USGS
science for a changing world

Physical Subdivision and Description of the Water-Bearing Sediments of the Santa Clara Valley, California

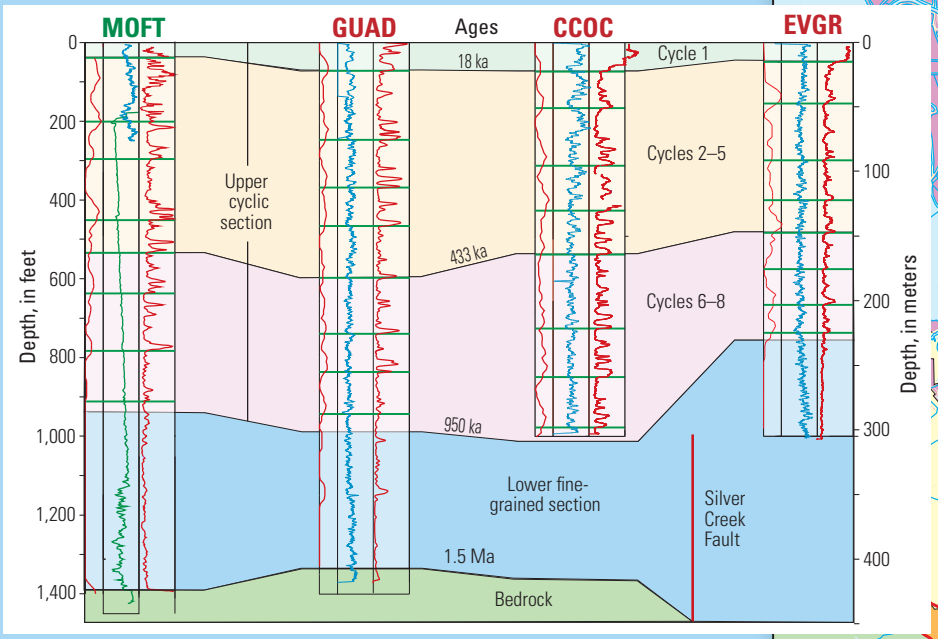

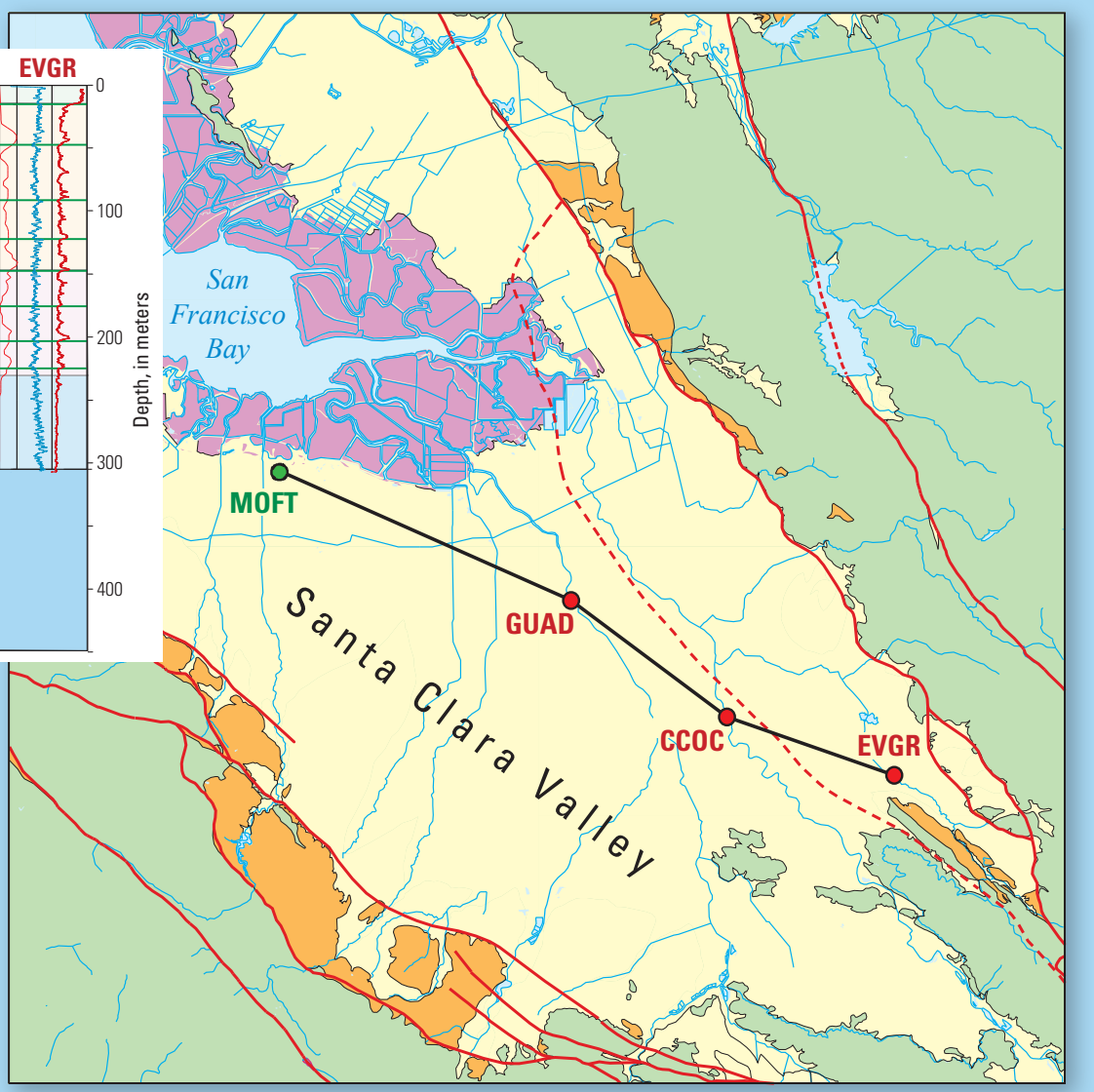

Scientific Investigations Report 2015–5017

U.S. Department of the Interior
U.S. Geological Survey

COVER

Summary cross section and map of the Quaternary sedimentary sequence beneath the Santa Clara Valley, California, showing four principal wells and their geophysical logs used to subdivide the sequence. The upper section consists of eight repetitive, upward-fining cycles that here are divided into the postglacial cycle 1, relatively permeable cycles 2–5, and less permeable cycles 6–8. It is this cyclic section that contains the groundwater aquifer system beneath the valley. The lower fine-grained section, beneath a mid-Quaternary unconformity, lacks abundant coarse layers and overlies an irregular bedrock surface estimated to be about 1.5 million years old.

Physical Subdivision and Description of the Water-Bearing Sediments of the Santa Clara Valley, California

By Carl M. Wentworth, Robert C. Jachens, Robert A. Williams, John C. Tinsley, and Randall T. Hanson

Scientific Investigations Report 2015–5017

U.S. Department of the Interior
U.S. Geological Survey

U.S. Department of the Interior
SALLY JEWELL, Secretary

U.S. Geological Survey
Suzette M. Kimball, Acting Director

U.S. Geological Survey, Reston, Virginia: 2015

Suggested citation:
Wentworth, C.M., Jachens, R.C., Williams, R.A., Tinsley, J.C., and Hanson, R.T., 2015, Physical subdivision and description of the water-bearing sediments of the Santa Clara Valley, California: U.S. Geological Survey Scientific Investigations Report 2015–5017, 73 p., 2 plates, *http://dx.doi.org/10.3133/sir20155017*.

Acknowledgments

This work was carried out in the context of a large study of the Santa Clara Valley that was supported by the U.S. Geological Survey and the Santa Clara Valley Water District and depended particularly on results from several new deep wells drilled under the sponsorship of the water district and the State of California. Collection of three seismic reflection profiles was also partially supported by the water district. We depended for most of the water wells in our dataset on the database of driller's logs developed by J.L. Fio and D.A. Leighton in their 1995 study of the basin.

Decisions concerning the possible use of the several studies of the unconsolidated surficial layer of sediment in the basin to help define sedimentary cycle 1 involved much discussion with M.J. Bennett, E.J. Helley, C.S. Hitchcock, T.L. Holzer, K.L. Knudsen, W.R. Lettis, and A.M. Rosinski. We thank them for their patience. Bennett also shared the results of his study of the Dumbarton well, including unpublished data.

Martha Merriam of the California Department of Transportation (CalTrans) generously arranged access to geophysical logs of three deep borings along the Dumbarton Bridge alignment, which proved most important in making cycle correlations from the Dumbarton well eastward onto the Niles alluvial cone.

Discussions with our colleagues were numerous and most helpful. In particular, we acknowledge the help of L.A. Beyer, who shared the results of his downhole gravity survey of well MOFT; E.A. Mankinen, whose paleomagnetic study of our well cores provided corroborative age control for the Quaternary section; P.J. McCabe, who suggested that borehole washouts might indicate loose sediment; R.J. McLaughlin, who patiently explained his work along the Monte Vista Fault Zone; R.G. Stanley, who aided our understanding of the buried Cupertino Basin and our interpretation of the Evergreen reflection profile; and C.F. Williams, for sharing and explaining his deep temperature logs.

Finally, we thank David W. Andersen, Jonathan D. Stock, and Donald S. Sweetkind for their helpful, even challenging, reviews of our manuscript, which stimulated considerable improvement in its content and organization.

This page left intentionally blank.

Contents

Figures

Tables

Plates

[Available online only at http://pubs.usgs.gov/sir/2015/5017/.]

Physical Subdivision and Description of the Water-Bearing Sediments of the Santa Clara Valley, California

By Carl M. Wentworth, Robert C. Jachens, Robert A. Williams, John C. Tinsley, and Randall T. Hanson

Abstract

A thick Quaternary alluvial section fills a sedimentary basin beneath the Santa Clara Valley, California, located within the San Andreas Fault system at the south end of San Francisco Bay. This section consists of an upper sequence about 1,000 feet thick containing eight sedimentary cycles and a lower fine-grained unit as thick as several hundred feet. Together these constitute the Quaternary Santa Clara Basin. The section overlies an irregular unconformity with more than 1,200 feet of relief cut into the underlying bedrock. This stratigraphy is determined through study of new wells and seismic reflection profiles, together with a sample of the many thousands of water wells in the valley. It represents a major change and improvement in understanding of the basin, particularly with regard to the upper cyclic sequence, which forms a large groundwater system that is an important resource in the San Francisco Bay region.

Each of the eight sedimentary cycles consists of a coarse-grained bottom interval overlain by a fine-grained top, with the coarse bottom forming a permeable sheet that is more or less continuous around the basin and the fine top forming a similarly extensive, relatively impermeable confining layer. This stratigraphic organization contrasts with most previous views, which have considered the coarse sediment in the basin to occur as scattered, discrete lenses and (or) sinuous channel sands, all embedded in a predominantly fine-grained section. Temperature logs in several wells demonstrate that the fine cycle tops do limit vertical movement of groundwater, although this may not be the case where those tops are thin to perhaps locally absent around parts of the basin margin.

Age control has been obtained from previous work, in which the sedimentary cycles were correlated with the marine oxygen isotope record and the ages of two deeper Quaternary unconformities were estimated, and from detailed paleomagnetic study of cores from the new wells by E.A. Mankinen. Despite careful search of the cores, very few fossils were found, and none that are helpful in subdividing the section. No tephra (volcanic ash) was recovered, and the few carbon samples found and dated radiometrically are limited to the upper 120 feet of the section. The upper cyclic section ranges in age from 0 to somewhat older than 718 thousand years (ka), and the lower fine-grained section lies between unconformities with estimated ages of 950 and 1500 ka.

Reflections in the seismic profiles indicate that layering in the basin is subparallel to the ground surface, and this fact, together with the continuous stratigraphic detail provided by geophysical logs of the new wells, allows the confident interwell correlation required to delineate the sedimentary cycles. The sequence of layers within any one cycle tends to persist laterally between the wells in the dataset, which are spaced 1 to 3 km apart, with most changes occurring gradually. The eight cycles, in contrast, tend to differ from each other in the details of their internal organization.

Maps and cross sections show the elevations of cycle boundaries and the underlying bedrock surface, the varying thicknesses of the cycles and of their fine tops and coarse bottoms, and the aggregate thickness of coarse layers in those bottom intervals. Coarse sediment is more abundant toward some parts of the basin margin and in the southern part of the basin. Cycle boundary surfaces are relatively smooth, and their shapes are consistent with having been intercycle topographic surfaces. The underlying bedrock surface has a relief of more than 1,200 feet and deepens toward the center of the basin and the west edge of the fault-bounded Evergreen Basin, which is concealed beneath the east side of the Quaternary basin. The absence of consistent abrupt changes in thicknesses or boundary elevations across the basin or in cross section indicates that the interior of the basin is largely unfaulted, with the Silver Creek strand of the San Andreas system at the west edge of the Evergreen Basin being the sole exception. The east and west margins of the Santa Clara Basin, in contrast, are marked by reverse and thrust fault systems.

Introduction

Study of eight recently drilled deep wells in the alluvial fill of the Santa Clara Valley of northern California and associated data has led to discovery of an unanticipated regularity in the upper 1,000 feet of section. That regularity defines eight separate

sedimentary cycles, which together constitute a large groundwater aquifer system that is a major source of water in the San Francisco Bay region. The primary goal of this report is to describe the sedimentary cycles and the sediment that forms them, together with the underlying bedrock unconformity and intervening earlier Quaternary section. Detailed hydrologic interpretation is not addressed, and the principal geologic description and interpretation are left for separate presentation. The study greatly improves understanding of the stratigraphy and structure of this alluvial basin and thus contributes to a better understanding of its aquifer system, earthquake response, and geologic history.

The Santa Clara Valley[1] is located within the California Coast Ranges between the San Andreas and Hayward Faults at the southern end of San Francisco Bay (fig. 1). The valley is floored by Quaternary deposits that overlie a large, subsiding Quaternary alluvial basin—the Santa Clara Basin (fig. 2). Many thousands of water wells have been drilled in the valley, and driller's logs of those wells have been the principal source of information about the basin sediments. Additional information has now been obtained about the basin from eight new deep wells and other geophysically logged wells, as well as three shallow seismic reflection profiles, which together yield new insights about the basin and provide a guide to interpreting the preexisting wells.

The material reported here is part of a large body of new work in the Santa Clara Valley that was stimulated jointly by the interest and support of the Santa Clara Valley Water District and projects funded by the National Geologic Mapping, Earthquake Hazards, and Water Resources Programs of the U.S. Geological Survey (USGS). The drilling, logging, and selective coring of the new wells in 2000–2003 were funded largely by the water district, and collection

Figure 1. Map showing location of the Santa Clara Valley in the southern San Francisco Bay region, California. Alluvial lowlands (yellow) are distinguished from bedrock uplands (green). Principal faults are shown in black; principal streams flowing into the study area are shown in blue: A, Alameda Creek, C, Coyote Creek, G, Guadalupe River, L, Los Gatos Creek.

[1] Santa Clara Valley here refers to the lowland extending from Coyote Hills southeast to Coyote narrows (southeast of Oak hill) (see fig. 2).

of the seismic reflection profiles was also partially supported by the district.

Recognition that the upper 1,000 feet or so of section in the basin consists of eight sedimentary cycles was made in the first new well drilled (Coyote Creek, or CCOC), and the rest of this study was directed largely at confirming that conclusion using other wells, and then mapping the cycles throughout the basin. The primary well dataset consists of geophysical logs and cores from the new wells, geophysical logs from 15 other wells, and driller's logs from 105 water wells. Material from other parts of the multidisciplinary project is also used, particularly seismic reflection profiles, paleomagnetic study of the cores, and high-precision temperature logs of the wells, and specific details are obtained from several other water wells.

Several methods were developed in this study specifically to help interpret and compare the well logs. These include a smoothed running measure of the concentration of coarse-grained layers through the section, quantitative display of driller's descriptions as continuous downhole logs, and the inference that unusually deep borehole washouts in coarse layers indicate less cohesive and thus more permeable sediment.

Each of the sedimentary cycles is subdivided into a coarse bottom and fine top, and those are mapped around the basin within the cycles. Systematic well-correlation sections containing all the wells in the primary dataset are presented with the cycles and their subdivisions shown. This assembly of wells provided a framework for compiling data, by well and by cycle, on aggregate thickness of coarse layers and other factors that are reported in data tables. Mapping the cycle boundaries and internal coarse/fine boundaries around the basin provided the basis for preparing elevation maps of those surfaces, and data on abundances of coarse and fine sediment supported mapping those factors as well. Representative cross sections were prepared from the elevation maps. The data also permitted the bedrock surface underlying the basin fill to be mapped in some detail.

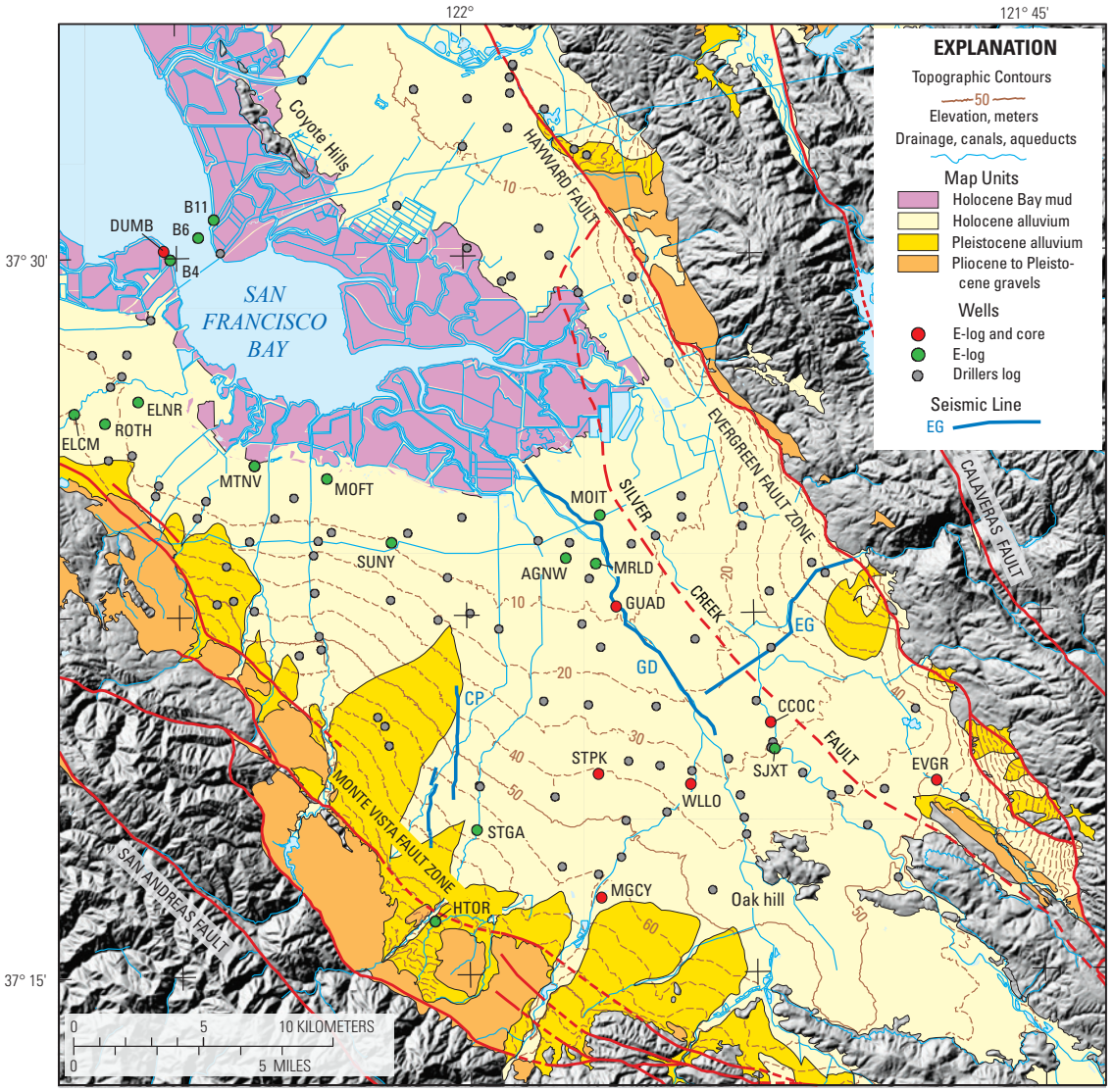

Figure 2. Map showing general surficial geology of the Santa Clara Valley and location of control wells, seismic reflection profiles, and principal faults (red, dashed where concealed). Symbols distinguish wells with geophysical logs and cores, geophysical logs only, and driller's logs. Well codes shown only for wells with geophysical logs (E-logs). Seismic reflection lines: CP, Cupertino, GD, Guadalupe, and EG, Evergreen. Upland bedrock areas in shaded relief (prepared from 30-m digital elevation model of Graham and Pike, 1998). Surface geology compiled from Graymer and others (1996), Wentworth and others (1998), Brabb and others (2000), Knudsen and others (2000), and Witter and others (2006).

The report begins with some background on previous work and geologic setting, describes the subsurface data used in the study, and then proceeds to describe the discovery of cyclicity in the section, testing of that conclusion, and then correlation of the cycles across the suite of 22 wells with geophysical logs. In the process, the procedures used to interpret and correlate the well logs are described and illustrated. The correlations between the 22 geophysically logged wells then provided a confident framework within which to identify and correlate the cycles in the 105 water wells represented by driller's logs. That set of wells, which forms a small sample of the many thousands of driller-logged wells in the basin, consists largely of a set chosen and categorized in an earlier study by Fio and Leighton (1995) and Leighton and others (1995). With the new stratigraphy defined, some general hydrologic implications are suggested, fault offset of the cyclic sequence is addressed, and the results are summarized. Appendixes present detailed descriptions of the cores, describe some of the detailed procedures used in the study, and list and describe the digital files that accompany the report. Those files include data tables, vector digital maps of areal geology and the wells, and raster grid maps of the numerous elevation surfaces and other data.

Illustrations are presented in three forms: figures scattered through the text, 19 well diagrams showing all the correlated wells in appendix B, and two suites of maps as plates 1 and 2. Although the illustrations are presented in the order of their principal reference and use in the text, some are also cited earlier.

Previous Work

Groundwater in the Quaternary Santa Clara Basin has been exploited for more than a century, and problems and information needs associated with that use have led to a long series of studies and reports (see, for example, the bibliographic list in California Department of Water Resources, 1975). In addition, there are relevant reports by Meade (1967), Poland and Ireland (1988), Iwamura (1995), Fio and Leighton (1995), and Leighton and others (1995), among others. Of these, for this analysis of the physical stratigraphy of the Santa Clara Basin, most of our attention can be focused on two reports by the California Department of Water Resources (1967 and 1975) and the three 1995 reports just noted, all of which address the whole basin.

In summary (based largely on Iwamura, 1995), the groundwater studies divide the basin fill into an upper unconfined to leaky confined aquifer zone with a clay cap and a lower confined aquifer zone, the two separated at a depth of about 150 feet by a thick and extensive aquitard. The result is that in most of the interior of the basin, beneath that aquitard, the groundwater is under artesian conditions, as initially mapped by Clark (1924). A so-called forebay facies consisting largely of coarse sediment is distinguished along the basin margins and considered the source of recharge for the deep aquifer system.

The sedimentary section has been considered to consist of generally impermeable silt and clay beds with interlayered sand and gravel beds, with many of the latter occurring as sinuous channel sands. Although gravels of the Santa Clara Formation exposed at the margin of the basin are considered essentially not water bearing, that same unit was presumed to occur in the subsurface within the basin, where it was considered to be an effective part of the aquifer system. Lateral continuity of coarse layers over considerable distances has not generally been recognized except in the Niles cone, where three aquifer zones extending to a depth of about 400 feet are named. Iwamura (1995) notes that below a depth of about 1,000 feet the section contains less coarse material.

The two studies by the California Department of Water Resources (1967 and 1975) and that by Iwamura (1995) represent major efforts to better understand the alluvial fill of the Santa Clara Basin, based largely on an extensive suite of driller's logs from water wells. Each of these reports presents cross sections from which the relative abundance of coarse and fine sediment and the inclination of layering relative to the ground surface can be estimated. Significant differences are evident between the three reports.

An intricate fence diagram in the 1967 report shows elongate discontinuous lenses of coarse sediment enclosed in much more abundant fine-grained sediment. Layering is shown as being more or less parallel to the ground surface. Cross sections in the 1975 report show even less coarse material occurring in thicker, more equant patches that are described as channel deposits. Inclination of layering, where evident at all, ranges from deepening basinward near the margins to subparallel to the ground surface. Iwamura (1995) shows much more abundant and laterally continuous coarse layers, with all but the shallowest layers deepening eastward across the basin. These different representations bear directly on the expected abundance and lateral continuity of coarse sediment, which forms the aquifer network in the basin, and on how the coarse intervals should correlate from well to well.

The 1975 interpretation by the California Department of Water Resources restricts the coarse sediment in the basin to a suite of isolated channel sands. These are shown in a set of maps representing 50-ft elevation slices down through the section. The maps show the coarse sediment in each elevation slice to form narrow, sinuous channels trending basinward that are typically about 0.2–0.65 miles wide, all immersed in much more abundant fine-grained sediment. Inspection of the maps shows that the channel boundaries are not closely constrained by the well control, although numerous wells containing "predominantly clayey materials" are shown between the channels within each elevation slice. Terminations of these inferred channels led to inference of numerous faults in the section.

Meade (1967), in a study of sediment in cores from two deep wells (SUNY and SJXT of our well dataset), concludes that the section is alluvial and contains no estuarine sediment at those drill holes, and reports a piece of redwood at a depth of 73 feet in SJXT with an uncalibrated ^{14}C age of 14,350±400 years before present. He also reports freshwater clams and snails below about 500 feet and one mollusk (*Fluminicola yatesiana*) at or below 760 feet in SUNY that was then considered to be no younger than late Pliocene.

The 1995 reports by Fio and Leighton and Leighton and others summarize some aspects of the previous work, but they are important to the present study largely because of their inclusion of a set of driller's logs for which the driller's descriptions are categorized in numeric, digital form.

In a very different kind of study, Koltermann and Gorelick (1992) developed mathematical procedures to model the formation of the Alameda Creek alluvial fan (Niles cone) in the northeast part of our study area. As one constraint in that modeling, they prepared an interpretation of the actual subsurface distribution of coarse and fine layers in that fan based on a rather dense array of 63 wells. They found the coarser sediment to be distributed in lenses large in plan extent and somewhat irregular in cross section, particularly in the upper half, and modeled them as forming six climate-controlled cycles that mimicked the ground surface in cross-sectional shape.

Previous reports arising from the present multidisciplinary study of the basin help provide context for this report. These include a series of papers presented at the 2005 meeting of the Geological Society of America in San Jose, California, particularly Andersen and others (2005), Jachens and others (2005), Mankinen and Wentworth (2005), Wentworth and others (2005), Wentworth and Tinsley (2005a), and Williams and others (2005). More extensive reports include a summary of the Coyote Creek well (Hanson and others, 2002), initial results of a paleomagnetic study of the Coyote Creek well (Mankinen and Wentworth, 2003), a summary of data for the new wells (Newhouse and others, 2004), geologic description of the Coyote Creek well (Wentworth and Tinsley, 2005b), and description and discussion of the geologic setting and history of the Silver Creek Fault (Wentworth and others, 2010). Hydrologic modeling by Hanson and others (2004), which predated the availability of the detailed stratigraphic subdivision presented here, is important here principally in its treatment of faults as impediments to water movement in the basin.

The areal geology of the Santa Clara Valley and surrounding uplands is delineated at scales of 1:62,500 to 1:100,000 on geologic maps by Graymer and others (1996), Brabb and others (1998), Wentworth and others (1998), and Brabb and others (2000). More detailed mapping of the Quaternary surficial deposits is presented by Knudsen and others (2000) and Witter and others (2006).

Geologic Setting

The Santa Clara Valley is relatively flat and consists of alluvial fans that extend from the surrounding hills down to a central drainage axis (Guadalupe River and Coyote Creek) and to San Francisco Bay, which is fringed and underlain by the estuarine San Francisco Bay mud (fig. 2). Late Pleistocene alluvium is exposed on the heads of the fans, particularly on the west side of the valley, whereas most of the valley surface consists of Holocene alluvium fining downslope toward the bay, with numerous natural levees expressed in the topography along present and earlier stream courses (Witter and others, 2006).

These surface deposits are only the uppermost part of a thick section of young alluvium that accumulated in this basin through much of Quaternary

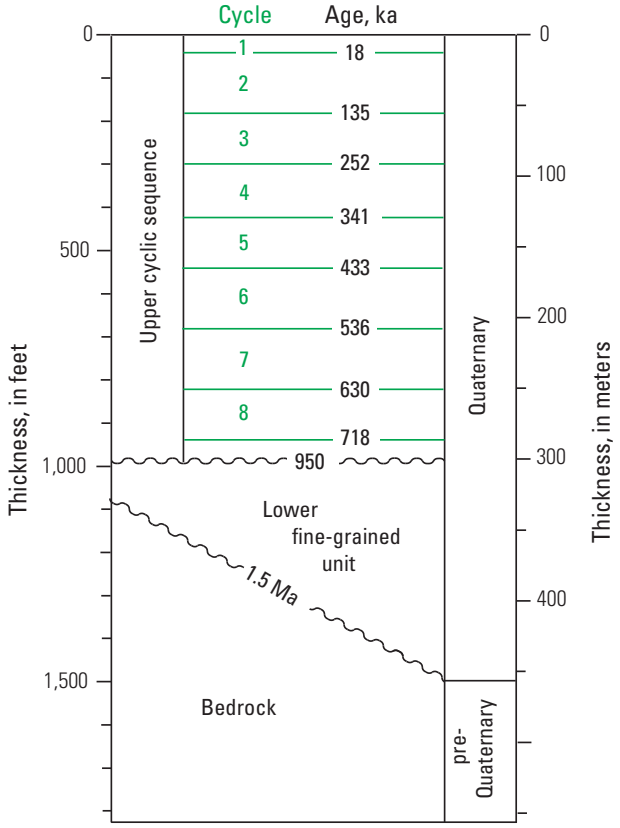

Figure 3. Stratigraphic diagram showing subdivision of the Quaternary sedimentary fill of the Santa Clara Basin. Ages in thousands of years (ka) except where noted. Bedrock consists of Miocene fill of the Cupertino Basin, Miocene(?)-Pliocene fill of the Evergreen Basin, and rocks of the Franciscan Complex and Coast Range Ophiolite. Ages modified from Wentworth and Tinsley (2005a) and Wentworth and others (2010).

time[2], as indicated by Wentworth and others (2010). The stratigraphic organization of the section, which is developed in some detail in this report, is summarized in figure 3. The basin subsided gradually to accommodate a sequence of clastic sediment that west of the Silver Creek Fault is as thick as 1,500 feet. Correlation of details in the section with the marine oxygen isotope record indicates that this subsidence proceeded at a regular rate of about 0.4 mm/yr over the past 718 thousand years during accumulation of the upper cyclic section (Wentworth and Tinsley, 2005b). The depositional environment was largely alluvial (Meade, 1967; Wentworth and others, 2010), although estuarine sediment is evident near the southern margin of San Francisco Bay (see, for example, Bennett, 1979). The sediment was derived from the adjacent uplands, and the presence of greenstone of the Franciscan Complex in gravel throughout the section in the new wells indicates that the source was largely the Santa Cruz Mountains to the west (Andersen and others, 2005; Wentworth and others, 2005).

The section is divided by a basinwide unconformity at a depth of about 1,000 feet that separates the principal water-bearing alluvial section above from a finer grained section below (fig. 3). The age of that unconformity is estimated to be slightly less than 1 million years (here, 950 ka) and that of the unconformity at the base of the Quaternary section to be about 1.5 million years (Wentworth and others, 2010). Contrary to earlier presumptions, none of the distinctive Santa Clara Formation or other Pliocene to Pleistocene gravel suites known from surface geology around the edge of the basin have been recognized within the basin, and they appear to be absent there (Andersen and others, 2005; Wentworth and others, 2010).

[2] The beginning of the Quaternary Period has recently been changed from 1.8 to 2.6 million years (Mascarelli, 2009; Walker and Geissman, 2009). Because all the work associated with this report took place in the context of the earlier definition of the period, however, that previous definition is retained here.

The Quaternary Santa Clara basin is underlain by two largely concealed Tertiary basins separated by a central basement high, which is composed of Franciscan Complex and Coast Range Ophiolite. The Miocene Cupertino Basin lies to the west and is bounded on the west by faults of the Monte Vista system, and the Miocene and Pliocene Evergreen Basin lies to the east and is a strike-slip pull-apart basin formed between the Silver Creek and Hayward Faults (Wentworth and others, 2010).

The Santa Clara Basin is separated from the mountain ranges bounding it on the east and west by basinward-directed systems of reverse or thrust faults that offset or truncate the alluvial section to various degrees (Monte Vista and Evergreen Fault systems, fig. 2). Groundwater modeling by Hanson and others (2004) suggests the presence of an outboard strand of the Monte Vista system that inhibits lateral movement of groundwater (located just northeast of the label for the Monte Vista Fault Zone on fig. 2), which they call the New Cascade fault. Wentworth and others (2003) suggested a possible blind fault in the Monte Vista system east of the mapped faults of figure 2 on the basis of geophysical modeling and the three-dimensional distribution of earthquakes. The California Department of Water Resources (1975) shows a variety of faults crisscrossing the basin that were inferred from apparent terminations of buried alluvial channels. Wentworth and others (2010), who reviewed past depictions of faults in the basin, concluded that the only fault that affects the interior of the Quaternary basin is the Silver Creek Fault (fig. 2). This fault, they demonstrate, offsets most of the Quaternary section, and the modeling of Hanson and others (2004) indicates that it does impede groundwater movement.

Subsurface Data

This study of the Quaternary sedimentary section of the Santa Clara Basin depends on three principal kinds of subsurface data—logs of wells (drilled largely for water), cores taken during the recent drilling campaign, and seismic reflection profiles. The sediment transected by the wells was sampled directly through cuttings and core—the former described largely by the drillers of the wells, the latter described carefully in the laboratory by geologists (see appendix A)—and through geophysical logs collected by raising instruments on a wire line up the height of the borehole.

Wells

The 127 wells used in this study of the sedimentary section (our primary well dataset) include 105 wells represented by driller's logs and 22 wells represented by continuous wire-line geophysical logs. Depths of the wells range from 110 to 1,535 feet, with about half deeper than 700 feet[3]. The wells are identified by codes that for some (such as GUAD) are based on well names or other features and for most (such as 731) by arbitrary numbers. These codes are used to identify the wells in the text, on the maps and figures, in the tables, and in the digital data files. The whole suite of wells is shown in map view on figures 2 and B1; in the former only those wells with geophysical logs are identified by code, while in the latter all the wells are so identified. The digital map layer wells (appendix E) contains all these wells.

Eight of the wells with geophysical logs (table 1; Newhouse and others, 2004) were drilled in 2000–2003 by the U.S. Geological Survey with funding from the Santa Clara Valley Water District (6 wells) and the State of California (2 wells). Geophysical logs were also obtained for 14 other wells in the valley, including 4 wells from the cities of Palo Alto (well codes ELCM and ROTH), Mountain View (MTNV), and Saratoga (HTOR); 2 wells drilled for emplacement of vertical extensometers in the valley for J.F. Poland in 1960

[3] A note about units. It is customary that depths in water wells are measured and described in feet, and that notation is retained here, including for thicknesses, depths, and elevations in the wells (3.28 feet = 1 meter). Other dimensions are reported in metric units.

(SUNY and SJXT; Poland and Ireland, 1988); and a deep well drilled at Ames Research Center, Moffett Field, in 1973 (MOFT; Beyer, 1980). One well (DUMB) was drilled near the Dumbarton Bridge by the U.S. Geological Survey in 1975–76 and studied by Bennett (1979). Logs of three deep geotechnical wells drilled along the Dumbarton Bridge alignment in 1992–93 (B-4, B-6, and B-11) were provided by the California Department of Transportation (CalTrans).

The remaining 105 wells are water wells. The driller's logs for most of these wells come from the database of wells prepared by Leighton and others (1995) as part of a general study of groundwater in the southern San Francisco Bay region (Fio and Leighton, 1995). It is these wells from the Leighton database that are identified by arbitrary numeric codes. The well CRIT, an unusually deep water well (1,535 feet) drilled in 1909–10, was reported by Crittenden (1951).

Wells were an important source of control in delineating the irregular surface of bedrock beneath the Quaternary basin. For this, 46 wells from the primary dataset that either reached rock or helped constrain the depth of the surface were supplemented by 18 other bedrock wells.

Table 1. Wells drilled in the Santa Clara Valley by the U.S. Geological Survey, 2000–2003.

[Elevations and depths in feet. Datum for latitude/longitude is North American Datum 1927 (NAD27). Negative longitudes are west of Greenwich. Surface elevations from 30-m digital elevation model (Graham and Pike, 1998)]

Well code	Surface elevation	Well depth	Depth to rock	Well name	Well number	Longitude	Latitude
CCOC	84.5	1,011	----	Coyote Creek	007S001E09L004	-121.86835	37.33702
ELNR	22.6	932	922	Eleanor	005S003W36P002	-122.14202	37.45026
EVGR	180.5	1,009	----	Evergreen	007S002E19C005	-121.79644	37.31616
GUAD	33.1	1,369	1,335.5	Guadalupe	006S001W26Q001	-121.93505	37.37770
MGCY	213.9	869	787	McGlincy	007S001W35L017	-121.94270	37.27670
STGA	225.2	1,000	----	Saratoga	007S001W29C003	-121.99653	37.30056
STPK	138.1	1,000	----	Santana Park	007S001W14P001	-121.94352	37.31967
WLLO	115.8	842	802.4	Willow	007S001E19B003	-121.90340	37.31581

Cores

Six of the newly drilled wells were cored, with the goal for most of collecting about 200 feet of core in each nominally 1,000-ft well. The exception was GUAD (drilled to rock at 1,336 feet), in which core from the upper 1,000 feet of the well was sought. The practical result was to recover 662 feet of core from 883 feet attempted in GUAD and 205 of 339 feet in CCOC, with similar proportions in the other four partly cored wells (EVGR, MGCY, STPK, and WLLO). The locations of the cores in the wells are shown graphically on the well sections of figure 14.

During coring, as the donut-shaped core bit advances downward, a central column of material remains and is captured in a plastic tube (liner) within the core barrel. The barrel assembly is then retrieved by wire line. Coring attempts were typically 5 feet, although a full 5 feet of core was rarely obtained. Principal causes of core loss were blockage of the mouth of the core barrel by a stone or concretion during advance of the drill and falling of cored material out of the open-ended liner during wire-line retrieval of the core barrel. In the laboratory, each core was split longitudinally and carefully described at centimeter scale in terms of such factors as color, grain size, and layering and other sedimentary structures. The procedures and resulting descriptive details for all the cores are presented in appendix A.

Well Logs

The principal means used to interpret the sedimentary sections in the wells were natural gamma and resistivity curves for the geophysically logged wells and driller's descriptions of textures (driller's logs) in the other wells. In some of the older geophysically logged wells, self potential (SP) logs served the same role as the natural gamma logs. The logs are shown graphically in the well diagrams using consistent symbols and positions, as illustrated in figure 4. Very detailed and irregular raw natural gamma curves from the new wells were smoothed using a running average to match the detail of commercial logs for the other geophysically logged wells. The geophysical logs respond to differences in the layered sedimentary section in characteristic ways that permit identification of different sediment types, which makes them standard tools used in the ground water and petroleum industries (see, for example, Asquith and Gibson, 1982).

Driller's logs describe the cuttings produced by drilling—typically collected for every10-foot advance of the drill bit down the hole—in terms that often require translation or interpretation to be useful geologically. Leighton and others (1995) went a step further and, for a selected set of wells, assigned the driller's descriptions to a set of numbered geologic categories (table 2). Those numeric categories are recast here to provide a simple textural spectrum ranging from fine to coarse grained sediment, plus rock (table 2). Driller's descriptions for wells CRIT and FWLR are interpreted in the same way. The resultant textural values are graphed in a fashion analogous to the geophysical logs to produce continuous downhole logs

of relative coarseness, as illustrated in figure 4. This method of representing the driller's logs was developed because comparison of driller's descriptions of cuttings from adjacent water wells had indicated that, although the specific descriptions differed considerably, the relative changes in coarseness with depth matched fairly closely. The simplicity of these curves, compared to the original descriptions, greatly facilitated comparison and interpretation.

Caliper logs, which measure the diameter of the borehole, were collected in all eight of the new wells. These are used here to identify where unusually deep washouts occurred in the borehole wall (fig. 18). Nearly continuous wire-line logs of P- and S-wave seismic velocity were also collected in five of the new wells (fig. 12; Newhouse and others, 2004; and see Wentworth and Tinsley, 2005b).

Another continuous downhole curve that proved crucial in the interpretations is the coarseness curve (examples shown in fig. 4), which is a running measure of the varying concentration of coarse layers down the hole that was prepared specifically for this study, as described below.

Before each of the six cored wells was drilled, a cone penetrometer sounding (CPT; see example in fig. 5*A*) was taken at the drill site (Noce and Holzer, 2003; Newhouse and others, 2004). Sounding depths, which depended on resistance to penetration and deflection of the probe by stones, reached a maximum of 122 feet. These soundings were part of a study in the Santa Clara Valley by T.L. Holzer and coworkers, who were collecting new CPT data throughout the valley in order to delineate thickness and properties of the unconsolidated surficial deposits that might be subject to liquefaction (Holzer and others, 2010; and see http://earthquake.usgs.gov/regional/nca/cpt). The CPT procedure measures resistance to downward advance of a conically tipped rod 3.6 cm in diameter, which can be interpreted in terms of sediment texture and consolidation (see Wentworth and Tinsley, 2005b). CPT logs are presented here for wells CCOC and GUAD (fig. 5b).

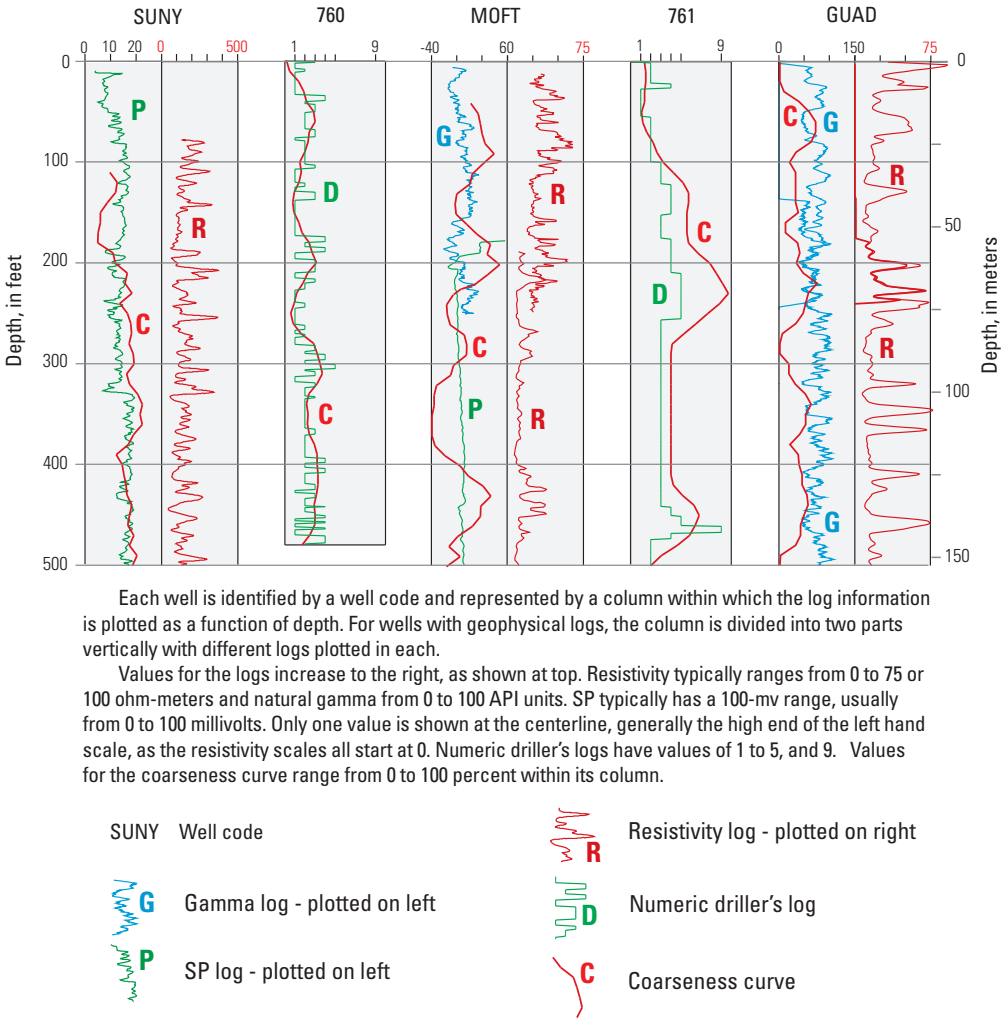

Each well is identified by a well code and represented by a column within which the log information is plotted as a function of depth. For wells with geophysical logs, the column is divided into two parts vertically with different logs plotted in each.

Values for the logs increase to the right, as shown at top. Resistivity typically ranges from 0 to 75 or 100 ohm-meters and natural gamma from 0 to 100 API units. SP typically has a 100-mv range, usually from 0 to 100 millivolts. Only one value is shown at the centerline, generally the high end of the left hand scale, as the resistivity scales all start at 0. Numeric driller's logs have values of 1 to 5, and 9. Values for the coarseness curve range from 0 to 100 percent within its column.

Figure 4. Explanation of symbols used for the various well logs shown in the well diagrams and sections. In some cases different logs represent the upper parts of the wells, as shown here where the deep logs for MOFT are supplemented by logs from a nearby shallow well, and in GUAD where shallow logs were run before the upper part of the well was cased. See text for description of how the numeric driller's logs and coarseness curves are constructed.

Table 2. Numerical representations of driller's log descriptions.

[Conversion of driller's descriptions of materials into numeric form: *A*, Initial conversion by Leighton and others (1995) and *B*, conversion of those values into the simple fine-to-coarse progression used here (F–C values), with the associated weighting factor used to plot the numeric driller's logs and compute the coarseness curves]

A.

Value	Description
0	unknown
1	rock, stone, shale, fractured shale
2	hard or cemented clay, hardpan
3	mud, clay, silt, silty clay, peat, clayey silt
4	sandy or gravelly clay, sandy silt, topsoil
5	tight, hard, or cemented sand, sandstone, tight, hard, or cemented gravel
6	clayey or silty sand, clayey or silty gravel
7	sand, gravelly sand
8	gravel, sandy gravel

B.

F–C value	Weight	Description (texture)	Leighton value
0	0	unknown	
1	0	clay to sandy silt	2, 3
2	0.1	sandy or gravelly clay	4
3	0.4	clayey or silty sand or gravel	6
4	0.7	sand, gravelly sand	7, 5
5	1	gravel	8
9	1	rock	1

Finally, a density curve is available for the deep well MOFT (fig. 15). This curve (Beyer, 1980; L.A. Beyer, written commun., 2005) is based on a downhole gravity survey that was collected in the well using an experimental downhole gravimeter (McCulloh and others, 1967).

Seismic Reflection Profiles

Three seismic reflection profiles aggregating about 25 km in length were collected across selected parts of the valley (fig. 2) by R.A. Williams and others using a minivibroseis energy source and multichannel receiver array (Williams and others, 2002; Williams and others, 2004; Williams and others, 2005). This procedure was very successful in imaging the Quaternary sedimentary section to depths of 1 km (3,300 ft) or more, despite difficult recording conditions that involved both urban noise and greatly varied ground conditions. Wentworth and others (2010) illustrate the western part of the Evergreen profile (EG), and its whole length to a depth of about 400 m (1,300 ft) is shown here in figure 13.

Interpreting the Geophysical Logs

Two of the new wells, CCOC and GUAD, which between them transected the whole Quaternary section and yielded 867 ft of core, provided an excellent look at the basin fill and posed all the basic issues involved in defining the sedimentary column from the well logs and cores. The cores indicated, as expected, that the section consists of mud, silt, sand, and gravel, and that these different textures are interlayered at various scales. But it was the geophysical logs that provided continuous information down the wells. The cores and logs from these two wells were used together to determine how to interpret all the geophysical logs for the purposes of this study.

In the saturated, predominantly freshwater environment of the Santa Clara Basin, the gamma and resistivity logs respond principally to clay content. Thus, natural gamma radiation is typically high in clay and low in sand, whereas electrical resistivity is low in clay and high in sand. Plotting these two logs together down the well column, with the gamma logs to the left and resistivity logs to the right, yields a pattern like the cross section of a complex spindle in which the narrow parts are finer grained (high gamma/low resistivity) and wider parts are coarser grained (low gamma/high resistivity). This pattern is evident in the logs for wells MOFT and GUAD in figure 4, and for wells CCOC and GUAD in figure 5*B* where the inferred layering is shown.

With this log response in mind, the detailed descriptions of cores from wells CCOC and GUAD were used to empirically calibrate interpretation of sediment textures from the geophysical logs. This was done in two steps, first by calibrating the log interpretation through visual comparison between core textures and the log features at equivalent depths, and second by testing that calibration through quantitative comparison with the core descriptions. In the first step, visual comparison of the textures observed in the cored intervals with the gamma and resistivity logs of the same intervals (see fig. 5*A* for a graphic example) guided establishment of a set of textures that could be inferred from the logs and then used to define layering in the section. The textures thus inferred from the logs are here called log textures (table 3), to distinguish them from those observed in the cores, which are called core textures (fig. 5*A*).

This visual comparison indicated that the most prominent gamma lows having corresponding resistivity highs represent medium-grained sand to gravel (see example E on fig. 5*A*), whereas higher gamma values that lack equivalent resistivity highs represent finer grained core material (B on fig. 5*A*). Unexpectedly, fine sand to silt could generally not be distinguished from silty clay and clay from the logs.

Table 3. Log textures.

[Textures interpreted from the geophysical logs (natural gamma, 16-inch normal resistivity, and caliper) according to relations defined from the detailed textural descriptions of the cores. Category B is the relatively fine-grained remainder after the other log textures are delineated. RES., resistivity]

	Size	Gamma	Res.	Caliper	Description
A	Consis-tently fine	High	Low	---	Principally clay, silty clay, and clayey silt
B	Mixed fine	Mod.-high	Low	---	Clayey silt to silt and fine sand
C	Mixed coarse and fine	Low	Mod.	---	Sand and gravel with abundant finer sediment
D	Coarse	Low	High	Was-houts	Principally medium to coarse sand and gravel, relatively loose and permeable
E	Coarse	Low	High	No wash-outs	Principally medium to coarse sand and gravel

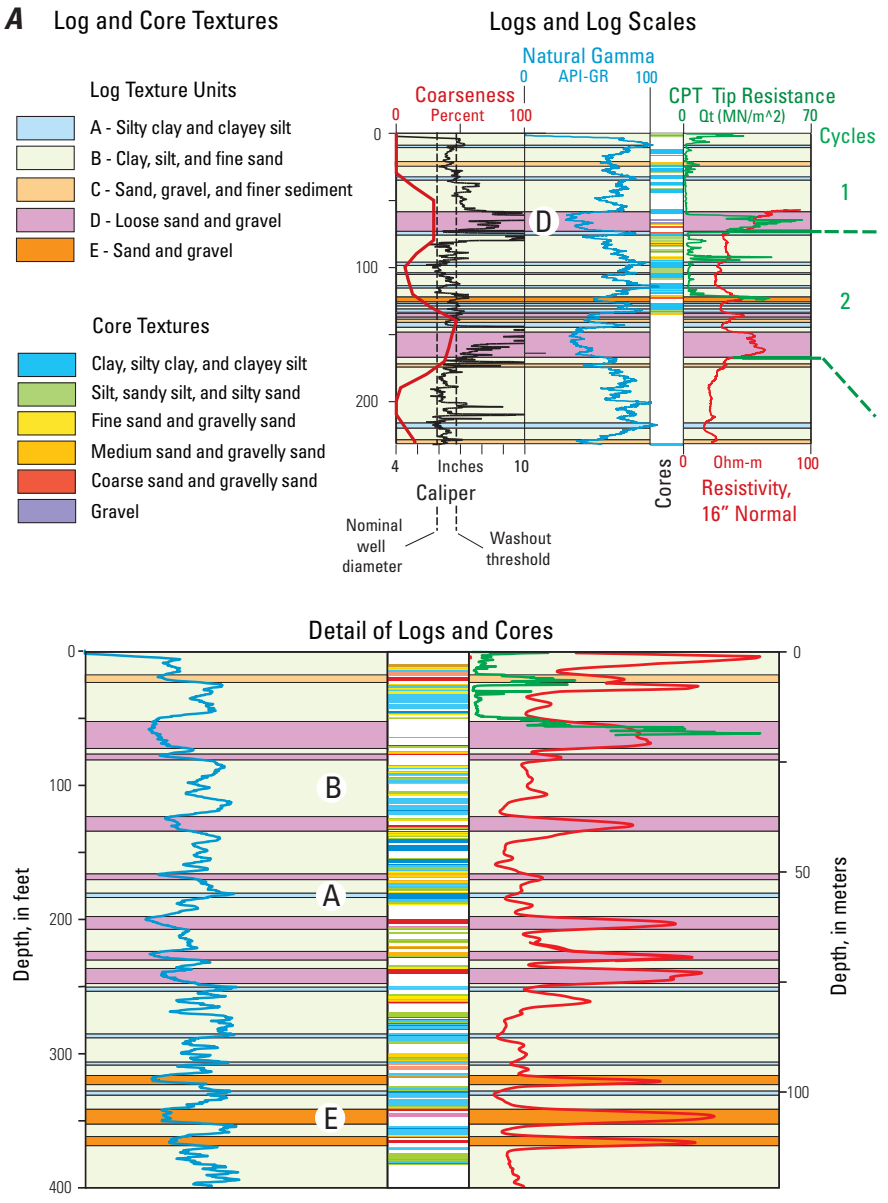

Figure 5. Stratigraphic interpretations of the sections in wells CCOC and GUAD derived from the electronic logs and examination of cores. ***A***, Explanation of symbols for logs, log textures, and core textures used in *B*. Log and Core Textures shows textural categories and color codes for log-texture units and core textures; Logs and Log Scales gives examples and scales for the various logs, including a CPT log plotted on the right in green; and Detail of Logs and Cores shows a portion of the layered section in GUAD to illustrate the relation between core textures and details of the natural gamma and resistivity curves from which the log textures are inferred. See text for description of log and core textures and for discussion of geophysical logs. Examples marked by circled letters are keyed to the text. ***B***, The sections in wells CCOC and GUAD showing logs, core textures, and log textures interpreted from the logs and cores. See *A* for explanation of symbols. Cycles, cycle boundaries and correlations in green. Example marked by C is keyed to text.

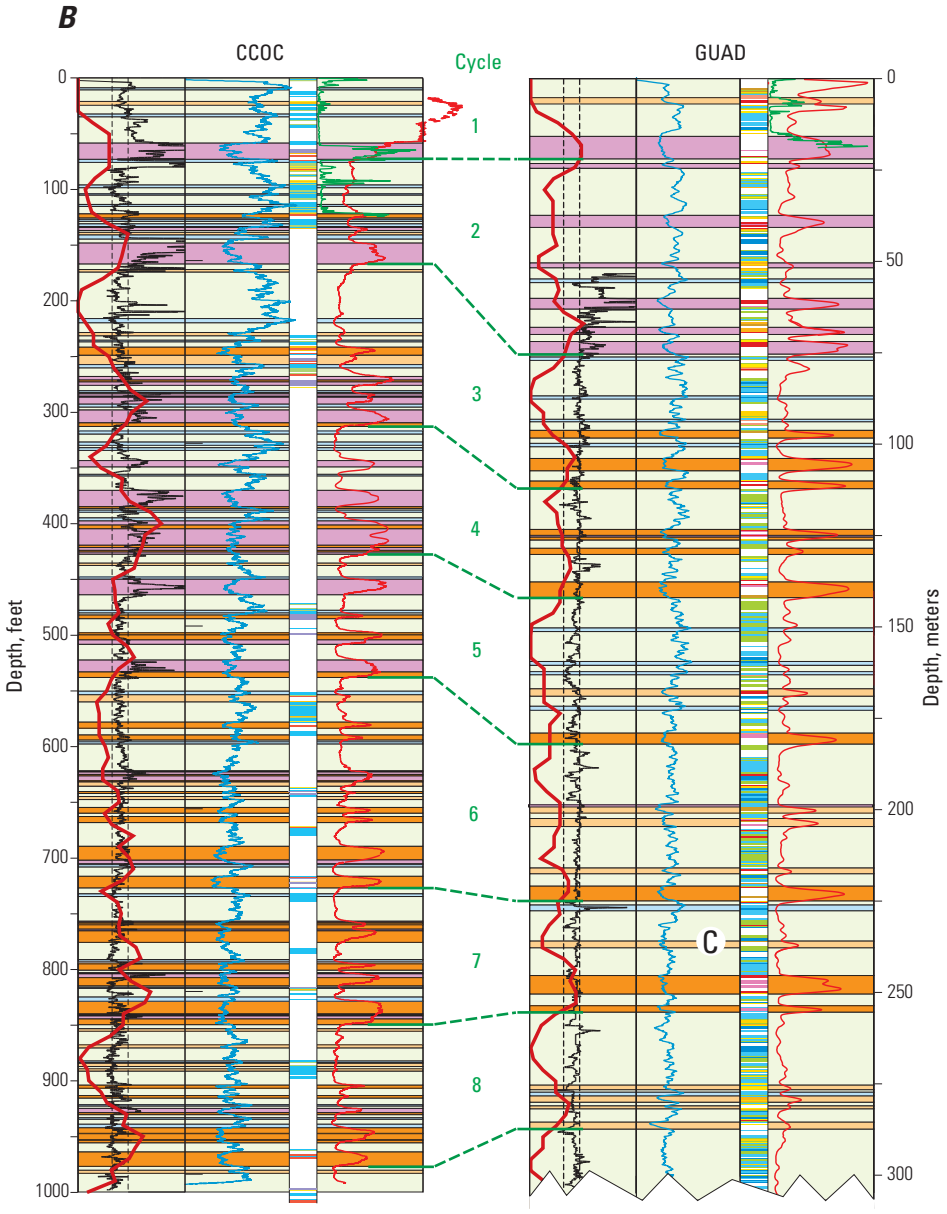

Given these relations, intervals in the section with strong gamma lows and equivalent resistivity highs were delineated as coarse sediment (medium-grained sand and coarser, log textures D and E) and the rest of the section as fine grained (clay to fine sand, log texture B). Exceptions to this twofold subdivision were few. In the fine-grained intervals, some occurrences of very high gamma values with equivalent low resistivity troughs did represent largely clay to clayey silt (log texture A; example A on fig. 5*A*). Within the coarser intervals, some resistivity highs with equivalent strong gamma lows are not nearly as high as most, and the cores indicate that here the sediment consists of mixed coarse and fine layers not resolved by the geophysical logs (C in GUAD column on fig. 5*B*). This is log texture C, which is also considered coarse. Because the geophysical logs tend to have high gradients at unit boundaries, the positions of the boundaries between these different intervals in the logs are relatively insensitive to the exact location of the picks.

Distinction between the coarse log textures D and E was made using the caliper log (fig. 5*A*). Amongst the various causes of changes in borehole diameter, it had been anticipated that differential washouts of the borehole wall might well occur in coarse-grained intervals where the material was relatively loose and permeable. Numerous unusually wide parts of the borehole within coarse log intervals do occur, to a well depth of 530 ft in CCOC and 240 ft in GUAD, and these were categorized as log texture D (D on fig. 5*A*). Those coarse log intervals lacking such deep washouts were categorized as log texture E. Surface casing in the upper 180 feet of GUAD prevented the collection of caliper data there, but it is assumed that the shallow coarse layers there have washouts as they do in CCOC.

The layering thus defined from the geophysical logs for these two wells is shown in figure 5*B*, together with the logs themselves: natural gamma, resistivity (16-inch normal), and caliper. In this figure the depths and textures of the cores are plotted in a column between the gamma and resistivity logs, using a generalization into six categories of the detailed textures originally described from the cores.

Testing the Log-Texture Interpretation

The log textures were defined by visual comparison of the core textures with the geophysical logs, and these categories were used in making the layer distinctions shown in figure 5. Then, in this second step, that interpretation was tested quantitatively by intersecting the textures observed in the cores from wells CCOC and GUAD (here aggregated into 12 core textures) with the log textures that had been defined in those wells. That is, the depth intervals for different textures observed in the cores were intersected with the layered sequence of log textures down each well (as illustrated in figure 6), and the results tabulated by log texture. The procedure is carried out by computer, compares the textures observed in the cores with the inferred log textures at equivalent depths, and yielded the numeric results displayed graphically in figure 7. The procedure depends on good registration between well depths measured by the drill string (core depths) and those measured by wire-line (log depths), which the results suggest was the case.

Figure 7 shows by colored curves the proportions of the various core textures determined by the intersection to occur within each of the five log textures (A through E). These curves show that the log categories successfully separate different aggregates of the twelve core textures, in the fashion indicated by the original visual comparison, although that separation is far from complete. Nor should it necessarily be so. Even at the relatively fine scale of the geophysical logs, many of the measurements are still of sets of beds rather than of individual textural intervals, which are as thin as one to a few centimeters. Some mismatch between core and log depths may also be involved.

These results help quantify the significance of placing the boundary between coarse and fine sediment in this work between medium- and fine-grained sand. The green curves in figure 7 indicate that log texture B (clay, silt, and fine sand), which forms most of the fine-grained category, contains about 25 to 40 percent clayey silt to silty sand.

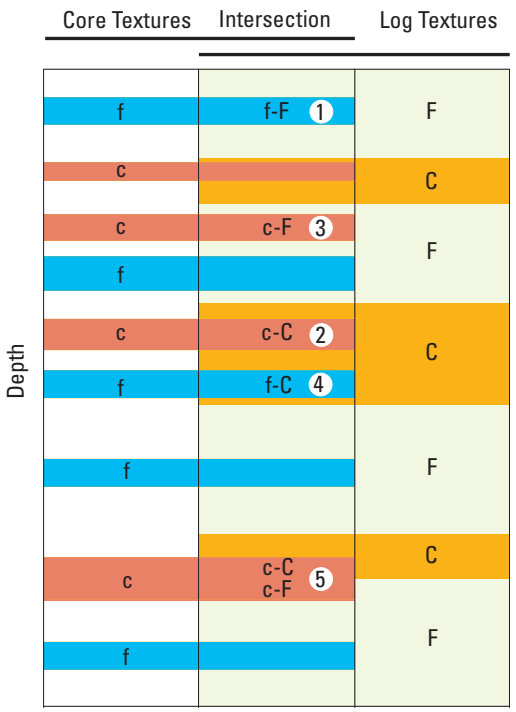

Figure 6. Diagrammatic vertical section showing simplified graphic example of intersecting the layering interpreted from the well logs (log textures) with the textures observed in the cores (core textures). The cores (on the left) and the continuous layering interpreted from the well logs (on the right) overlap (intersect) in the column at center. White = no core, c and C = coarse texture, f and F = fine texture. The intersected result f-F (at 1) represents a core of fine sediment that occurs within a layer identified from the logs as fine grained, and c-C (2) represents a coarse core within a coarse log layer. In contrast, c-F (3) and f-C (4) represent cases where coarse and fine cores occur within log layers of the opposite texture. At (5) the coarse core is split by the coarse-over-fine contact in the log column, which results in two intersected layers, a c-C interval above and a c-F interval below. See text for further discussion.

Note also that the amount of lost core (attempted but not recovered) is related to log texture, with more coarse than fine material being lost. This is as expected, for coarse sediment is more likely to disaggregate and fall out of the core barrel during its retrieval.

These textural interpretations from the geophysical logs are much more detailed than the textural descriptions by Newhouse and others (2004, their figs. 3 and 7) for the same wells and differ considerably from them in the relative abundance of coarse sediment, particularly for CCOC. Those earlier descriptions, in a fashion similar to driller's logs, were based largely on cuttings taken at 10-ft depth intervals and seem to emphasize the coarser materials relative to the abundant fine-grained sediment inferred here from the geophysical logs and confirmed by comparison with the cores.

The Coarseness Curve

Inspection of the layering defined from the geophysical logs in well CCOC (using the procedures just described) suggested local concentrations of coarse layers in the section (that is, of log textures C, D, and E). In order to quantify the depth distribution of coarser layers, a smoothed measure of coarseness was developed by calculating the percent of coarse section in a 50-ft-high window that was moved by short steps down the well (variously 0.1, 1, or 10 ft). The resulting curve was marked by several prominent, simple to complex peaks separated by distinct lows (fig. 5*B*). The peaks mark local concentrations of coarse layers, the lows their relative absence. The 50-ft height was selected by inspection to capture the effect of several layers together. Testing on the layered sequence of CCOC with a suite of window heights ranging from 10 to 200 ft (fig. 8) demonstrates that the result is not a function of window height. Rather, the curves show different degrees of generalization of the same layered section, and the 50-ft window provides good discrimination of its varying coarse and fine elements.

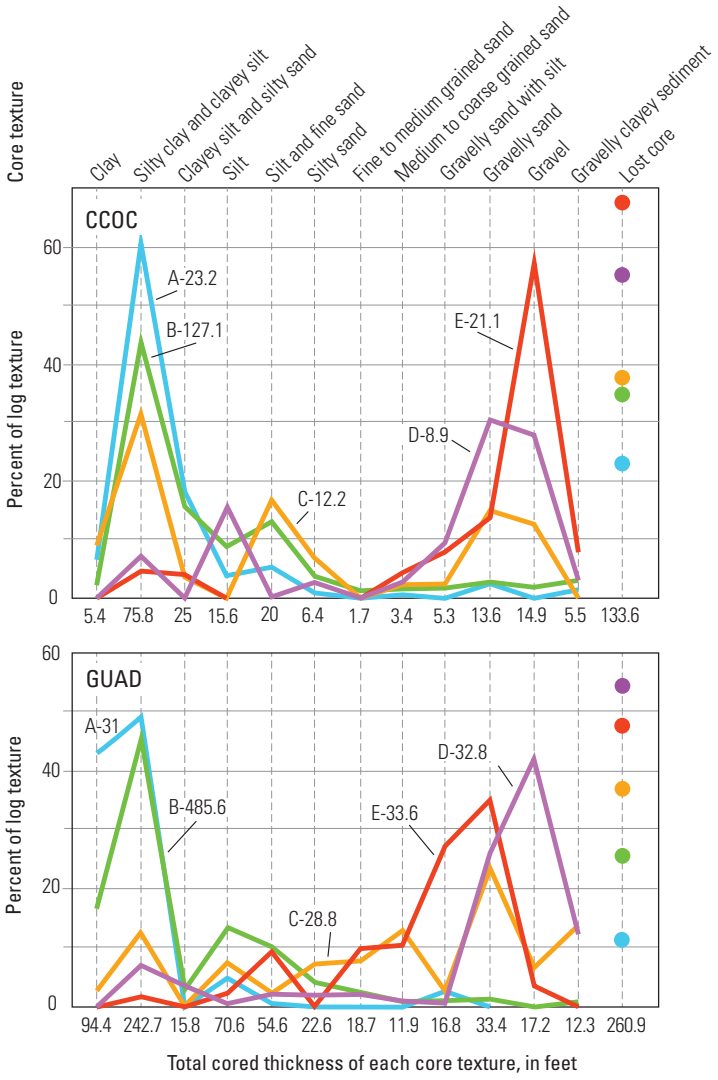

Figure 7. Chart showing intersected core textures within each log-texture category for wells CCOC and GUAD. The colored curves represent the range (X axis) and abundance (Y axis) of core textures that occur within each log texture (*A* through *E* of figure 5*A*). Labels for the curves indicate log texture (letter) and total thickness of that log texture cored (in feet). Dots at right indicate percentage of core lost (attempted but not recovered) within each log texture (dot colors match curve colors).

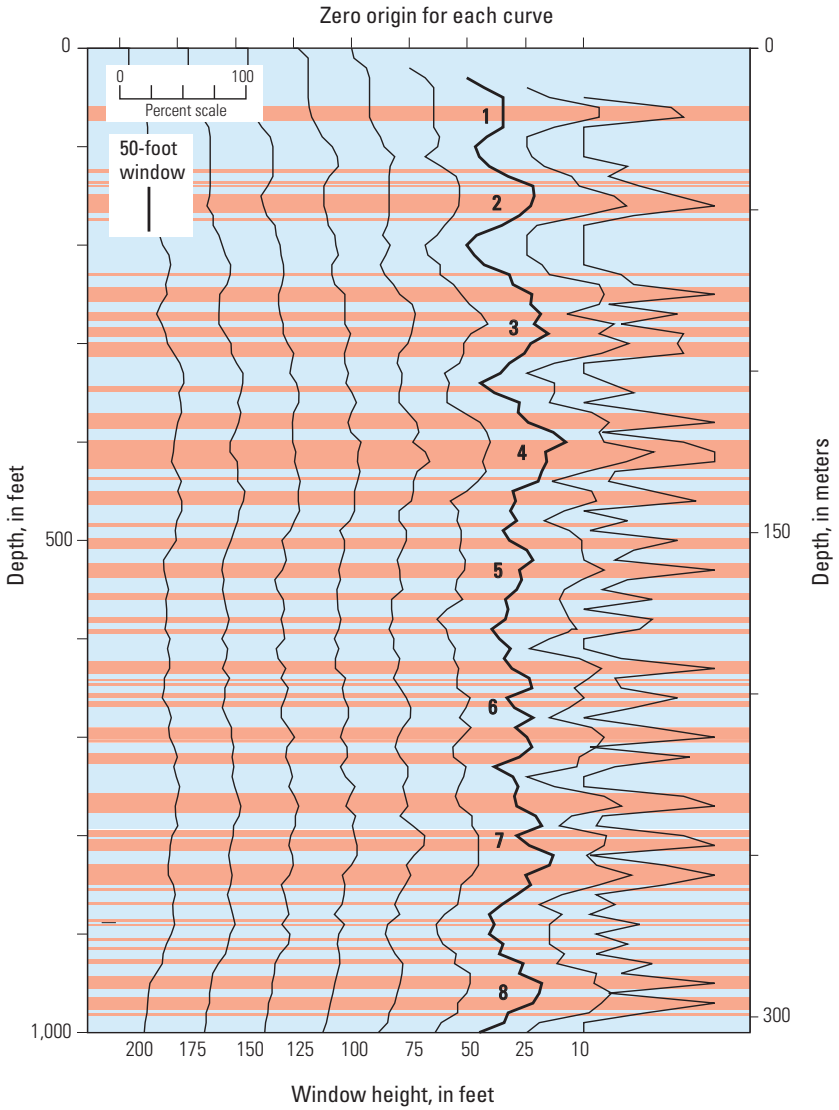

Figure 8. Vertical section for the Coyote Creek well (CCOC) with coarseness curves determined for a wide range of window heights. The scale shows the percent of coarse material separately for each curve, with its zero origin marked at top. Log textures for the well are simplified from the categories of figure 5 to either coarse (red) or fine (blue). Principal peaks in the 50-foot curve are numbered (compare with figure 9).

After the value of the coarseness curves was demonstrated in wells CCOC and GUAD (and later in WLLO), where they were calculated from the detailed layer interpretation of the geophysical logs, similar curves were calculated for most of the other geophysically logged wells directly from the resistivity logs. In this procedure, a varying base line was defined along minimum values (troughs) in the curve, and a threshold was defined part way up the typical peak amplitude. Resistivity values exceeding that threshold were considered to represent coarse intervals, the others fine. For the most part the shapes of the resulting coarseness curves were found to be relatively insensitive to the particular threshold chosen, except where small resistivity peaks representing thin coarse layers were present.

For the driller's logs, coarseness curves were calculated from the F-C values of table 2 using the weighting values as the measure of coarseness (F-C stands for Fine-Coarse). That is, instead of being either fine (0) or coarse (1) at each sample point (as is the case for the log textures based on the geophysical logs), here where the categories generally involve mixed textures, each F-C texture is assigned a degree of coarseness according to the associated weighting value (thus, 0, 0.2, 0.4, 0.7, or 1). For these logs, the step distance for moving the sampling window down the well was 10 ft. For a few wells, the coarseness curves were calculated by hand from the geophysical or driller's logs. Here, also, the longer (10 ft) step in window position was used.

Sedimentary Cycles

The sedimentary section traversed by well CCOC, the first drilled of the new wells, consisted of clay, silt, sand, and gravel, as expected, but the layered organization of those materials contained a regularity that was not expected. That regularity, clearly revealed by the coarseness curve for the well, posed questions that drove much of the remainder of this study.

The one feature that was expected, based on the pioneering work of Helley (1990), was an uppermost interval of unconsolidated sediment deposited during postglacial time. To test this, a CPT sounding was taken at the CCOC well site before drilling began. That sounding reached a depth of 122 feet and showed a fine-grained unconsolidated surface layer with a coarse base overlying a somewhat more consolidated section (fig. 5; Wentworth and Tinsley, 2005b). That contact was targeted in the coring program, and was found to consist of unconsolidated sand overlying a truncated soil developed in clayey silt and silty sand at a depth of 74 ft. Carbonaceous material collected from above and below that contact in CCOC and dated with carbon 14 brackets the contact between ages of 32.8 and 12.4 ka (see fig. 14*C*).

Peaks in the coarseness curve show that the coarse layers in CCOC are concentrated in eight limited intervals (figs. 5 and 8). The upper five (1–5) and the lowermost (8) peaks in the curve are relatively simple, whereas peaks 6 and 7, though still distinct, are more complex (see figure 9, where the curve and its features are most readily seen). Inspection of the layering in the context of the coarseness curve shows that each concentration of coarse layers is underlain by a distinct fine interval that is thicker than most of those within the overlying groups of coarse layers.

In this stratigraphic section, then, there are eight cycles, each consisting of a coarse bottom and fine top. These are not simply interlayered coarse and fine intervals, however, for the base of each cycle is marked by an abrupt coarse-over-fine contact (shown in green on fig. 9), whereas in most of the cycles the transition upward from coarse bottom to fine top is to some degree gradational. That is, the thickness and (or) abundance of coarse layers decreases upward from the coarse bottom to fine top of a cycle. Thus this 978-ft section in CCOC consists of a sequence of eight, upward-fining sedimentary cycles. Cycle thicknesses are all within a factor of two (93–188 ft), except for cycle 1, which is thinner (74 ft).

This is a remarkable pattern of organization of the section that, if characteristic of the Quaternary basin as a whole, would define a framework for characterizing the stratigraphic organization of the whole aquifer system. It would also have important geological implications. The possibility that this pattern applies to the whole basin was tested with the second well to be analyzed, GUAD, and that section showed the same organization.

The well GUAD was drilled to a greater depth than CCOC, but layering in the upper 1,000 feet or so of section shows the same cyclicity (figs. 5*B* and 9), despite the fact that this well is located 7.4 km downstream from CCOC and transects a finer grained section (22.8 percent coarse material, versus 37.3 percent in CCOC). The same concentrations of coarse layers occur in GUAD, and they compare well with those in CCOC, cycle by cycle. Note that in defining the cycles and cycle boundaries, the coarseness curve and layering details were used together. Peaks in the curve locate the concentrations of coarse layers, and the base of each cycle is then placed below the lowest prominent coarse layer overlying a prominent fine interval. The CPT sounding for GUAD (fig. 5*B*), like that for CCOC, shows an unconsolidated layer at the surface but was unable to penetrate its basal coarse interval. Although there is a general decrease in the number and thickness of coarse layers from CCOC to GUAD, the details of the two coarseness curves, peak by peak, show striking similarity (fig. 9). Dated carbonaceous material collected from above and below the base of cycle 1 in GUAD brackets that contact between ages of about 58 and 14.2 ka (see fig. 14*B*).

The implications of the similarity between these two wells are that the eight cycles are stratigraphically correlative between the two wells, that equivalent cycles represent the same deposition sequence, albeit considerably finer grained in GUAD, and that the coarse layers are, to the degree that they persist from CCOC to GUAD, the same layers.

This correlation between the two wells is quite rigorous. Eight fine-over-coarse cycles occur within the same depth range in each well. The shape of the peak in the coarseness curve for each cycle is similar to that of the equivalent in the other well and is largely different from those of the other peaks. The sequence of cycles is thus the same, compared cycle by cycle. The layering within each cycle can also be compared directly. In some, such as cycle 3, the fine top is relatively thick, whereas in others, such as cycle 4, it is less prominent. In some the upward fining is more evident than in others. And progressive lateral change is a guide. GUAD contains a finer grained section than CCOC, such that most coarse layers thin toward GUAD and some drop out. Finally, equivalent cycles occur at similar depths in the two wells, which is consistent with the indication from the seismic reflection profiles that the sedimentary layering is subparallel to the ground surface.

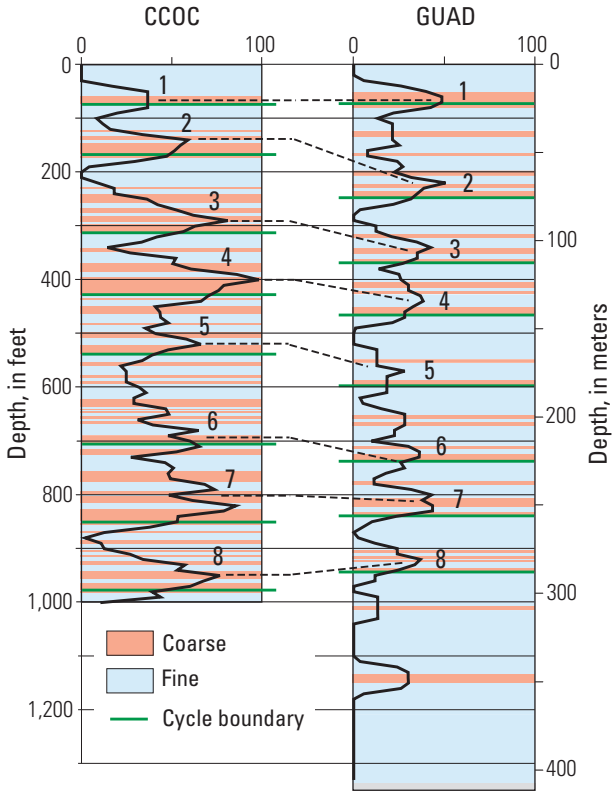

Figure 9. Vertical sections with coarseness curves for wells CCOC and GUAD. Equivalent peaks in the curves are correlated (dashed lines) and numbered. Log textures are simplified from the categories of figure 5 to either coarse (red) or fine (blue).

The evidence thus indicates that the layered sequences in wells CCOC and GUAD represent, in fact, the same stratigraphic section and contain the same eight upward-fining cycles within a thickness of about 1,000 feet. That conclusion, reached early in the investigation, led Wentworth and Tinsley (2005a) to correlate the cycles observed in CCOC and GUAD with the dated marine oxygen-isotope record, and that correlation permitted the ages of the cycles to be determined (see fig. 3). They attributed the sedimentary cyclicity to the variation in climate that has driven the Quaternary glacial cycles. The sharp base of each cycle should thus be marked by an unconformity, associated with a glacial low stand of sea-level and a low sediment supply, and be overlain by the coarse lower part of the next sediment cycle that formed as the climate warmed (Wentworth and Tinsley, 2005a; Wentworth and others, 2010).

The ages assigned to the cycles apply to their unconformable bases, and they indicate durations for cycles 2 through 8 of 88 to 122 k.y., with an average of 100 k.y. The length of cycle 1 is much shorter (18 k.y.), as the present glacial cycle is only about 20 percent complete.

Expanding the Correlation

With a set of eight correlative cycles demonstrated in wells CCOC and GUAD, the next test of whether this cyclicity is a basinwide characteristic was to examine the rest of the geophysically logged wells in the dataset. Those logs provide a far more accurate and detailed measure of the sedimentary sections transected by the wells than do the driller's logs, which are addressed later. Well HTOR is also reserved for later consideration, as it lies west of the Monte Vista frontal fault at the west side of the basin (fig. 2).

The layering in this second group of wells was examined in the context of the experience gained from working with wells CCOC and GUAD. It seemed unnecessary to distinguish all the log textures of table 3, but only to distinguish coarse from fine layers, as is done in figures 8 and 9. Log textures A and B are thus grouped together as fine, and textures C, D, and E as coarse. The coarseness curves for most of these wells were calculated directly from the resistivity logs. These coarseness curves are less sensitive to layering details than those determined from detailed layer interpretation, with the result that details of the curves that might help distinguish one cycle from another are muted. The resistivity logs alone were generally a sufficient guide to the layering. The natural gamma logs were important, however, particularly to confirm some coarse layers, refine boundary positions, and complete the uppermost parts of the wells where the resistivity logs are missing or uninterpretable.

Considerable emphasis in this analysis was placed on correlating the cycles directly from the coarseness curves. Other factors emphasized were the sequence of cycles down a well and correlation to similar depth. As almost all of the wells are more than 1 km apart, a depth difference as large as 100 ft for the same cycle boundary between wells seemed reasonable, although most correlations involved much smaller differences. Cycle 1 was identified using the pattern from CCOC and GUAD as a guide (a fine unconsolidated upper interval with a relatively thin, coarse base). Once the base for that cycle was determined, the bottom of the next deeper coarseness peak was taken to identify the base of cycle 2.

Within each cycle, lateral stratigraphic continuity of its layered sequence between adjacent wells was sought, as was sharp definition of cycle bases with prominent coarse layers overlying a thick, or especially fine-grained, fine interval. In this process it proved important to inspect the coarseness curves and the details of the geophysical logs together, in part because the coarseness curves based solely on the resistivity logs are more generalized than those prepared from the detailed log-texture interpretations.

The eight newly drilled wells (table 1), which have minimum spacings greater than 3 km, were correlated first, and the correlation was then extended from these wells into the others with geophysical logs. This produced a network of 21 correlated wells with most minimum spacings between adjacent wells ranging from about 1 to 5 km (fig. 10). Not only can the sequence of cycles be found in all these wells, with minor exceptions, but equivalent cycles in adjacent wells typically show similarity in the internal sequences of layering and the shapes of the coarseness curves. This is the case even in the initial, more widely spaced set of eight wells. Differences in the depth to correlated cycle boundaries between adjacent wells range from 0 to 70 ft, with most being less than about 40 ft. The network covers most of the basin, except for the area east of Coyote Hills (Niles cone) and east of the Silver Creek Fault.

The resultant correlations within this set of 21 wells are shown in the three well sections of figure 11. The northern well section (fig. 11*A*) runs northeast from well ELNR across the neck in San Francisco Bay at Dumbarton narrows to well B-11, and the sedimentary sequence here tends to be quite fine grained. It is so fine, in fact, that the bases of cycles 6 and 7 cannot be distinguished in well ELCM, nor can the base of cycle 2 in B-11. The central well section (fig. 11*B*) tends to become finer grained as it runs westward around the south edge of the bay from GUAD to MTNV. Along the southern section (fig. 11*C*), in contrast, the deposits become generally

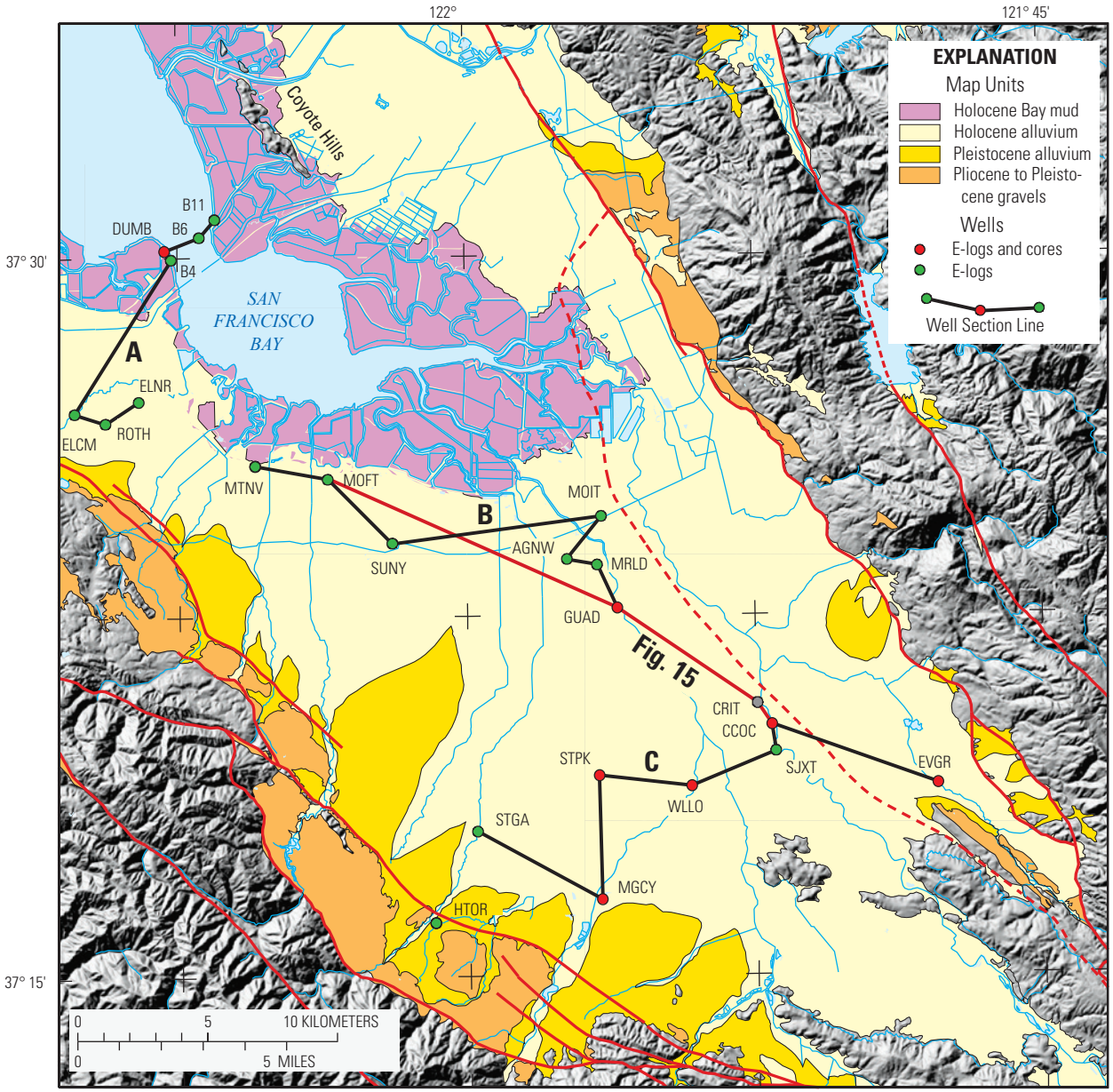

Figure 10. Map showing locations of the master well sections *A*, *B*, and *C* of figures 11*A*–*C* and 14*A*–*C* and of the stratigraphic section of figure 15 (red). Principal faults in red. Geology and shaded relief as for figure 2.

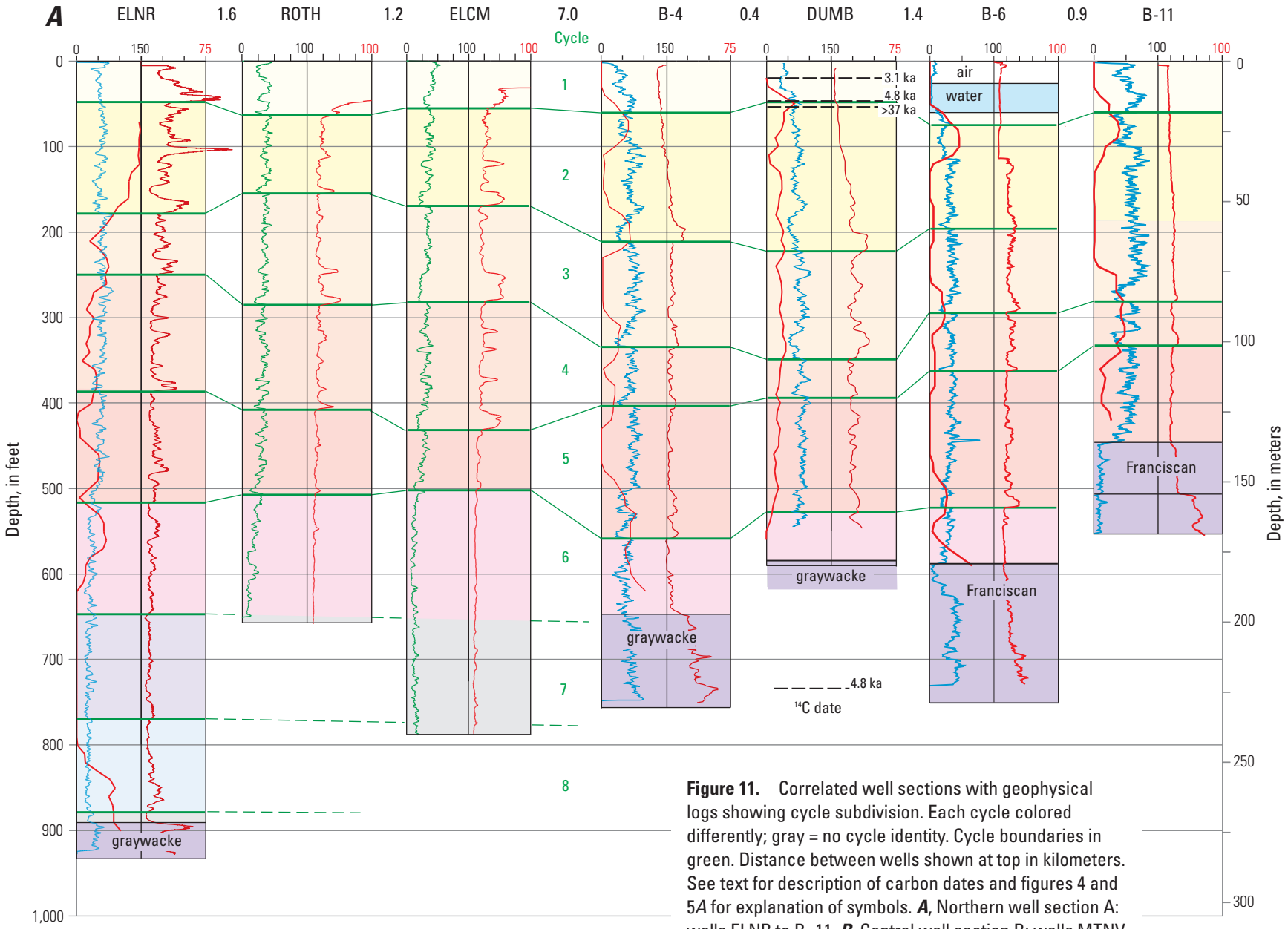

Figure 11. Correlated well sections with geophysical logs showing cycle subdivision. Each cycle colored differently; gray = no cycle identity. Cycle boundaries in green. Distance between wells shown at top in kilometers. See text for description of carbon dates and figures 4 and 5*A* for explanation of symbols. ***A***, Northern well section A: wells ELNR to B–11. ***B***, Central well section B: wells MTNV to GUAD. ***C***, Southern well section C: wells STGA to EVGR.

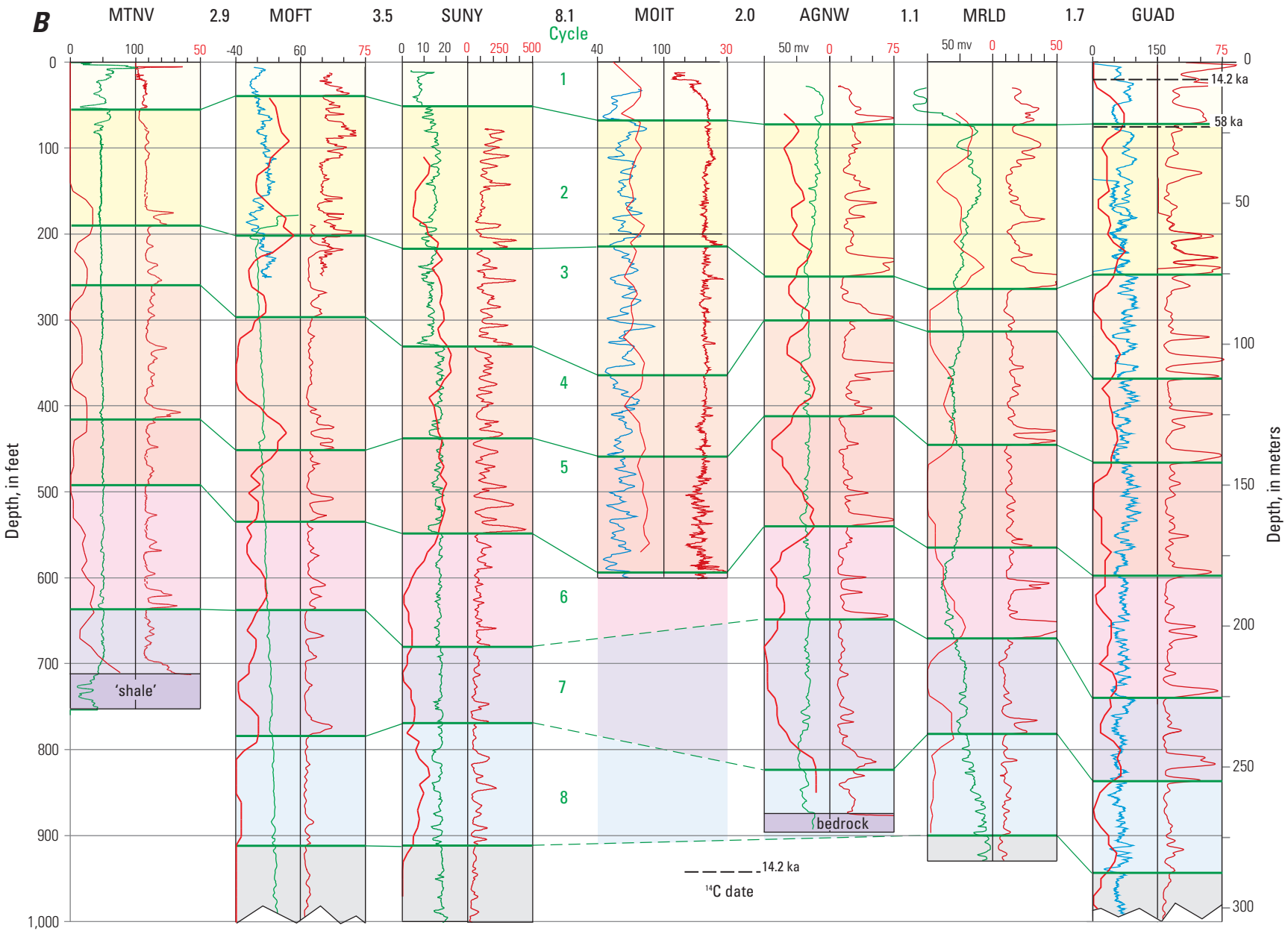
B
MTNV
2.9
MOFT
3.5
SUNY
8.1
MOIT
2.0
AGNW
1.1
MRLD
1.7
GUAD
Cycle
1
2
3
4
5
6
7
8
'shale'
bedrock
14.2 ka
14C date
14.2 ka
58 ka
Depth, in feet
Depth, in meters

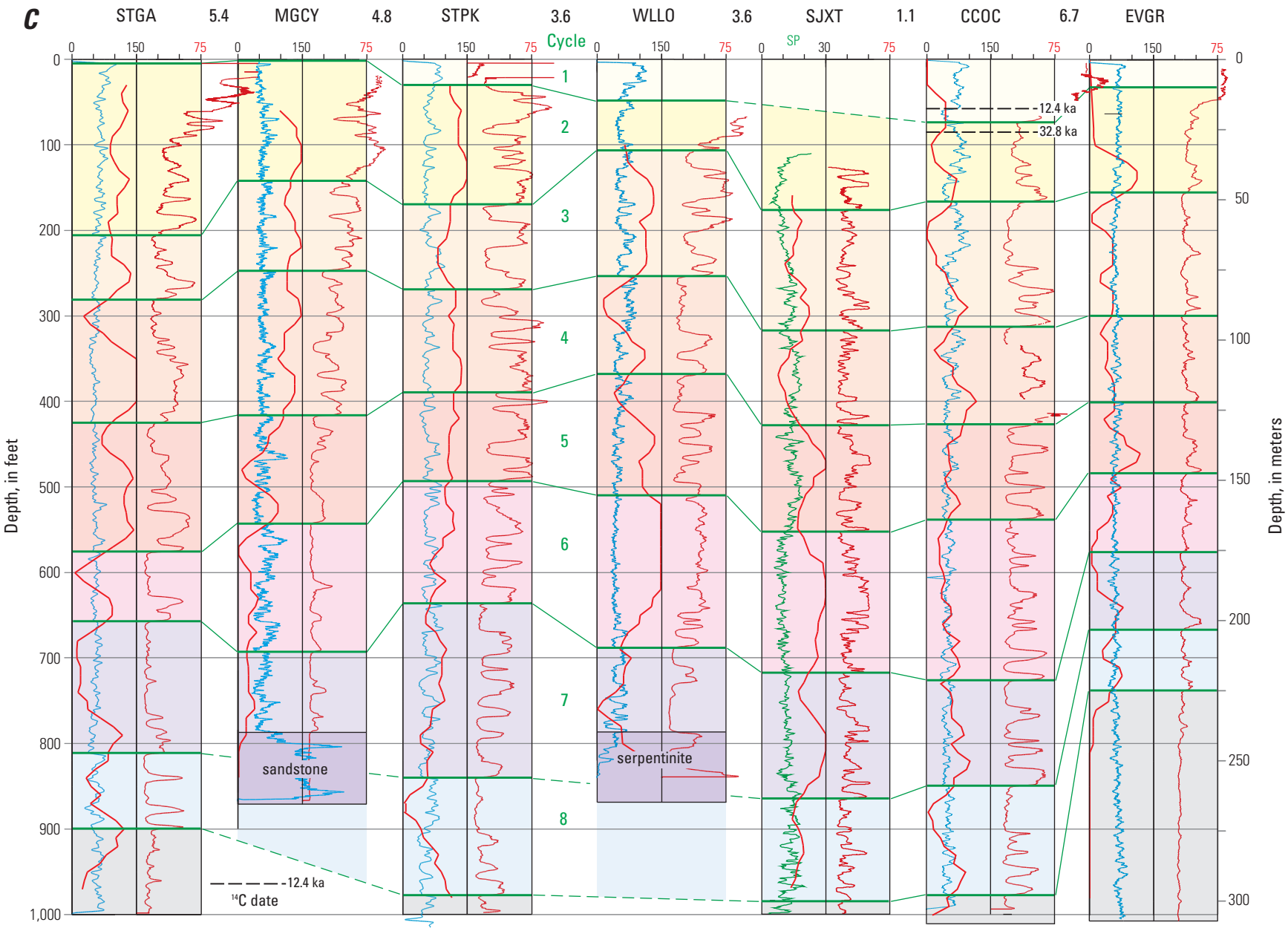
C
STGA 5.4
MGCY 4.8
STPK 3.6
WLLO 3.6
SJXT 1.1
CCOC 6.7
EVGR
Cycle
SP
0 150 75
0 30 75
1
2
3
4
5
6
7
8
12.4 ka
32.8 ka
sandstone
serpentinite
12.4 ka
14C date
Depth, in feet
Depth, in meters
0
100
200
300
400
500
600
700
800
900
1,000
50
150
250

coarser running from the drainage axis at well CCOC southwestward up the alluvial fan complex to STGA. The somewhat atypical well EVGR is added to that well section southeast of CCOC.

Inspection of the well sections of figure 11 indicates that, although equivalent cycles are similar in adjacent wells, the internal layering of the cycles tends to change progressively from well to well. Cycle thicknesses are variable, but generally change gradually, though some abrupt changes are evident. The pattern within a cycle typically involves a basal sequence of one to several coarse layers that persists with only limited change across the well section, supplemented above by other coarse layers that appear, disappear, divide, and merge progressively across the well section.

This set of correlations indicates that the Quaternary section throughout much of the Santa Clara Basin is, in fact, characterized by eight generally fining-upward sedimentary cycles, as originally suggested by interpretation of wells CCOC and GUAD (in effect, the discovery wells). There are ambiguities in places, and a few unidentifiable cycles in some wells, but a consistent set of cycles can be defined in all the geophysically logged wells in the dataset. This result involving the best data in the set indicates that the cyclic sequence is present throughout all of the basin sampled by the wells.

Cycle definition is least obvious in some of the relatively fine-grained well sections near the bay and in some of the largely coarse-grained well sections on the fan complex in the southern part of the basin. In the former, it can be difficult to distinguish a coarse cycle base, and in the latter it is the fine cycle top that can be difficult to define. The difficulty encountered in the northern fine-grained wells has already been noted. Of the coarser wells, WLLO is notable in the definition of the base of cycle 5. There, a contrast between borehole washouts above (log texture D) and very few, thin washouts below (log texture E) emphasizes the very thin fine-grained layer at which the base of the cycle is placed (figs. 14*C* and 18). In the coarser grained wells, also, any gradational change from coarse cycle bottom to fine top is least evident.

There are other departures from a simple sequence of eight upward-fining cycles. In some wells the lower part of the cyclic sequence is cut out by shallowing bedrock. At Dumbarton narrows, the base of cycle 2 is only barely evident in well B-6 and is not expressed at all in well B-11, although the other cycles above bedrock are all present in these two wells. The base of cycle 1 is not everywhere clear—high on the alluvial fans in STGA and MGCY, for example, because it is so thin that it is not resolved by the logs, and in SJXT because the logs start below the top of cycle 2. Well DUMB is different again, for no coarse base is present in cycle 1 and the underlying coarse interval belongs to cycle 2 according to the carbon dates (fig. 11*A*) reported by Bennett (1979).

Defining Cycle 1

The layering that defines cycle 1 is clearly evident in wells CCOC and GUAD, where the eightfold cyclicity of the upper Quaternary section was first discovered. There, the CPT soundings and cores indicate that cycle 1 consists of unconsolidated fine sediment with a relatively thin coarse base. We had initially intended (Graham and Wentworth, 2005) to extend identification of this uppermost layer across the basin using the pioneering work of Helley (1990) and several subsequent efforts to delineate the unconsolidated Holocene section in the Santa Clara Valley from geotechnical borings. This method proved unfeasible, however, as explained below.

The California Geological Survey was pursuing such work in support of its Seismic Hazard Zoning Program (Clahan and others, 2002; see also http://www.conservation.ca.gov/cgs/shzp/Pages/Index.aspx); C.S. Hitchcock and E.J. Helley of William Lettis and Associates were doing similar work under a grant from the National Earthquake Hazards Reduction Program of the U.S. Geological Survey (Hitchcock and Helley, 2003); and T. L. Holzer and associates were collecting new cone penetrometer data in the valley in order to delineate thickness and properties of the unconsolidated surficial deposits (Holzer and others, 2010; see also http://earthquake.usgs.gov/regional/nca/cpt). The position chosen for the base of the surficial unconsolidated interval in those studies, however, was generally shallower than the base of cycle 1 where it could be defined from good control, such as in CCOC.

This disparity seems to result largely from not all the basal coarse sediment of cycle 1 being considered unconsolidated in those studies. As a result, the correlation of the base of cycle 1 was determined from the logs in our primary dataset, guided by its expression and confident location in many of the geophysically logged wells. The CPT logs were also useful for some of the new wells. The resulting cycle 1 boundary lies almost everywhere below the base of unconsolidated sediment determined in those other studies (limited to south of San Francisco Bay), with depth differences largely less than about 25 ft but ranging up to local maxima of 40 to 56 ft.

The carbon 14 dates on carbonaceous material from above and below the base of cycle 1 in wells CCOC and GUAD (figs. 14*B* and 14*C*) demonstrate that cycle 1 represents the postglacial alluvial cycle (see figs. 3 and 15). The uncalibrated date of 14.35 ka reported by Meade (1967) on a piece of redwood from 73 feet in SJXT is consistent with this interpretation, thus placing the otherwise undetermined base of cycle 1 in that well at or somewhat below that sample depth.

Evidence from Velocity Logs

The cycles are also evident in continuous seismic velocity logs that were collected in five of the new wells (fig. 12). Velocity is a completely different property than is measured by the natural gamma and resistivity logs, but inspection of the figure indicates that the peaks and troughs in the velocity curves have patterns similar to those other logs. Wentworth and Tinsley (2005b) demonstrated that these velocity variations correlate

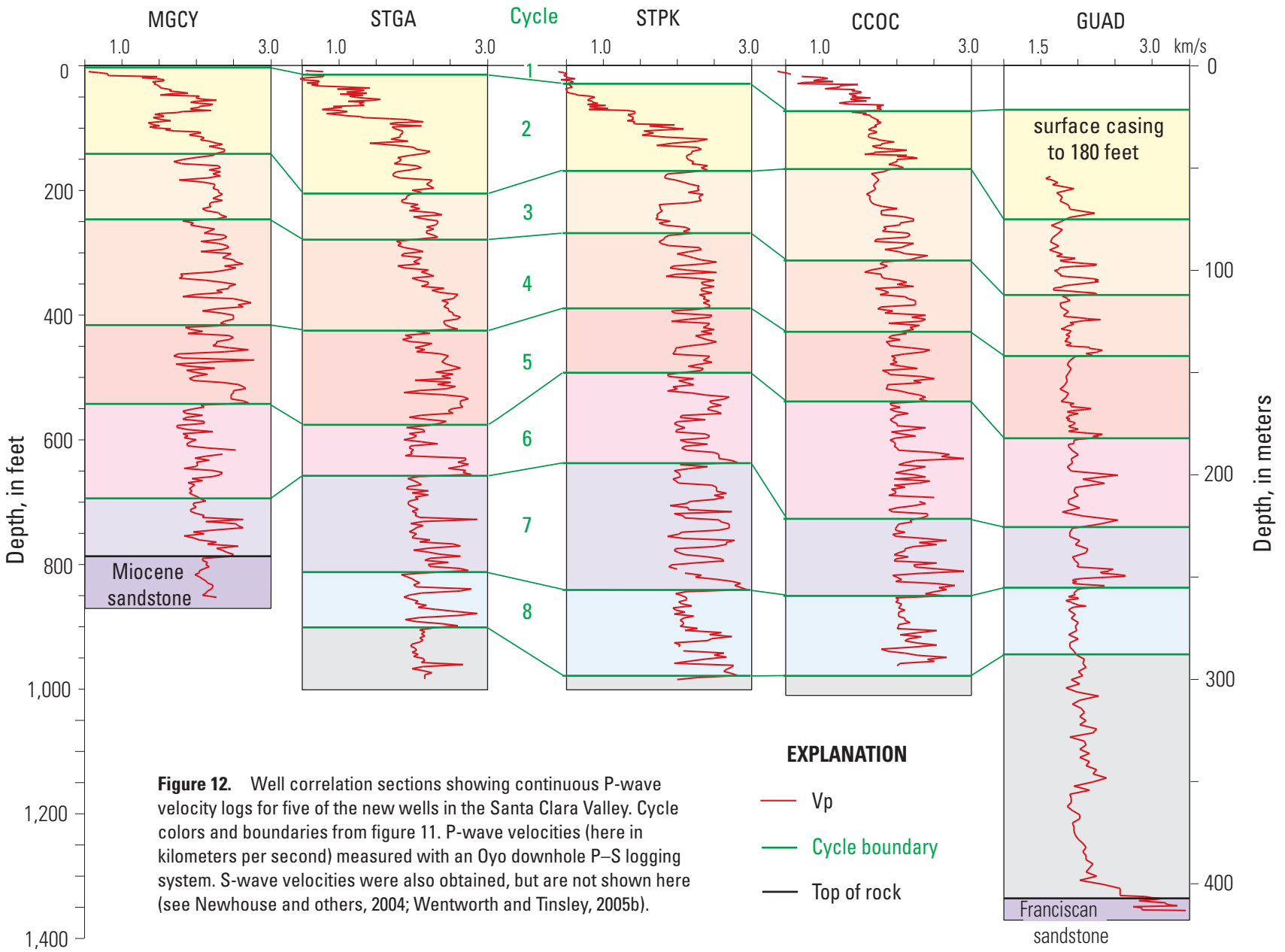

Figure 12. Well correlation sections showing continuous P-wave velocity logs for five of the new wells in the Santa Clara Valley. Cycle colors and boundaries from figure 11. P-wave velocities (here in kilometers per second) measured with an Oyo downhole P–S logging system. S-wave velocities were also obtained, but are not shown here (see Newhouse and others, 2004; Wentworth and Tinsley, 2005b).

closely with the layering determined from the natural gamma and resistivity logs. The velocity logs show the same coarse bottom-fine top pattern for the cycles, and comparison of equivalent cycles across the set of wells shows the same kinds of similarities and lateral changes as do the gamma and resistivity logs. These similarities within equivalent cycles are especially impressive here because of the large spacing between the five wells (5.1 to 7.4 km).

Confirmation from Paleomagnetic Analysis

If each of the eight cycles represents sediment accumulated during a particular glacial cycle, then each cycle represents a distinct interval of time. The cycle boundaries are thus approximate time lines (or surfaces), the ages of which were estimated through correlation with the marine oxygen isotope curve, as previously described. Although no fossils or tephra (volcanic ash) were found to provide independent age control that might confirm the cycle correlations, paleomagnetic study of cores from the new wells does just that (Mankinen and Wentworth, 2004; E.A. Mankinen, written commun., 2008).

A polarity reversal correlated with the Brunhes/Matuyama boundary at 780 ka was discovered just below the 718-ka bottom of cycle 8 in well CCOC. That result was considered when the cycles were correlated with the marine record by Wentworth and Tinsley (2005a) and found to be consistent with the correlated age of the base of cycle 8. Later discovery of that reversal in similar positions in wells GUAD and STPK further supports that consistency. Similarly, a magnetic excursion correlated with the Big Lost excursion at 565 ka was found just below the 536-ka base of cycle 6 in four wells (GUAD, CCOC, STPK, and MGCY).

The bases of cycles 6 and 8 are thus independently confirmed to be approximate time surfaces, and their ages determined from the marine oxygen isotope record are stratigraphically consistent with the associated paleomagnetic events. And these facts, in turn, support the eightfold subdivision of the cyclic section, because a different number of cycles would change the correlation with the marine oxygen isotope record and thus break those age consistencies.

The 32-ka Mono Lake paleomagnetic excursion was also found just below the base of cycle 1 in several wells, including CCOC (Mankinen and Wentworth, 2004), although that relation does not provide constraint on the deeper cycles as do the Big Lost excursion and Brunhes/Matuyama boundaries.

Mapping the Cycles

The correlations between the wells with geophysical logs in figure 11 formed a confident framework across much of the basin from which the cycles could then be interpolated and extrapolated into the more densely and widely distributed wells with driller's logs. The goal was to obtain sufficient control to map the cycle boundaries throughout the basin. This was a less confident process than the correlation between geophysical logs, but the driller's logs proved very useful.

Those logs are based on visual inspection by the driller of cuttings collected during drilling of the well. But even the careful sampling and textural descriptions of cuttings from the new USGS-drilled wells produced relatively poor representations of the layered sequences in those wells, as previously noted, and the initial expectation was that the driller's logs would not be accurate or detailed enough to be of much use. This expectation proved wrong, though not all cycles were evident in all the driller's logs, and in many wells no pick was possible for particular cycles. Figure 4 illustrates the wide variation in detail in the driller's logs, ranging from that of well 760, for example, where the detail approaches that of a resistivity curve, to that of well 761, which shows very little detail in either layering or grain size. The quality of the driller's descriptions certainly depends on the skill and attention of the observer, but also on factors that can distort the representativeness of the cuttings sampled. These include selective destruction of fine or coarse sediment by the drill bit, time lag and sorting of cuttings during their transport up the well in the drilling fluid, and selective survival of cuttings extracted from the mud. In some driller's descriptions it would seem that one observed texture may be given unwarranted emphasis; in many it can be inferred that a described interval actually consists of layers of both coarse and fine material.

Interpretation of the driller's logs here uses the relative changes in coarseness evident in the numeric curves, which are based on the textural categories of Leighton and others (1995). The original driller's descriptions were generally not consulted except in some cases to confirm bedrock. As with the geophysical logs, the process involved working laterally, comparing adjacent wells, and correlating to similar depths. In contrast to the geophysical logs, however, the limited detail of many of the driller's logs made it impossible to find an equivalent for every cycle. Some of the picks of cycle boundaries in the driller's logs are far from unique or really confident, but those chosen are reasonable. Depth differences required to find correlative intervals between wells were typically similar to those encountered in the earlier correlations between wells with geophysical logs, but some are considerably larger.

The detail with which the coarse and fine textures are distinguished in the driller's logs correlates with the success in identifying the sedimentary cycles. For those wells, or large sections of wells, where the logs are relatively detailed (nearly half the set of 105 wells), cycle identification is nearly complete, whereas in the others it is far less so. Difficulties in cycle identification arise particularly where the textures are reported to be nearly constant for

considerable lengths in the well, either fine or coarse, and reported contrasting textures are only thin and (or) rare over such long constant intervals. Numerous cycle boundaries were picked in these less detailed logs, albeit with lowered confidence—in many cases on only thin coarser or finer intervals or small steps in relative coarseness.

Identification of cycle 1 from the driller's logs was particularly difficult, because in many of the wells the shallow detail is insufficient. Here, the work proceeded outward from geophysically logged wells in which the cycle was clear, looking for similar patterns and depths. In many of the wells the log detail was insufficient, and in others the absence of lateral similarity prevented confident correlation. In some parts of the basin, cycle 1 is too thin to be resolved by the logs, and it is completely absent where the alluvium at the surface is late Pleistocene (fig. 2). A further complication is that the uppermost part of cycle 2 may be coarse, as is the case in DUMB (Bennett, 1979). That issue is discussed below.

Addition of wells with driller's logs to the correlated network of wells fills many holes in the coverage, carries the correlations northwest from well MGCY along the western margin of the basin to ELNR, and extends the correlations eastward across the Silver Creek fault and beyond the Coyote Hills onto the Niles alluvial cone. The whole suite of 126 correlated wells, both those with geophysical logs and those with driller's logs, is shown in figures B3-B21 (appendix B; see fig. 20 for HTOR), with the well section lines shown on the map of figure B1. (Note that in these well sections the cycles are divided into a coarse bottom and fine top, as discussed below.) The section lines of figure B1 define a network of closed loops, and a severe test of the success of the correlations is whether, along any and all routes through that network, the cycles match at their junctions. That proved to be the case, for all the circuits do close properly, despite difficulty in interpreting many of the less detailed driller's logs.

Correlation Across Faults

The only fault within the basin that may affect the cyclic section is the Silver Creek Fault (fig. 2), which is described by Wentworth and others (2010) as a large strike-slip fault that almost ceased moving before deposition of the cyclic sedimentary section (see section on "Faults Within the Basin" below, for further discussion). The Evergreen seismic reflection profile (fig. 13; location shown on fig. 2), which imaged the layered sedimentary section across the eastern part of the basin, shows that the effect of the Silver Creek Fault within the cyclic section is quite limited. The layering of the cycles can easily be traced across the length of the profile, which raises the possibility that this profile might be used to extend the cycle correlations east of the fault, where well control is sparse.

To test that possibility, the locations of the cycle boundaries in the reflection profile were determined by projecting the coarseness curve and cycle boundaries for well CCOC northwestward parallel to the Silver Creek Fault to the seismic profile (fig. 13). The correlation between coarseness peaks for CCOC and the reflections is clear. From there, the positions of the cycle boundaries can be readily carried eastward across the profile to the east edge of the basin. Cycle boundaries and coarseness curves for wells 710 and 702, located along the profile to the east, correlate with the same reflections, thus indicating lateral persistence of the close relation between the cycles and the reflections. This gives confidence that the reflections are responding to the layering that defines the cycles, and in the process provides further evidence that the cycles are laterally continuous. The depths of cycle boundaries in the reflection profile were thus picked at several recording stations, as shown in figure 13, and these control points are used to supplement control from the few nearby wells.

Faults near the margins of the basin do affect the Quaternary section (see section on "Faults Within the Basin" below), but not all to the extent that the cycle boundaries can't be mapped across them. The Quaternary section extends west of the Monte Vista Fault system near the west side of the basin only locally, and the cycle boundaries are not extended across it. As discussed below, the section there has been offset by hundreds of feet. In the northeastern part of the study area, the cycle boundary mapping is locally extended across the southern Hayward Fault, although the mapped gradual elevation changes in the boundaries there might better be assigned as abrupt offsets at the fault itself. In the southeast, uplift above an underlying thrust at well EVGR does not seem to involve discrete fault offset of the cyclic section.

Gridding the Cycle Boundaries

Once the cycle boundaries were correlated through the whole primary well dataset, those correlations could be used to define continuous surfaces. The depths of the cycle boundaries in the wells were converted to elevations, the elevations for each boundary were gridded by computer to produce a continuous surface, and that surface was contoured (the procedure is described in appendix C). Each of these surfaces was once a topographic surface, and the results of the gridding were tested against that standard. Correlations that produced local depressions in a surface were thus suspect. Although the real surfaces may actually be irregular in detail, the control is not dense enough to delineate such local relief. These anomalous correlations could be correct, but their influence in the gridding distorts the surfaces far beyond their immediate vicinity. Relatively smooth surfaces were thus sought, and those correlations that caused local depressions or other severe anomalies in the surfaces were rejected. The final surfaces are relatively smooth and simple (plate 1), even where the differences in depths between nearby wells are fairly large.

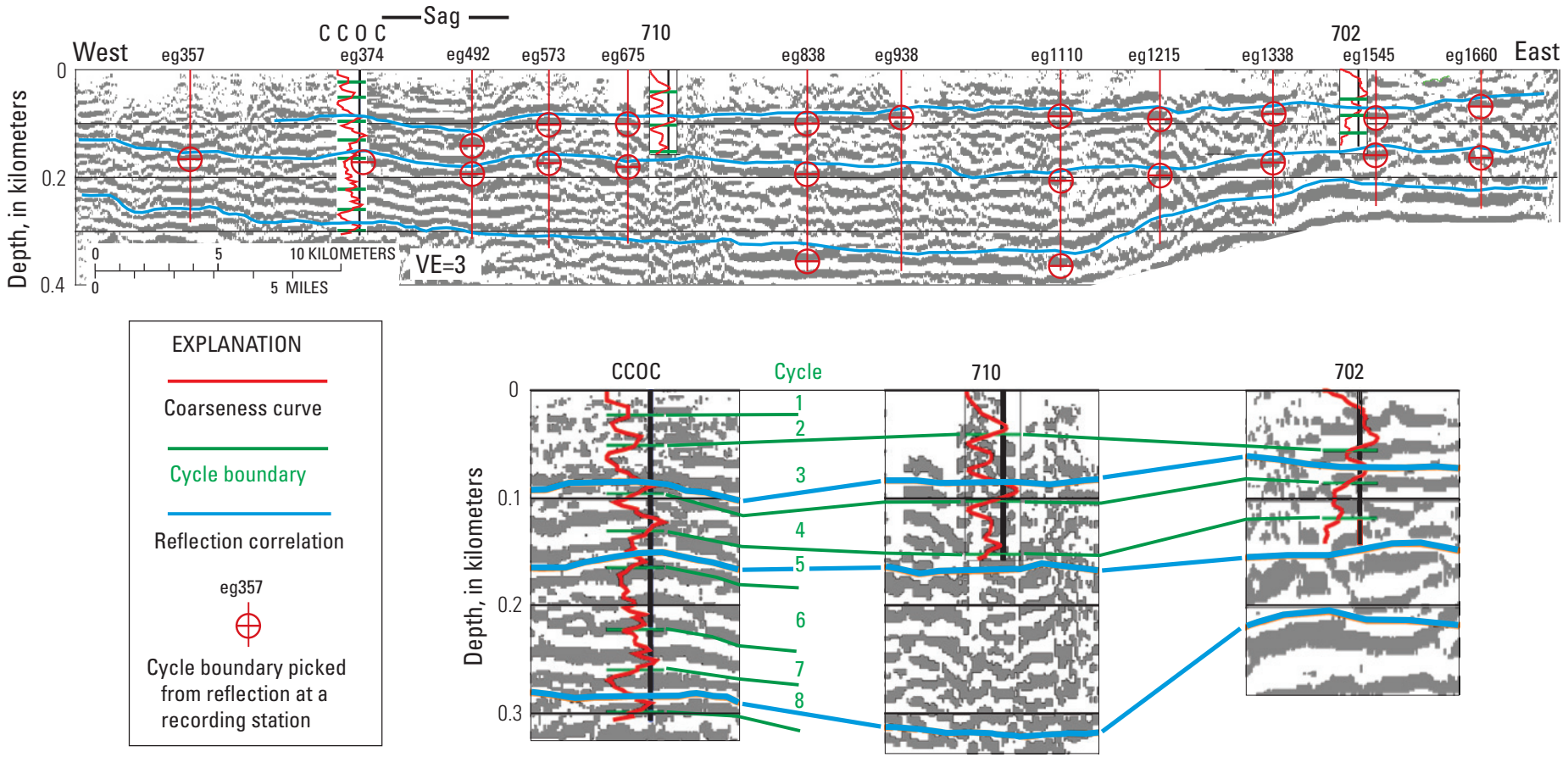

Figure 13. Upper part of the Evergreen seismic reflection profile (to a depth of about 400 meters), showing (1) correlations along selected reflections, (2) wells CCOC, 710, and 702 projected to the reflection profile line (with coarseness curves and cycle boundaries), (3) enlargements of those three wells to illustrate the parallelism of the reflections with the cycle boundaries, (4) the locations (and recording stations) where cycle boundaries were picked and depths determined, and (5) location of the structural sag above the Silver Creek Fault near well CCOC (see Wentworth and others, 2010). See figure 2 for location of the reflection profile (EG).

The locations of the rejected correlations are shown on the maps of plate 2 (row A) and in the well diagrams of figures B3 to B21, where they are distinguished by dashed symbol from those actually used in the final gridding of the surfaces. Only a few correlations per cycle were rejected (appendix C, table C1), ranging from zero (cycles 1 and 8) to eight (cycle 5). None of the rejects are in wells with geophysical logs, and most are in driller's logs that have relatively poor detail.

The cycle boundaries slope inward toward the center of the basin and thence, for the shallower boundaries, northwestward toward the bay, in a fashion similar to the present topographic surface (fig. 2 and plate 1) and in accord with their general parallelism with that surface. The deeper surfaces, however, are at least partially terminated to the northwest by the buried bedrock ridge that extends from well DUMB across Dumbarton narrows and Coyote Hills to wells 204 and 210. The crest of that ridge seems deepest east of Coyote Hills, where it lies just below the base of cycle 6 (see fig. 17 and plate 1, map 11). The truncation of the cycles by the buried bedrock surface (see section on "Bottom of the Basin" below) as it rises northward toward Coyote Hills and southward toward Oak hill is shown on plate 1 by areas of bedrock subcrop (see section on "Subcrop Areas" below).

The modern surface subsidence and underlying compaction in the Santa Clara Valley documented by Poland (1971) and Poland and Ireland (1988) must have deformed these cycle boundaries to some extent. The effect on the shapes of the surfaces is small, however, particularly for the deeper cycle boundaries. The surface subsidence increased inward from the valley margins and southward from Coyote Hills to a maximum near the subsidence center in San Jose. There the measured surface subsidence for the period 1916–1969 (at benchmark P7) was 12.88 feet (see Poland and Ireland, 1988, fig. 21). The aquiclude compaction that produced the subsidence occurred at depths between 200 and 1,000 ft, but cannot be assigned a more specific depth with available data.

Subdividing the Cycles

The basic fining-upward character of the sedimentary cycles offered the possibility that the cycles could be divided into a coarse bottom and fine top and those divisions mapped around the basin. In making this subdivision, the internal boundary between the divisions was placed at the top of the uppermost principal coarse layer, such that fine layers were generally subordinate to coarse below the boundary and coarse subordinate to fine above it. In doing this, a guiding principal was to maintain lateral stratigraphic continuity between wells to the extent possible.

Each top and bottom subdivision was then characterized by (1) the abundance of coarse layers (aggregate coarse thickness, percent coarse material), (2) the thickness of the thickest resolvable fine layer, and (3) the number of resolvable layers. Note that the number of layers evident depends greatly on the type of log, with more layers evident in a geophysical than a driller's log for an equivalent sedimentary interval. The data are tabulated in data file subdivs.xls (see appendix E). This characterization was done, where the data permitted, for each fine top and coarse bottom for which the adjacent cycle boundary (above the fine top or below the coarse bottom) was used in the final gridding. The resultant top/bottom boundaries are shown in the well sections of figures 14 and B3 to B21 and in the cross sections of figure 17.

An anomalous departure from this generally fining-upward pattern within the cycles occurs in the top of cycle 2. In the original cycle analysis of the wells, the base of cycle 1 was selected in the context of its definition and location in many of the geophysically logged wells and without placing much weight on the coarseness curves, which are generally not well defined at such shallow depths. As it turned out, this left a remainder of coarse layers near the top of cycle 2 in some wells. Although not initially evident in the discovery wells CCOC and GUAD, an upper coarse interval in cycle 2 is prominent and unavoidable in the interpretation of the Dumbarton well (DUMB; figs. 11 and 14). Carbon 14 dates[4] from that well (Bennett, 1979) demonstrate that there, at the margin of the bay, cycle 1 has no coarse base and the top of cycle 2 consists of a 41-foot-thick coarse layer. Without those dates, that layer might well have been considered a locally thick coarse interval at the base of cycle 1.

This upper cycle-2 interval at well DUMB forms the bulk of the Newark aquifer, which extends eastward beneath the bay and up the Niles alluvial cone (Wentworth and others, 2010; see also fig. 17, section FG, and fig. B-21), an area where we have no independent control on thickness of an unconsolidated surface layer. Inspection of the other wells with geophysical logs (fig. 14) shows that an upper coarse interval in cycle 2 can be distinguished throughout the basin if it is allowed to contain fine layers above a coarse base, although it is generally not discriminated by the coarseness curves. Weakly expressed coarse bases to an upper cycle 2 interval can, in fact, be defined from a single coarse layer in GUAD and a thin coarse peak in the CPT log of CCOC, and a prominent coarse interval in the appropriate position is evident in the intervening water well CRIT (fig. B-3). Prominent coarse tops in cycle 2 can be distinguished in wells on the alluvial fans to the west, most clearly in STGA and least so in WLLO. Thus, driven by the evidence from DUMB, cycle 2 was subdivided into a lower coarse interval, a central fine interval, and an upper coarse interval (cycle 2a), but otherwise the same conventions and descriptive elements were used as for the other cycles. This coarse top to cycle 2 is somewhat forced in some wells (including GUAD and CCOC) and is not as confidently defined as the cycles themselves. Similar coarse tops are not evident in the other cycles.

[4] Bennett (1979) reports uncalibrated ^{14}C dates on oysters from the middle and base of cycle 1 in well DUMB of about 3 and 5 ka, respectively, and one greater than 37 ka on a piece of wood from near the top of cycle 2 (see DUMB in fig. 14*A*).

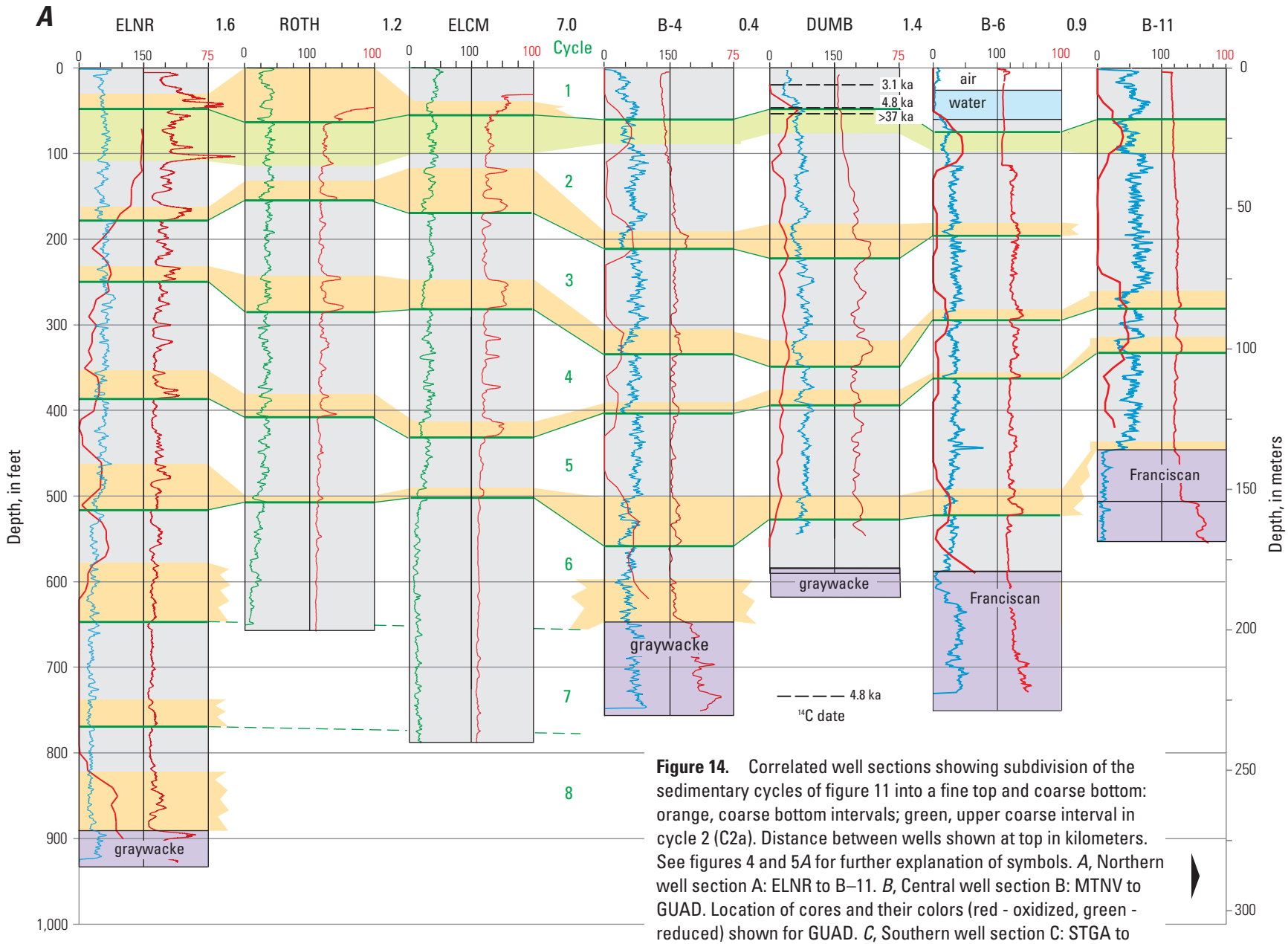

Figure 14. Correlated well sections showing subdivision of the sedimentary cycles of figure 11 into a fine top and coarse bottom: orange, coarse bottom intervals; green, upper coarse interval in cycle 2 (C2a). Distance between wells shown at top in kilometers. See figures 4 and 5*A* for further explanation of symbols. *A*, Northern well section A: ELNR to B–11. *B*, Central well section B: MTNV to GUAD. Location of cores and their colors (red - oxidized, green - reduced) shown for GUAD. *C*, Southern well section C: STGA to EVGR. Location of cores (black) shown for those wells with cores.

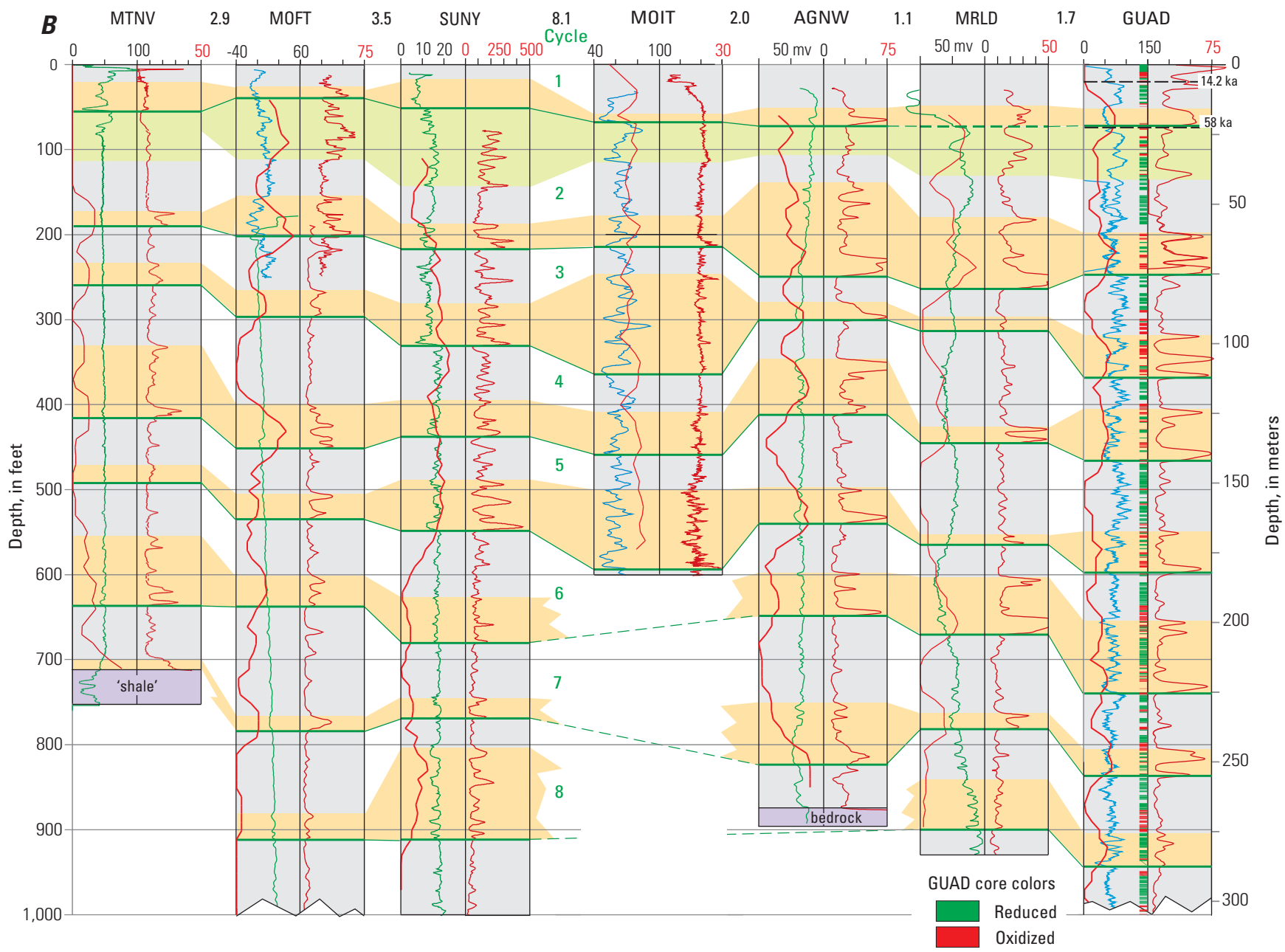
B
MTNV
2.9
MOFT
3.5
SUNY
8.1
MOIT
2.0
AGNW
1.1
MRLD
1.7
GUAD
Cycle
1
2
3
4
5
6
7
8
'shale'
bedrock
14.2 ka
58 ka
Depth, in feet
Depth, in meters
GUAD core colors
Reduced
Oxidized

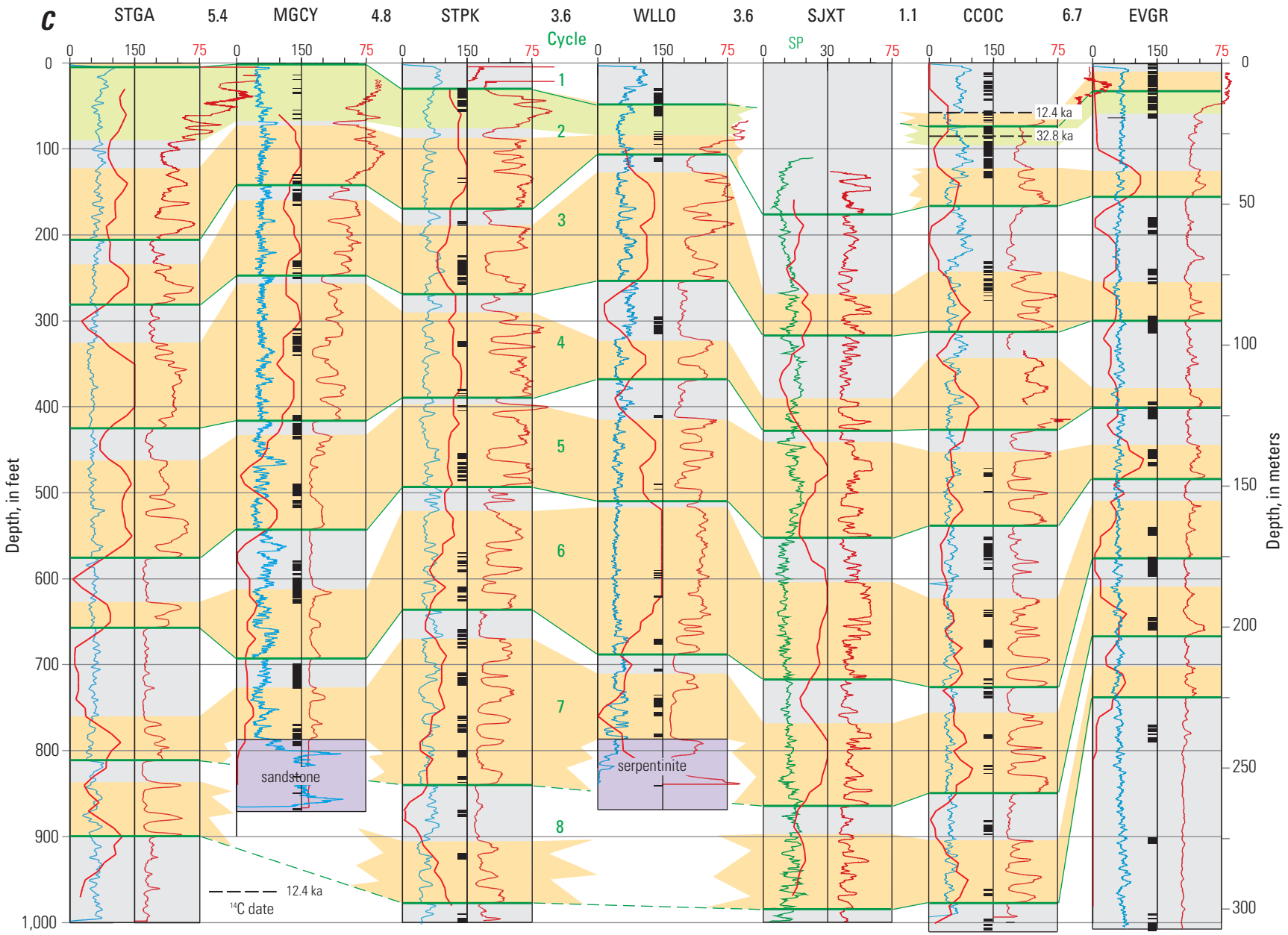
c
STGA
5.4
MGCY
4.8
STPK
3.6
WLLO
3.6
SJXT
1.1
CCOC
6.7
EVGR
Cycle
SP
0
150
75
30
1
2
3
4
5
6
7
8
12.4 ka
32.8 ka
sandstone
serpentinite
12.4 ka
14C date
Depth, in feet
Depth, in meters
0
100
200
300
400
500
600
700
800
900
1,000
50
150
250

Bottom of the Basin

The bottom of the Quaternary sedimentary section is an unconformity eroded across bedrock of Franciscan Complex and related rocks and the marine Miocene fill of the Cupertino Basin, which is buried beneath the western part of the Quaternary basin (Stanley and others, 2002; Wentworth and others, 2010). East of the Silver Creek Fault, the Quaternary section overlies the poorly known late Cenozoic fill of the Evergreen Basin, where its basal unconformity is offset 650 ft down into the basin across that fault (Wentworth and others, 2010).

Control on the position of the buried bedrock surface (plate 1, map 11) is provided both by wells that bottom in rock and those that do not but are deep enough to constrain the surface. Other control is provided by the seismic reflection profiles by Williams and others (2002, 2004, 2005), refraction profiles by Hazelwood (1974, 1976), and the elevation of mapped depositional contacts of alluvium on bedrock.

The wells that reach bedrock consist of 26 in our primary dataset and 19 others (including those shown by Hazelwood). Brief summaries of reported rock types encountered in the bottom of these holes (other than the Hazelwood wells) are reported in digital data layer bdrk (and see appendix C section on "Bedrock Surface"). Seismic reflections from the basement surface in the Guadalupe and Evergreen seismic profiles are relatively clear. In the Cupertino profile, however, selection of where to pick the bedrock was guided by elevations of rock in nearby wells (–650 to –750 ft), which match a change in the character of reflections in the Cupertino profile. An additional source of control in the northern part of the study area is the suite of refraction profiles collected in the 1970's by Hazelwood around the south end of San Francisco Bay (Hazelwood, 1974, 1976; see also Wentworth and others, 2010). These different sources are distinguished by symbol on the bedrock surface map of plate 1 (map 11).

All the direct control was used to grid the bedrock surface by computer, in the same fashion used for the sedimentary cycle boundaries (see appendix C). Inspection of that initial gridded surface in the context of all the wells in the primary dataset identified several wells that are intersected by that surface but do not reach rock. The surface must be made to pass beneath those wells. To accomplish this, elevations just below the bottoms of 19 wells were added to force the final gridded surface down (points shown as "well, no rock" on plate 1, map 11). Remaining artifacts in the surface around the north side of Oak hill were constrained by the addition of two constructed elevation points (plate 1, map 11).

The resulting bedrock surface slopes inward toward the center of the basin and eastward toward the Silver Creek Fault and the Evergreen Basin beyond it. More specifically, the surface daylights around the south side of the basin, lies at elevations of –400 to –800 feet along the Monte Vista Fault system at the western margin of the basin, and to the north extends along a bedrock ridge that runs eastward across the Dumbarton narrows. There, it is as deep as –600 feet at Dumbarton narrows, daylights at Coyote Hills, and then drops to about –700 feet to the east beneath the Niles alluvial cone. That elevation for the bedrock surface east of Coyote Hills, which is based on wells, is consistent with the surface defined by inversion of gravity with control from wells that is reported by Wentworth and others (2010), although the latter indicates that beyond the well control the surface rises eastward. From all those outer shallow boundaries, the bedrock surface slopes down inward and is deepest at the edge of the Evergreen Basin, where its elevation is lower than –1,445 feet at well CRIT. The deepest well control runs east and southeastward from well 819 toward that basin, passing through MOFT and GUAD and beneath CRIT, with well 819 lying in a closed depression defined by well MTNV (see below).

The deep embayment produced by forcing the surface to pass beneath well STGA raises the possibility that STGA actually bottoms in Miocene rock of the Cupertino Basin. No core was obtained from STGA, but no bedrock was recognized from cuttings by the geologist at the well during drilling, and there is no indication in the geophysical logs that the bottom of the well is different, as there is in MGCY where it bottoms in Miocene sandstone and siltstone. The eight alluvial cycles can be defined in STGA and correlated eastward to MGCY and STPK without problem. Cuttings from STGA described by a geologist (Newhouse and others, 2004) indicate abundant gravel in the lower part of the well, which would be anomalous for marine Miocene rock. The bedrock surface is thus placed below the bottom of STGA, and also below well 947, the other well that controls the embayment. That well is not reported to bottom in rock, and the fact that the details of cycle 8 in well 947 match those in STGA gives added confidence to the conclusion.

The bedrock surface thus defined can be divided into two principal topographic elements. The wells and Cupertino reflection line define a shallow surface of low relief located at the west side of the basin at an elevation of about –600 to –700 ft that can be correlated with the bedrock lows on either side of the Coyote Hills. That relatively simple surface is dissected by a rougher, more deeply eroded surface that drains eastward to the edge of the Evergreen Basin. The roughness of this second surface is best defined by the bedrock reflection in the Guadalupe reflection line, which has a local relief of almost 750 ft and a drainage spacing of about 2½ km (see plate 1, inset profile on map 11). The "string of beads" appearance to the contoured surface along that reflection line results from the lack of similar density of elevation data in the surrounding area. The depressions at wells 819 and MOFT are probably artifacts of the generally sparse control. Given the drainage spacing indicated by the Guadalupe profile, there is more than enough room for drainage lines to run across the bounding ridges in areas of no control. The ridge west of GUAD may also be such an artifact.

The alignment of the east-facing step in the bedrock surface along the Cupertino reflection profile with the frontal fault mapped to the northwest is simply coincidence, as continuous subhorizontal reflections in the reflection record do not permit a dip-slip fault here.

Subcrop Areas

The inward slope of the bedrock surface along the northern, western, and southern margins of the Quaternary basin requires that the extent of bedrock exposed at the base of each sedimentary cycle increases downward from the present topographic surface. These buried bedrock areas—subcrop areas beneath each overlying sedimentary cycle—are shown in the maps of plates 1 and 2 (light green areas). They were determined by intersection of the bedrock surface with the basal surface of each cycle (or the base of the upper fine interval for cycle 8 in map 18, plate 2) and locally simplified and better fitted to the well control. Although the maps seem to imply that the whole cycle terminates abruptly at the subcrop boundary, that termination is actually gradual across the subcrop width between the base and top of a cycle, as is evident in the cross sections of figure 17.

Stratigraphy

The Quaternary section overlying the basal bedrock surface in the Santa Clara Valley consists, where most complete, of an upper cyclically layered sequence almost 1,000 ft thick and a lower finer grained sequence as thick as 500 ft or more, as is shown in the stratigraphic diagram of figure 3. In figure 15 that stratigraphic sequence is placed in the context of the four principal wells used to define it: CCOC, the well in which the cyclic sequence was first recognized; GUAD, in which the lower sequence was first recognized; and MOFT and CRIT, which also transect the whole cyclic sequence and thick sections of the underlying fine-grained sequence.

The cyclically layered sequence that was first defined in CCOC and corroborated in GUAD is also present to the northwest in MOFT and in the driller's log of CRIT. That log, which from its age (1909–10) was probably based on cuttings recovered by systematically bailing a well drilled by cable tool, is nearly as detailed as the resistivity logs of the other wells. As in all the wells with good logs (see especially fig. 14), the eight sedimentary cycles can be correlated between these four wells (except for the base of cycle 1 in CRIT), and comparison of each cycle indicates a distinctive and persistent similarity in its internal sequence across the wells.

The mapping of the cycles around the basin leads to the conclusion that each of these generally fining-upward cycles is a separate, laterally continuous stratigraphic interval that is marked by an unconformable base overlain by a generally prominent basal coarse interval. These coarse basal intervals form largely continuous, basinwide sheets of interbedded coarse and fine sediment. Fine intervals form the upper part of most cycles (in cycle 2, its central interval); they range widely in thickness and may locally pinch out, particularly in the southern part of the basin. The change from coarse base to fine top within a cycle is generally gradational to some degree. This cyclic sequence is largely alluvial, as indicated in the cores by sedimentary structures, the general lack of fossils, and relict soils scattered through the section. Near the bay, however, at least some of the section is estuarine.

A different interpretation in past work, based on driller's descriptions of the color of cuttings (such as California Department of Water Resources, 1975), is that sediment with reduced colors (blue, green, gray to black) is estuarine sediment deposited during interglacial high stands of sea level. The cores indicate, however, that the distribution of colors is erratic, and includes reduced colors and oxidized colors (red, brown, yellow) in both fine- and coarse-grained sediment, within the same core and even locally intermixed. Such erratic distribution is evident in the cores from well GUAD (fig. 14), where about a third of the cores showed oxidized colors, the rest reduced. It is clear that color does not provide a useful guide to depositional environment in this basin.

It is likely, considering how renewed alluviation might occur at the beginning of each climate-driven cycle, that initial sedimentation on a basal unconformity was not everywhere coarse. Overbank flooding would presumably spread finer sediment beyond the confines of any one alluvial channel. In this analysis, any such initial fine sediment that was preserved beneath the first coarse layer is included in the top of the underlying cycle. For hydrologic applications, at least, this should not be significant, as it is the lateral continuity of the coarser intervals and the vertical coarse-over-fine basal boundary that are important.

The lateral continuity of the cycles and consistency of an eightfold cyclic sequence is supported by the paleomagnetic analysis of Mankinen, as previously described. The 780-ka Brunhes/Matuyama magnetic reversal occurs just below the 718-ka base of cycle 8 in three wells, and the 565-ka Big Lost excursion occurs just below the 536-ka base of cycle 6 in four wells. The apparent absence of these events in the other cored wells is probably due to some combination of incomplete stratigraphic section and lack of properly located, relatively fine-grained cores.

The upper cyclic sequence is separated from the lower finer grained sequence by an unconformity of mid-Quaternary age (fig. 15; Wentworth and others, 2010). This is indicated at the base of the cyclic sequence in GUAD by missing section within the Matuyama reversed paleomagnetic epoch (E.A. Mankinen, written commun., 2008), and by an abrupt density step in MOFT revealed by the downhole gravity survey referred to earlier. The unconformity is also evident in the Evergreen seismic reflection profile at the same stratigraphic position beneath the projected location of well CCOC (Wentworth and others, 2010).

The age range of the mollusk *Fluminicola yatesiana*, reported from the lower 240 feet of the 1,000-ft-deep SUNY well by Meade (1967), can

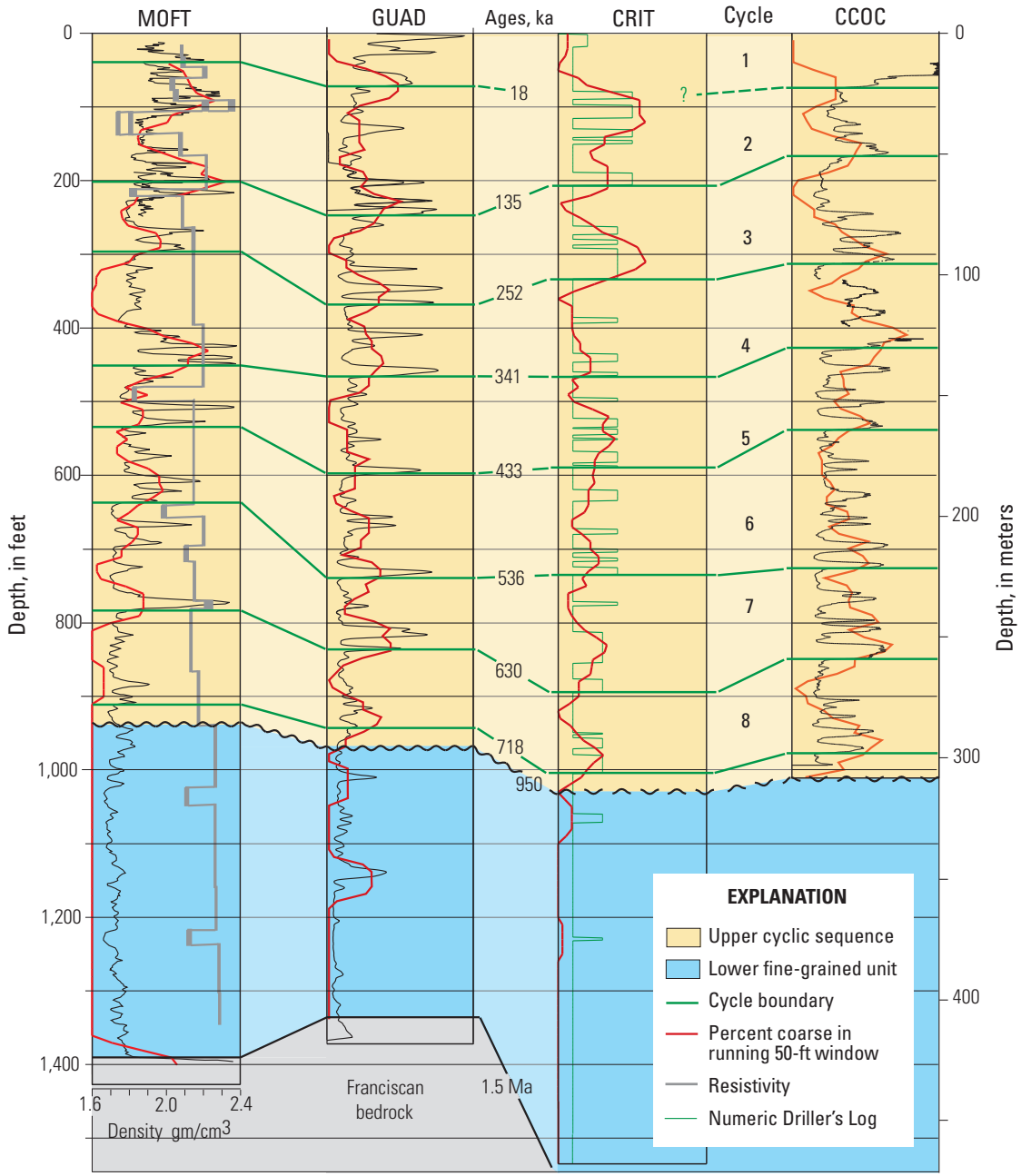

Figure 15. Correlated well section showing stratigraphic subdivision of the Quaternary fill of the Santa Clara Basin and the principal wells used to define the subdivisions. Compare with figure 3. Ages of cycle boundaries from correlation with marine oxygen isotope record modified from Wentworth and Tinsley (2005a) and Wentworth and others (2010); ages of mid-Quaternary and bedrock unconformities estimated by Wentworth and others (2010). Resistivity curves in black; density curve in well MOFT in gray, with scale at bottom. See figure 10 for location of section line.

today be extended from the late Pliocene limit that he cited to as young as about 600 ka (specifically, older than 600 ka; C.L. Powell, written commun., 2014). The fossil is thus consistent with the age constraints determined here, for its minimum depth of 760 ft lies just above the 630 ka base of cycle 7 in this well.

The finer grained unit beneath this mid-Quaternary unconformity is known particularly from the three deep wells MOFT, GUAD, and CRIT (fig. 15). Wells MOFT and GUAD transect the whole lower sequence and reach underlying bedrock, thus defining the unconformable base of the section, whereas CRIT transects 500 feet of the lower sequence without reaching rock. This lower unit lacks the abundant coarse layers of the upper cyclic sequence. It also lacks fossils, and in one core taken near its base in well GUAD it is poorly sorted, with clasts consisting of serpentinite and altered felsic volcanics.

The thickness of the lower finer grained unit in the basin west of the Silver Creek Fault ranges from zero to at least 500 feet (in CRIT) as a function of the depth to the bedrock surface (see fig. 17 and plate 1, map 11). The lower unit is completely cut out by rising bedrock at the north, west, and south margins of the basin, and reaches its greatest thickness along a deepening axis running from well 819 to CRIT near the edge of the Evergreen Basin.

Note that none of the Santa Clara Formation or other Pliocene to Pleistocene gravel lithologies known from surface geology are recognized within the upper or lower Quaternary sequence in the basin, or between the lower sequence and underlying bedrock (fig. 15; Andersen and others, 2005; Wentworth and others, 2010). Although exposed at the sides of the basin, any such gravels must have been eroded from the interior of the basin before deposition of the early Quaternary lower fine-grained sequence (Jachens and others, 2005). Dissection of the shallow element of the bedrock surface by a deeper, more irregular surface that drains to the edge of the Evergreen Basin offers just such an erosional episode.

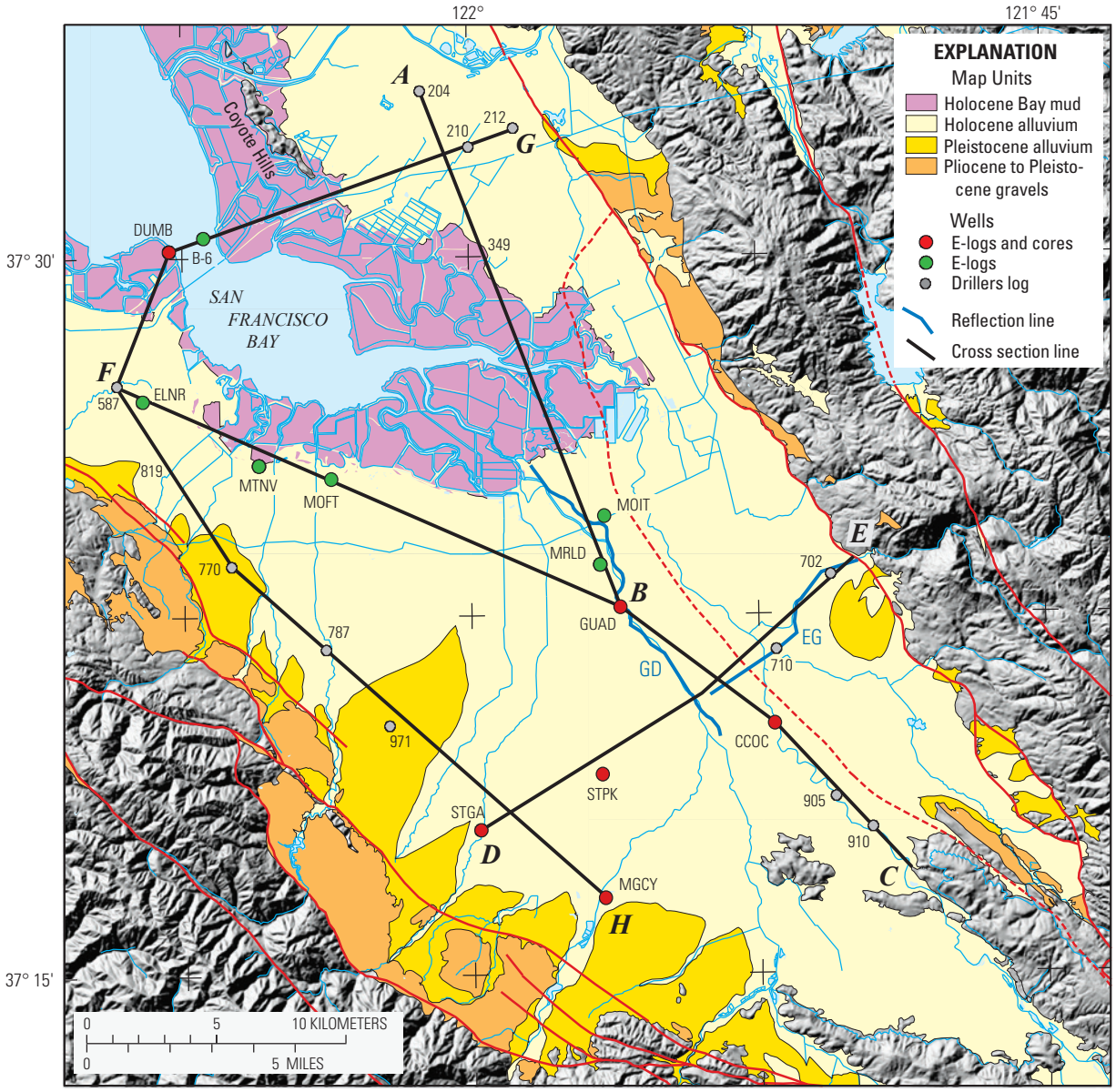

Figure 16. Map showing location of the cross sections of figure 17, the Evergreen and Guadalupe seismic reflection lines, and the nearby wells shown on the cross sections. See figures 2 and B1 and plates 1 and 2 for all the wells used in preparing the gridded surfaces from which the cross sections were generated. Surface geology and shaded relief as for figure 2.

Cycle Maps and Cross Sections

The gridded cycle boundaries and internal top/bottom surfaces provide the basis for preparing a suite of maps and cross sections (plates 1 and 2; figs. 16 and 17), using the procedures described in appendixes C and D. The 11 maps of plate 1 show the present topographic surface, the shape and elevation of the bases of the sedimentary cycles, and the shape of the buried bedrock surface. Plate 2, an array of 36 small-scale maps, shows the shapes of the cycle boundaries and the internal top/bottom boundaries, and the thickness of the cycles and of the upper fine and lower coarse interval in each cycle. Also shown are the amount of coarse sediment as a percent of that lower interval thickness and the aggregate thickness of coarse sediment in the lower interval. Inspection of these maps shows that areal variation of the several parameters is, for the most part, quite regular.

The cross sections (fig. 17) were constructed directly from the gridded cycle and internal top/bottom boundaries. The sections show the cycle boundaries (including the anomalous cycle 2a), the coarse lower intervals of the cycles, and the bedrock surface. They clearly illustrate the generally smooth variations in thickness and the depositional termination of the lower cycles laterally against bedrock highs.

Distribution of Coarse and Fine Sediment

The cross sections (fig. 17) show the general style of cyclic layering in the Quaternary sedimentary section, including the lateral continuity of both the upper fine and lower coarse intervals in each cycle that is indicated by correlation of the well sections. Although distinguished as largely fine or coarse grained, the upper fine and lower coarse intervals both consist largely of alternating coarse and fine layers. Lateral variations in thickness of the intervals tend to be gradual, with considerable pinch and swell evident in places.

The lower coarse intervals are thicker in the southern part of the basin (see cross-sections AC and DE in fig. 17). The most prominent pinch and swell in cycle thickness occurs high on the alluvial fans along the west side of the basin (section FH). The upper fine intervals in each cycle are laterally continuous, and the well dataset provides no evidence that they actually pinch out (except in cycle 1), although they can be quite thin (3–5 ft). That is particularly true both in the southern part of the basin and high on the Niles cone, where vertically adjacent coarse intervals may join in places.

The maps of plate 2 provide areally continuous representations of these variations, together with the distribution of control points. The thickness of most of the cycles (plate 2, row A) is in the range of 100–150 ft, with cycle 1 anomalously thin (appropriate for its incomplete duration—it is still ongoing). Cycle 2a is relatively thin and lacks the local thickness highs characteristic of the deeper cycles. The map locations of these thickness highs change from cycle to cycle, such that the highs in each cycle tend to occur over the thinner areas of the previous cycle.

The upper fine intervals (plate 2, row B) range widely in thickness across the basin, but with no simple pattern. The intervals tend to be thicker toward the center of the basin, but not exclusively so, nor are the intervals uniformly thinnest near the basin margins. The thicker parts of the fine intervals do fall within the much more extensive areas of thicker complete cycles.

There is reasonable correlation between cycle thickness and thickness of the lower coarse intervals, although the highs in cycle thickness tend to be more extensive than those of the lower coarse intervals (plate 2, contours in rows C and D), and some areas of high cycle thickness contain no high in the thickness of the coarse interval. There is fairly good correlation between the thickness of the lower coarse intervals and the aggregate thickness of coarse material in those lower intervals, but there is little or no correlation with the percent of coarse material in those intervals. That is because thin lower coarse intervals can contain a high percentage of coarse material even though the aggregate thickness of that coarse material is relatively small.

Hydrologic Aspects

The conclusion that much of the coarse sediment in the upper 1,000 ft or so of the Quaternary fill of the Santa Clara Basin is distributed basinwide across the bottoms of eight cyclic sequences has important hydrologic implications. Those coarse basal intervals are laterally continuous, and thus presumably hydrologically continuous as well. In most of the basin each coarse bottom interval is overlain by a fine upper interval that should greatly impede vertical movement of groundwater. Thermal evidence is presented below that this is in fact the case. Vertical continuity between cycles may be at least locally present, however, where the upper fine intervals are thin to perhaps locally absent toward the margins of the basin and particularly in its southern part and high on the Niles cone. The regularity of the cyclic sequence allows prediction of the approximate depths at which each cycle will be encountered in wells. The distribution of borehole washouts, presented below, indicates that the coarse bases of cycles 1 through 5 should have greater permeability than those of the deeper cycles, at least toward the center of the basin.

In previous work, uncertainty about how to correlate coarse intervals between wells led to differing interpretations. The results of this study provide a model that can be applied: identify clusters of coarse beds in a well, locate their unconformable base over a

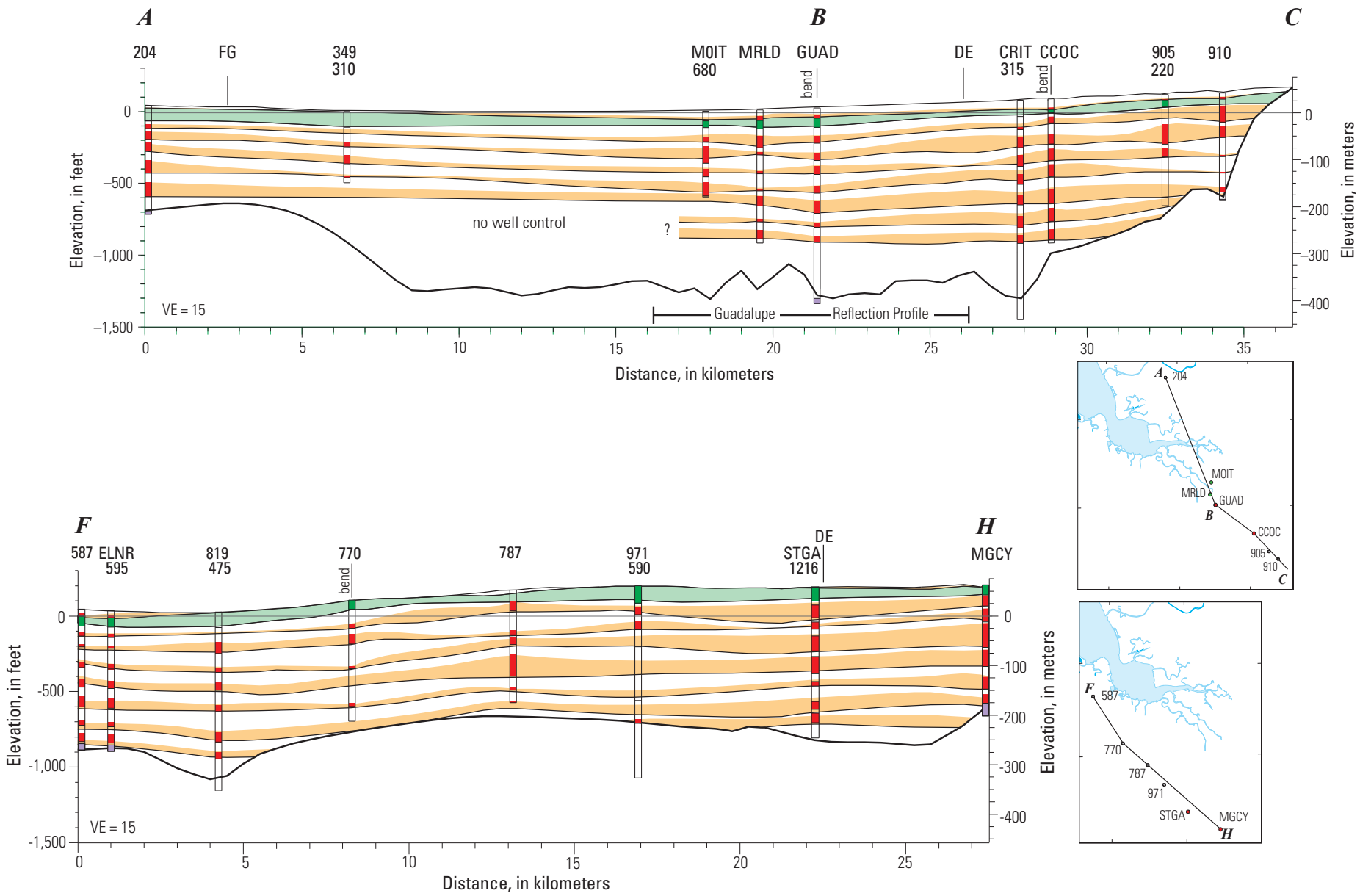

Figure 17. Cross sections showing the eight sedimentary cycles and their lower coarse intervals, the anomalous coarse interval at the top of cycle 2 (C2a), the bedrock surface at the bottom of the Quaternary sedimentary section, and the same features in selected control wells on or near the section lines. VE, vertical exaggeration. See figure 16 for locations of section lines.

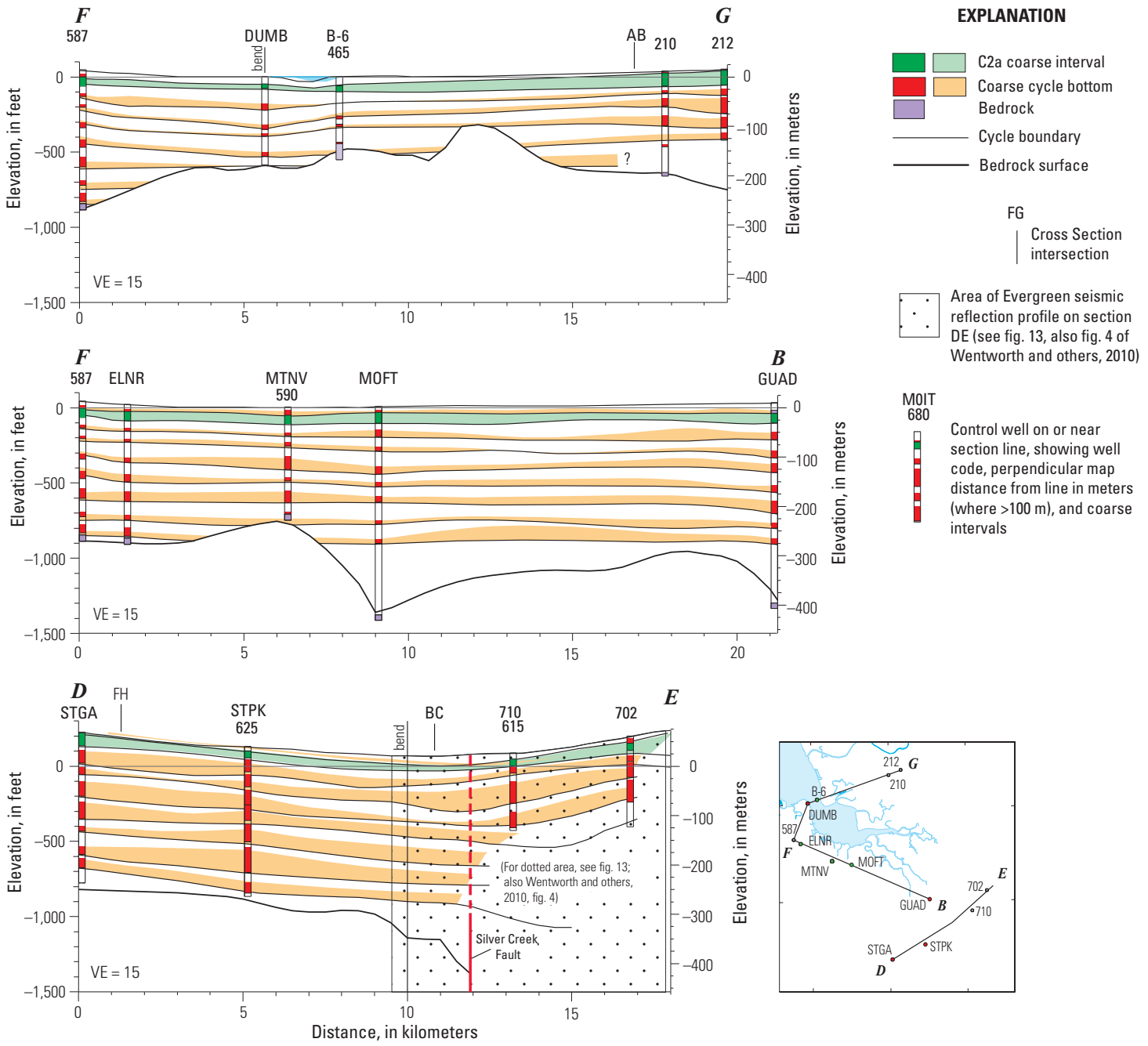

Figure 17.—Continued

prominent fine interval, and correlate to equivalent coarse clusters at similar depths in nearby wells.

Despite the correlation differences, some similarities between the present results and earlier work on the groundwater system can be identified. The surficial clay cap corresponds to the upper fine interval of cycle 1 throughout much of the interior of the basin where the cycle is relatively thick. The prominent aquiclude separating the upper and lower aquifers at a depth of 100–200 ft corresponds approximately to the fine central interval of cycle 2. On the Niles cone, where a sequence of aquifers has been named (California Department of Water Resources, 1968, 1973), the Newark aquifer corresponds to the coarse interval C2a and perhaps parts of the over- and underlying coarse bases of cycles 1 and 2, and the top of the Centerville aquifer seems to correspond to the top of the lower coarse interval of cycle 3. Deeper comparisons become progressively less clear. The forebay facies of earlier work—there considered to be vertically continuous sections of coarse material adjacent to the margins of the basin—is not clearly evident in the present study, although our well control does not sample the very edges of the basin. Some parts of the basin margin may have nearly continuous coarse material through much of the upper cyclic section, particularly around the southern part of the basin and high on the Niles cone, but that is not demonstrable with our data.

In a study to mathematically model the accumulation of an alluvial fan through time, using the Niles cone east of Coyote Hills as an example, Koltermann and Gorelick (1992) found that sedimentary layering there could be represented by six coarse intervals separated by finer layers. That result closely resembles the result presented here, both in the cyclic assembly of the section and the presence of six principal coarse intervals in that fan (see fig. 17, sections AC and FG).

The lower finer grained interval, several hundred feet thick in the center of the basin, contains few coarse layers compared to the overlying cyclic section, and thus is probably not a significant carrier of accessible groundwater. The marine Miocene section beneath the western part of the Santa Clara Basin is relatively shallow (depths of about 700–900 ft), and in deeper wells may not be recognized as such from cuttings. This Miocene section is oil-bearing (Stanley and others, 2002), which can account for traces of oil reported in nearby water wells.

Distribution of Borehole Washouts

Numerous borehole washouts are indicated in the new wells by unusually wide caliper readings (fig. 18). The coarse log texture D (fig. 5*A*) was distinguished in these wells by such washouts in coarse beds, with the inference that they resulted from coarse sediment with relatively low cohesion being eroded by the circulating mud during drilling. That inferred low cohesion suggests that these intervals have relatively high permeability. Such analysis in the eight wells for which we have digital caliper logs (fig. 18) indicates that these washouts also have stratigraphic significance. Deep washouts in coarse sediment are present in the upper parts of four wells that extend across the southern part of the basin (STPK, WLLO, CCOC, and EVGR), but end downward abruptly near the base of sedimentary cycle 5. This abrupt termination argues against a downward decrease in washouts resulting from shorter exposure to the circulating mud, as that exposure changed only gradually as drilling proceeded. The distribution of the washouts suggests an abrupt downward increase in the coherence of the coarse layers, compared to many layers in the upper part of the sequence. This contrast is not evident in the wells at the west side of the basin (MGCY and STGA), where few washouts are recognized, and to the north, where the section tends to be finer grained, the contrast becomes shallower (GUAD) to absent (ELNR).

Evidence from Downhole Temperatures

The gross hydrologic behavior of the upper cyclic sequence is indicated by high-precision temperature logs collected in several wells in the Santa Clara Valley (C.F. Williams, written commun., 2009 and 2012; Newhouse and others, 2004). All the temperature curves (fig. 19) show similar features: (1) a lower, relatively straight sloping segment that marks the stable geothermal gradient rising from depth, (2) an upward steepening of the curve that is maintained by long-term recharge and flow of groundwater toward San Francisco Bay, and (3) local perturbations of that upper segment that result from modern groundwater movement due to pumping or other management practices (C. F. Williams, written commun., 2009; see also Williams and others, 1994). In most of the wells, the upward steepening and modern perturbations occur above the base of cycle 5, in parallel, perhaps, with the distribution of washouts described above, although limits on bayward drainage by the bedrock ridge across the north side of the basin may also be involved. In the more northerly wells MOFT and GUAD, marked effects on the geothermal gradient are limited to the upper two or three sedimentary cycles.

The perturbations of the upper, steeper parts of the curves, attributed to modern groundwater movement, show considerable relation to the boundaries of the sedimentary cycles. Their common termination at those boundaries indicates a general lack of vertical movement of groundwater across them.

Faults Within the Basin

Faults that offset the Quaternary section in the Santa Clara Basin could well create barriers to lateral flow of groundwater and thereby affect the behavior of the hydrologic system, and some are known to do so. Quaternary reverse or thrust faults bound the basin

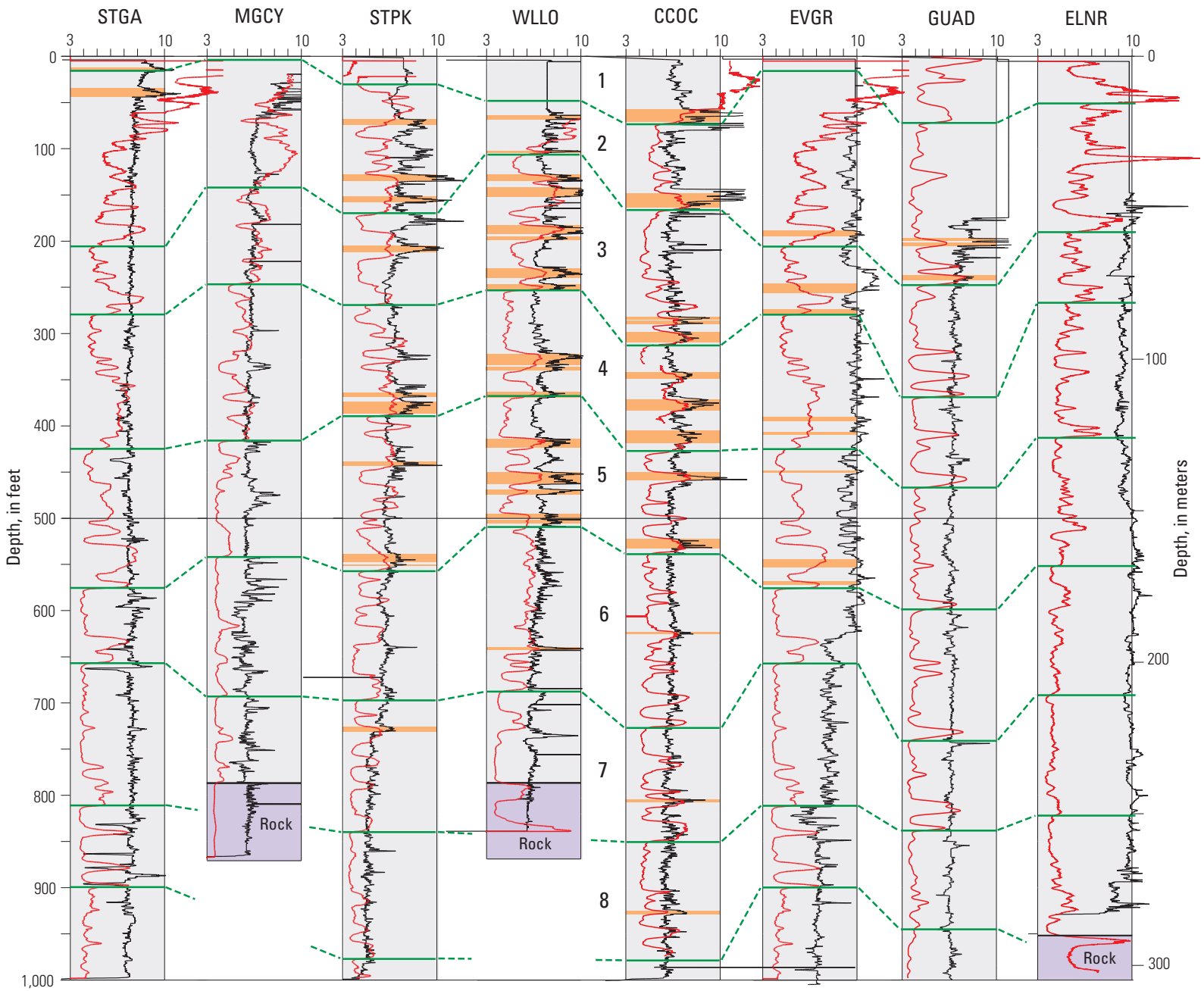

Figure 18. Correlated well section showing borehole washouts within coarse sediment layers inferred from caliper logs in the eight newly drilled wells. Coarse layers are indicated by peaks in the resistivity logs (red curves). Coarse layers in which unusually deep washouts occurred, as determined from the caliper logs (black, with scale at top in inches), are highlighted in orange. Sedimentary cycle boundaries and their correlations shown in green, with cycles numbered at center of section. See figure 5*A* for a calibrated example of a caliper log.

on the east and west, the Hayward Fault extends southward into the northeast part of the study area, and a major strike-slip fault (the Silver Creek Fault) is buried beneath the eastern part of the basin (fig. 2). These faults are recognized and demonstrable, but numerous other faults have been suggested within the basin as well.

Earlier reports have shown extensive suites of faults crossing the Santa Clara Basin that supposedly offset the Quaternary section. These include faults inferred from truncations of presumed alluvial channels (California Department of Water Resources, 1975), faults inferred from gravity anomalies (California Department of Water Resources, 1967, plate 3), faults inferred from magnetic anomalies (Brabb and Hanna, 1981), and faults patterned after those shown in the earlier reports (Jennings and Bryant, 2010). Wentworth and others (2010) trace this history of fault depictions for the basin, and conclude that most of the suggested faults do not exist in the Quaternary section.

The evidence for that conclusion is the continuity and simplicity of the cycle boundaries. No faults crossing the interior of the basin are required or, within the resolution of the data, are permitted by those boundaries. The boundary surfaces (plate 1) indicate that there can be very little dip slip anywhere within the basin, and no systematic offsets exist that extend vertically through the section or along persistent strike lines. Although the cycle boundary surfaces are subhorizontal, their shapes together with the varying thickness of the cycles and lower coarse intervals do place constraints on any strike-slip offset. No abrupt and systematic changes in shape or thickness in either plan or cross section that might indicate lateral offset are present (plate 2).

The Silver Creek Fault (fig. 2) is the sole exception to this absence of faults within the basin, as discussed by Wentworth and others (2010), although its effect on the cyclic section is limited. The fault shows about 650 feet of dip separation on the base of the Quaternary section, east side down, but little or no offset on the mid-Quaternary unconformity located just below the base of sedimentary cycle 8 (see fig. 15). Considerable strike slip accompanying the dip separation is presumed on the fault during that early Quaternary interval based on the prior behavior of the fault, but in the upper cyclic sequence the fault is marked only by a shallow structural sag with accompanying scattered small offsets (fig. 13). These small offsets are apparently sufficient to affect groundwater flow, for a partial groundwater barrier does occur at the trace of the Silver Creek Fault in the cyclic section, as indicated both by an abrupt subsidence boundary in InSAR imagery (Galloway and others, 1999 and 2000; see also Wentworth and others, 2010) and the groundwater modeling of Hanson and others (2004).

East of the Silver Creek Fault, in Quaternary deposits near the northern tip of Yerba Buena ridge, the well EVGR shows evidence of local uplift. All eight sedimentary cycles are recognized in that well, but the bases of cycles 6, 7, and 8 are unusually shallow and the cycles themselves abnormally thin (fig. 14*C*). This thinning seems to be due to uplift

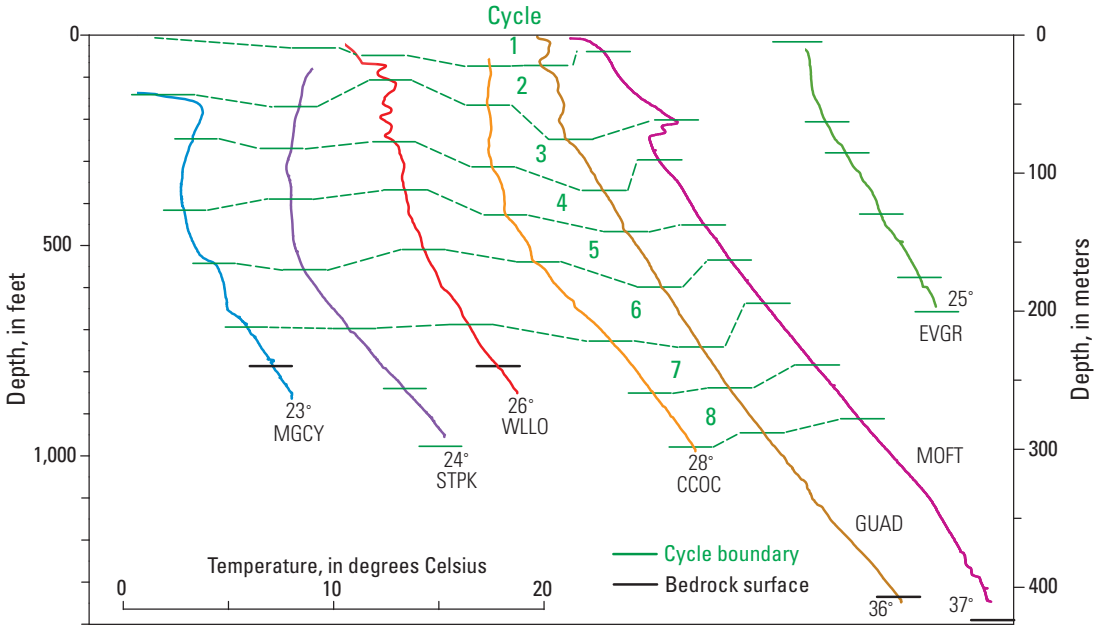

Figure 19. Graph of temperature variation with depth for seven wells in the Santa Clara Valley, showing distortions in the smooth geothermal gradient that rises from depth and its relation to the sedimentary cycles. Temperatures at the bottom of each log shown above well code. Cycle boundaries and their correlations shown in green. Temperature curves from C.F. Williams (Newhouse and others, 2004; C.F. Williams, written commun., 2009 and 2012).

during sedimentation over an underlying thrust fault in the Evergreen Fault system, above which the EVGR section is riding, but no associated steep faults are evident.

The strike-slip Hayward Fault extends southeastward into the study area across the head of the Niles alluvial cone (fig. 2), where it produces a groundwater barrier (California Department of Water Resources, 1968, 1973). The deepest of the five control wells in our dataset that lie east of that fault, well 214, extends to a depth of 400 ft and contains cycles 2 through 5 (figs. B19 and B20; see fig. B1 for well and section locations). Those cycles are correlated westward across the fault to well 212 (no cycle 1 is present). All the equivalent cycle boundaries west of the fault in well 212 are deeper (west side down), with the depth differences increasing downward from 53 to 87 ft for the four cycles. Similarly, correlation of cycles 1 through 3 from well 214 (east of the fault) to well 341 (west of the fault) also step down to the west, by 28 to 32 feet. If these depth differences occur at the fault, then a modest dip-slip component with basin-side down is present here in the shallow Quaternary section across the Hayward Fault, a sense that is consistent with surface geology (fig. 2).

The Monte Vista Fault, at the west side of the basin, has undergone late Cenozoic dip-slip offset that extended into the Quaternary, as summarized by McLaughlin and others (1999). At the surface this offset juxtaposes Pleistocene alluvium of the basin against Pliocene to Pleistocene gravels to the west (fig. 2). Well HTOR was drilled in late Pleistocene alluvium on the western, upthrown thrust block, where it transects only about 400 ft of sediment above inferred Santa Clara Formation (fig. 20). The history of that upthrown block could have involved episodes of both subsidence and uplift and erosion, which would have complicated accumulation of simple fining-upward cycles like those to the east within the continuously subsiding basin. Interpretation of the logs for well HTOR indicates four separate sedimentary intervals: an upper interval (A) for which coverage by the logs is incomplete; two apparently simple fine-over-coarse intervals (B and C) whose patterns resemble the cycles within the basin; and a lower interval (D) that shows a different gamma log signature and larger peaks in the resistivity log. This lower interval is probably Pliocene to Pleistocene Santa Clara Formation like that exposed at the surface nearby on the upthrown block (see fig. 2). The nearest well east of the Monte Vista Fault with which to compare the HTOR section is STGA (figs. 20 and B1). Searching downward in STGA for a correlative to interval B, the first similar cycle is cycle 4. Cycle 2 is not a good match, because its fine top is too thin relative to its coarse bottom, and cycle 3 is too thin.

If interval B in HTOR correlates with cycle 4 in STGA, then interval A represents the time interval of cycles 2 and 3 (no cycle 1 deposits are present at HTOR), but not necessarily the same depositional history. The vertical separation across the Monte Vista Fault implied by this correlation between the base of interval B (elev. 87 ft) and the base of cycle 4 (elev. –200 ft) would indicate 296 feet of dip slip since about 340 ka (see fig. 15 for age). That yields an offset rate of 0.26 mm/yr, which is similar to the rate since middle Pleistocene of 0.2±0.1 mm/yr of McLaughlin and others (1999). If, instead, the base of interval B were correlated with the base of cycle 5, which is both deeper and older, the resulting offset rate is a somewhat higher 0.32 mm/yr, but this alternative leaves a less satisfactory correlation of interval C with the much thinner cycle 6. Dip-slip offset across the Monte Vista zone in excess of the typical thickness of a sedimentary cycle in the basin necessarily would break stratigraphic continuity across the cyclic system, and thus make it likely that the fault forms at least a partial groundwater barrier.

Hanson and others (2004) see impediments to groundwater movement across the Monte Vista Fault zone, including their New Cascade fault, which lies

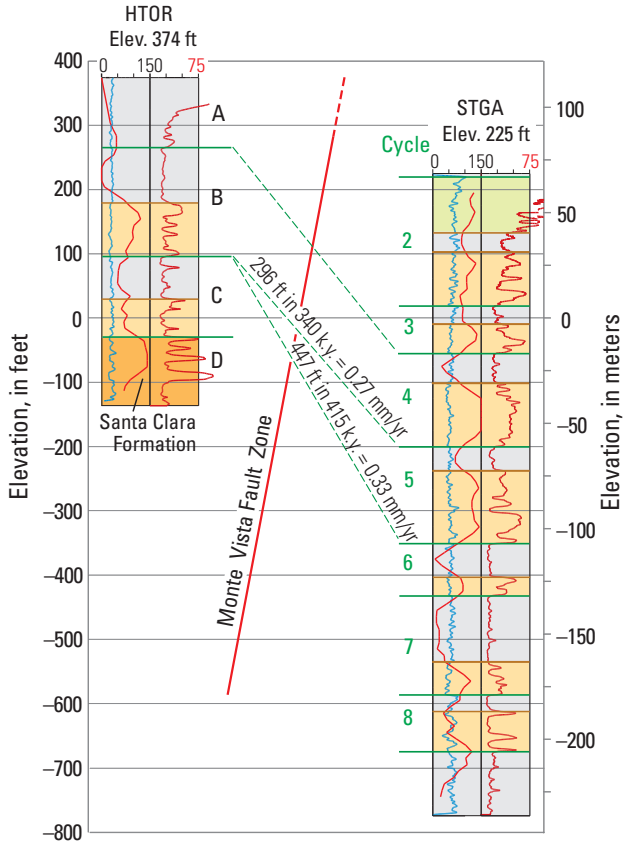

Figure 20. Well sections showing correlation of sedimentary cycles between wells HTOR and STGA across the Monte Vista Fault Zone. Note that the vertical axis here is elevation, not depth. Four sedimentary intervals (*A–D*) are recognized in well HTOR. Possible correlations of these with cycles defined in well STGA yield two possible rates of vertical offset on the fault, as shown. Distinction of coarse intervals within the cycles as in figure 15. See figures 2 and B1 for location.

east of the fault traces shown in figure 2. Although small fault offsets can have such an effect, as shown by those in the structural sag across the Silver Creek Fault (fig. 13), no faults (large or small) are evident in the southern end of the Cupertino reflection profile, which crosses the proposed trace of the New Cascade fault.

Summary and Conclusions

This study finds that the upper 1,000 ft of Quaternary section in the Santa Clara Basin consists of eight sedimentary cycles that can be mapped continuously around the whole basin. This unexpected conclusion and other insights into the anatomy and history of the basin are made possible by geophysical logs and cores from several newly drilled wells, three new seismic reflection profiles, and the gathering of geophysical logs from a number of other wells. These lines of evidence, in turn, provide guidance in interpreting a sample of the much larger body of driller's logs from water wells in the basin.

The discovery of cyclicity in the Quaternary section arises from recognition that two newly drilled wells near the middle of the basin contain clusters of coarse layers that define eight distinct sedimentary cycles. From those wells (CCOC and GUAD) the cycles are correlated into a set of 21 wells with geophysical logs that are scattered around much of the basin, and from that primary framework they are then correlated into a network of 105 water wells with driller's logs. Identification of the cycles is nearly complete in all the wells with geophysical logs and in those with fairly detailed driller's logs. The fact that the cycles are evident in the more detailed driller's logs indicates that the less detailed logs are less accurate and should be given less weight, particularly in parts of those logs where no lithologic changes are indicated.

The cycle correlations are guided by the fact that layering in the section is subparallel to the ground surface, as indicated by the seismic reflection profiles. A reflection profile also aids correlation of the cycles eastward across the Silver Creek Fault to the eastern edge of the basin, and that correlation helps to corroborate the lateral continuity of the cycles. Further evidence for the cycles is seen in logs of seismic velocity in five of the new wells, downward termination of deep borehole washouts in several wells at a common cycle boundary (cycle 5), and limitation at cycle boundaries of thermal anomalies due to groundwater movement.

The bases of the eight cycles were correlated with low stands of sea level using the marine oxygen isotope record (Wentworth and Tinsley, 2005a), and that relation indicates that those surfaces are unconformities. That correlation also permits ages to be assigned to those surfaces, with the oldest (base of cycle 8) being about 718 ka. Paleomagnetic analysis by E.A. Mankinen shows a magnetic reversal just below the base of that cycle that represents the 780-ka Brunhes/Matuyama boundary. Similarly, a magnetic event identified as the 565-ka Big Lost excursion occurs just below the 536-ka base of cycle 6. This consistent relation between stratigraphic ages assigned using the glacial climate record and the ages of two underlying, somewhat older paleomagnetic events helps constrain and confirm the identification of the cycles.

Analysis of the wells was aided by several procedures the development of which was stimulated by examination of the well data. Interpretation of the resistivity and natural gamma logs from the geophysically logged wells was calibrated through quantitative comparison with sediment textures observed in many hundreds of feet of core from wells CCOC and GUAD. A key result of this was that the separation between fine and coarse sediment in the section was placed at the boundary between fine and medium sand, because the distinction between fine sand to silt and silty clay to clay was generally not possible from the logs.

Recognition in the first well examined (CCOC) that the distribution of coarse layers had some regularity led to development of a smoothed, downhole measure of the local concentration of coarse layers—the coarseness curve—which was then applied to all the wells. Visual evaluation of the driller's logs and comparison with the geophysical logs was facilitated by converting the driller's descriptions to numeric measures of coarseness and plotting those values down the well column in a fashion similar to the other logs. Caliper logs from the new wells were used to identify excessive washouts in coarse layers, which were inferred to be less cohesive and therefore more permeable. These deep washouts terminate downward in the section at the base of cycle 5 in several wells.

The coarseness curves provide a summary of the distribution of coarse layers in each well. For the deeper wells, these curves typically show eight principal coarse peaks, with some of the peaks simple and some more complex. Each peak is associated with a concentration of coarse layers, and that coarse interval forms the lower part of a sedimentary cycle. Each cycle thus consists of that coarse bottom and an overlying fine top, with the base of the cycle marked by a generally prominent coarse-over-fine contact. Although that basal contact is sharp, the change from coarse bottom to fine top within a cycle is generally gradational to some degree. The eight cycles tend to differ from one another in their detailed internal organization. Within any particular cycle, however, the internal sequence of beds tends to persist laterally when compared from well to well, with most changes occurring gradually despite typical well spacings of 1 to 3 km.

The uppermost cycle (cycle 1) represents the postglacial depositional sequence that forms an unconsolidated blanket across most of the basin and includes the estuarine Bay mud. Identification of the base of this cycle proved difficult, both because the logs tend to be incomplete at that shallow level and because the top of cycle 2 includes considerable coarse material in some parts of the basin. Delineation

of the base of unconsolidated sediment susceptible to liquefaction by others did not prove a satisfactory match for the base of cycle 1, although that work aided in its identification. Coarse material evident near the top of cycle 2 in some wells, anomalous in the context of the eight cycles, led to mapping of an uppermost coarse interval in cycle 2 (C2a) that, with some uncertainty, was carried throughout the basin. This interval forms the bulk of the Newark aquifer of the Niles alluvial cone.

The lower part of the cyclic section is cut out around the edges of much of the basin by bedrock rising to shallow levels away from the interior of the basin. There, in the interior, where the bedrock surface west of the Silver Creek Fault is deepest, the cyclic section is underlain by several hundred feet of largely fine-grained Quaternary sediment, with the two units separated by a mid-Quaternary unconformity. Although the Santa Clara Formation and other Pliocene to Pleistocene gravels are exposed around the margins of the basin, none have been found in the subsurface above that buried bedrock surface, contrary to earlier presumptions that these gravels floor the basin.

The Quaternary stratigraphic sequence is summarized in figure 3 and illustrated in figure 15 in the context of four principal wells. The cycles are subdivided throughout the basin into coarse bottoms and fine tops, as shown in figures 14 and B3–B21. This subdivision provides a measure of the varying abundance of coarse material around the basin and also emphasizes the typically gradual stratigraphic change from well to well within each cycle. Aggregate thickness of coarse layers and other data assembled during this subdivision are reported in digital data files (appendix E).

Sedimentary structures and soils recognized through study of hundreds of feet of core indicate that most of the basin fill is alluvial, although estuarine sediment does occur near the margin of and beneath San Francisco Bay. Earlier use of color to distinguish alluvial from estuarine sediment is not consistent either with this evidence or the distribution of oxidized and reduced colors in the cores.

The upper cyclic sequence forms the principal groundwater aquifer system of the Santa Clara Valley, which has been the subject of considerable previous study. In that context the present results are particularly important. Rather than forming small local lenses or long sinuous channel sands embedded in a predominantly fine-grained section, as earlier studies suggested, this study finds that the coarse sediment in the basin forms eight basinwide sheets separated by fine-grained intervals. This implies that there should be lateral hydrologic continuity within those sheets and only limited movement of water across the intervening fine intervals. Perturbations in thermal gradients measured in several wells in the basin and attributed to groundwater management practices do not cross cycle boundaries, confirming that those boundaries are strong impediments to water movement.

Around the margins of the basin, and particularly in its southern part, the fine cycle tops are thin to perhaps locally absent, and these may thus provide little to no impediment to vertical water movement. This would provide surface water access to the deeper aquifer system, as suggested by previous work. In the interior of the basin, abrupt downward termination of deep wellbore washouts at the base of cycle 5 suggests that aquifer sediment above that boundary is less consolidated, and thus more permeable, than below it.

The widespread confining aquiclude that is described by previous workers as occurring at depths of about 100 to 200 ft is very approximately equivalent to the central fine interval of cycle 2. The fine tops of the deeper cycles are not greatly dissimilar in thickness, however, as is evident from figure 17.

With the cycle boundaries identified in the suite of wells, their elevations were determined and used to prepare continuous (raster) representations of the surfaces by computer. Those digital surfaces were then used to prepare cross sections along representative section lines. The boundary surfaces are relatively smooth and, after removing a few poorly fitting control points determined from driller's logs, satisfy the test that they were once topographic surfaces. The cross sections show the lateral continuity of the cycles and of their coarse bottoms and fine tops, as well as the presence of gradual pinch and swell in cycle thickness, a feature that is most evident along the western part of the basin near the heads of alluvial fans. That pinch and swell, and the varying location of thicker areas from cycle to cycle seen in maps of cycle thickness, suggest the filling of topographic lows in each successive depositional cycle, an expectable pattern in such an alluvial depositional system.

The continuity and simplicity of the cycle boundary surfaces provide a severe constraint on the presence of any faults offsetting the Quaternary section within the basin. Other than the bounding fault systems at the east and west sides of the basin, no faults are required or, within the resolution of the data, permitted by those boundaries. This result is in conflict with earlier depictions of faults within the basin. The boundary surfaces indicate that there can be very little dip slip anywhere within the basin, and no systematic offsets exist that extend vertically through the section or along persistent strike lines in plan. Similarly, the varying thicknesses of the cycles and lower coarse intervals show no abrupt and systematic changes in thickness in either plan or cross section that might indicate significant lateral offset. It is precisely this evidence from the mapped cycles that led Wentworth and others (2010) to conclude that the Quaternary section in the basin is largely unfaulted, contrary to earlier suggestions. The exception within the basin is the Silver Creek Fault (Wentworth and others, 2010), which in the upper cyclic sequence is marked by a shallow structural sag about 750 m (2,500 feet) wide with scattered small fault offsets that do produce a partial groundwater barrier. Our well dataset is too sparse to reveal that narrow sag in the cycle boundaries.

References Cited

Andersen, D.W., Metzger, E.P., Ramstetter, N.P., and Shostak, N.C., 2005, Composition of sediment from deep wells in Quaternary alluvium, Santa Clara Valley, California: Geological Society of America, Abstracts with Programs, v. 37, no. 4, p. 37.

Asquith, G.B, and Gibson, C.R., 1982, Basic well log analysis for geologists: The American Association of Petroleum Geologists, Methods in Exploration Series, 216 p.

Bennett, M.J., 1979, Depositional environments and geotechnical properties of Quaternary sediment from south San Francisco Bay, San Mateo County, California: California State University at San Jose, Masters thesis, 133 p.

Beyer, L.A., 1980, Borehole gravity program of the U.S. Geological Survey (1963–1975)—brief history and basic data: U.S. Geological Survey Open-File Report 80–903, 76 p.

Birkeland, P.W., 1984, Soils and geomorphology: Oxford University Press, 372 p.

Brabb, E.E., Graymer, R.W., and Jones, D.L., 1998, Geology of the onshore part of San Mateo County, California—a digital database: U.S. Geological Survey Open-File Report 98–137, scale 1:62,500.

Brabb, E.E., Graymer, R.W., and Jones, D.L., 2000, Geologic map and map database of the Palo Alto 30’ x 60’ quadrangle, California: U.S. Geological Survey Miscellaneous Field Studies Map MF–2332, scale 1:100,000.

Brabb, E.E., and Hanna, W.F., 1981, Maps showing aeromagnetic anomalies, faults, earthquakes epicenters and igneous rocks in the southern San Francisco Bay region: U.S. Geological Survey Geophysical Map GP–932, scale 1:125,000.

California Department of Water Resources, 1967, Geology, appendix A *of* Evaluation of ground water resources—South Bay: California Department of Water Resources Bulletin 118–1, 153 p.

California Department of Water Resources, 1968, Evaluation of ground water resources South San Francisco Bay, Fremont study area: California Department of Water Resources Bulletin 118–1, v. 1.

California Department of Water Resources, 1973, Evaluation of ground water resources South San Francisco Bay, additional Fremont area study: California Department of Water Resources Bulletin 118–1, v. 2.

California Department of Water Resources, 1975, Evaluation of ground water resources—South San Francisco Bay: California Department of Water Resources Bulletin 118–1, v. 3, Northern Santa Clara County area, fig. E, double-page map, scale approximately 1:140,000.

Clahan, K.B., Mattison, M.E., Rosinski, A.M., Bott, J.D., and Knudsen, K.L., 2002, Preliminary maps of (1) Pleistocene alluvial surface, (2) depth to historical high ground water, and (3) thickness of Holocene alluvium—and their use in liquefaction hazard mapping, Santa Clara Valley and the east San Francisco Bay plain, California [abs.]: Eos (American Geophysical Union Transactions), v. 83, no. 47, p. F1312.

Clark, 1924, Ground water in Santa Clara Valley, California: U.S. Geological Survey Water-Supply Paper 519, 209 p.

Crittenden, M.D., Jr., 1951, Geology of the San Jose-Mount Hamilton area, California: California Division of Mines Bulletin 157, 74 p., plate map scale 1:62,500.

Fio, J.L., and Leighton, D.A., 1995, Geohydrologic framework, historical development of the ground-water system, and general hydrologic and water-quality conditions in 1990, south San Francisco Bay and Peninsula area, California: U.S. Geological Survey Open-File Report 94–357, 46 p.

Galloway, D., Jones, D.R., and Ingebritsen, S.E., eds., 1999, Land subsidence in the United States: U.S. Geological Survey Circular 1182, 175 p.

Galloway, D.L., Jones, D.R., and Ingebritsen, S.E., 2000, Measuring land subsidence from space: U.S. Geological Survey Fact Sheet 051–00, available online at http://pubs.usgs.gov/fs/fs-051-00/.

Graham, S.E, and Pike, R.J., 1998, Elevation maps of the San Francisco Bay region, California—a digital database: U.S. Geological Survey Open-File Report 98–625. scale 1:275,000.

Graham, S.E., and Wentworth, C.M., 2005, Derivation of a Pleistocene topographic surface map and a Holocene deposit thickness map for Santa Clara Valley, California [abs.]: Geological Society of America, Abstracts with Programs, vol. 37, no. 4, p. 91.

Graymer, R.W., Jones, D.L., and Brabb, E.E., 1996, Preliminary geologic map emphasizing bedrock formations in Alameda County, California—a digital database: U.S. Geological Survey Open-File Report 96–252, scale 1:75,000.

Hanson, R.T., Newhouse, M.W., Wentworth, C.M., Williams, C.F., Noce, T.E., and Bennett, M.J., 2002, Santa Clara Valley Water District multi-aquifer monitoring-well site, Coyote Creek Outdoor Classroom, San Jose, California: U.S. Geological Survey Open-File Report 02–369, 4 p.

Hanson, R.T., Zhen, Li, and Faunt, C.C., 2004, Documentation of the Santa Clara Valley regional ground-water/surface-water flow model, Santa Clara County, California: U.S. Geological Survey Scientific Investigations Report 2004–5231, 75 p.

Hazelwood, R.M., 1974, Preliminary report of seismic refraction survey along the east side of the San Francisco Bay, Alameda County, California: U.S. Geological Survey Open-File Report 74–1046 [OFR number assigned later], 11 p.

Hazelwood, R.M., 1976, Contour map and interpretive cross sections showing depth and configuration of bedrock surface, South San Francisco Bay region, California: U.S. Geological Survey Miscellaneous Fields Studies Map MF–796, map scale 1:62,500.

Helley, E.J., 1990, Preliminary contour map showing elevation of surface of Pleistocene alluvium under Santa Clara Valley, California: U.S. Geological Survey Open-File Report 90–633, scale approx. 1:35,971.

Hitchcock, C.S., and Helley, E.J., 2003, Characterization of subsurface sediments, southern San Francisco Bay area: U.S. Geological Survey, National Earthquake Hazards Reduction Program, Final Technical Report, Award Number 99-HQ-GR-0097, 27 p., map scale 1:100,000.

Holzer, T.L., Noce, T.E., and Bennett, M.J., 2010, Maps and documentation of seismic CPT soundings in the central and eastern United States: U.S. Geological Survey Open-File Report 2010–1136, 80 p.

Iwamura, T.I., 1995, Hydrogeology of the Santa Clara and Coyote Valleys groundwater basins, California, *in* Sangines, E.M., Andersen, D.W., and Buising, A.V., eds., Recent geologic studies in the San Francisco Bay area: SEPM (Society for Sedimentary Geology), Pacific Section, volume 76, p. 173–192.

Jachens, R.C., Wentworth, C.M., Graymer, R.W., Stanley, R.G., McLaughlin, R.J., Simpson, R.W., Williams, R.A., Andersen, D.W., Ponce, D.A., and Langenheim, V.E., 2005, Late Cenozoic stratigraphic and tectonic history of the Santa Clara Valley, California [abs.]: Geological Society of America, Abstracts with Programs, v. 37, no. 4, p. 59.

Jennings, C.W., and Bryant, W.A., 2010, Fault activity map of California: California Geological Survey Geologic Data Map No. 6, map scale 1:750,000.

Koltermann, C.E., and Gorelick, S.M., 1992, Paleoclimate signature in terrestrial flood deposits: Science, v. 256, p. 1775–1782.

Knudsen, K.L., Sowers, J.M., Witter, R.C., Wentworth, C.M., Helley, E.J., Nicholson, R.S., Wright, H.M., and Brown, K.M., 2000, Preliminary maps of Quaternary deposits and liquefaction susceptibility, nine-county San Francisco Bay region, California—a digital database: U.S. Geological Survey Open-File Report 00–444, scale 1:275,000.

Leighton, A., Fio, J.L., and Metzger, L.F., 1995, Database of well and areal data, south San Francisco Bay and Peninsula area, California: U.S. Geological Survey Water-Resources Investigations Report 94–4151, 47 p.

Mankinen, E.A., and Wentworth, C.M., 2003, Preliminary paleomagnetic results from the Coyote Creek Outdoor Classroom drill hole, Santa Clara Valley, California: U.S. Geological Survey Open-File Report 03–187, 32 p., available at http://pubs.usgs.gov/of/2003/of03-187/.

Mankinen, E.A., and Wentworth, C.M., 2004, Mono Lake excursion recorded in sediment of the Santa Clara Valley, California: Geochemistry Geophysics Geosystems, v. 5, no 2, Q02H05, doi:10.1029/2003GC000592.

Mankinen, E.A., and Wentworth, C.M., 2005, The paleomagnetic record as means of correlating sedimentary sequences encountered in research wells of the Santa Clara Valley, California [abs.]: Geological Society of America, Abstracts with Program, v. 37, no. 4, p. 91.

Mascarelli, A.L., 2009, Quaternary geologists win timescale vote: Nature, v. 459, 4 June 2009, p. 624.

McCulloh, T.H., La Coste, L.J.B., Schoelhamer, J.E, and Pampeyan, E.H., 1967, The U.S. Geological Survey–La Coste and Romberg precise borehole gravimeter system – test results: U.S. Geological Survey Professional Paper 575–D, p. D92-D100.

McLaughlin, R.J., Langenheim, V.E., Schmidt, K.M., Jachens, R.C., Stanley, R.G., Jayko, A.S., McDougall, K.A., Tinsley, J.C., and Valin, Z.C., 1999, Neogene contraction between the San Andreas Fault and the Santa Clara Valley, San Francisco Bay region, California: International Geology Review, v. 11, p. 1–30.

Meade, R.H., 1967, Petrology of sediments underlying areas of land subsidence in central California: U.S. Geological Survey Professional Paper 497–C, 89 p.

Munsell Color, 2000, Munsell soil color charts: New Windsor, New York, Munsell Color.

Newhouse, M.W., Hanson, R.T., Wentworth, C.M., Everett, R.R., Williams, C.F., Tinsley, J.C., Noce, T.E., and Carkin, B.A., 2004, Geologic, water-chemistry, and hydrologic data from multiple-well monitoring sites and selected water-supply wells in the Santa Clara Valley, California, 1999–2003: U.S. Geological Survey Scientific Investigations Report 2004–5250, 132 p., available at http://pubs.usgs.gov/sir/2004/5250/.

Noce, T.E., and Holzer, T.L., 2003, Subsurface exploration with the cone penetration testing truck: U.S. Geological Survey Fact Sheet 028-03, 2 p.

Poland, J.F., 1971, Land subsidence in the Santa Clara Valley, Alameda, San Mateo, and Santa Clara Counties, California: U.S. Geological Survey Open-File Report [not numbered], map scale 1:125,000 (San Francisco Bay Region Environment and Resources Planning Study, Technical Report 2).

Poland, J.F., and Ireland, R.L., 1988, Land subsidence in the Santa Clara Valley, California, as of 1982: U.S. Geological Survey Professional Paper 497–F, 61 p.

Shepard, F.P., 1954, Nomenclature based on sand-silt-clay ratios: Journal of Sedimentary Petrology, v. 24, p. 151–158.

Stanley, R.G., Jachens, R.C., Lillis, P.G., McLaughlin, R.J., Kvenvolden, K.A., Hostettler, F.D., McDougall, K.A., and Magoon, L.B., 2002, Subsurface and petroleum geology of the southwestern Santa Clara Valley ("Silicon Valley"), California: U.S. Geological Survey Professional Paper 1663, 55 p., available at http://pubs.usgs.gov/pp/1663/.

Walker, J.D., and Geissman, J.W., compilers, 2009, Geologic time scale: Geologic Society of America, doi: 1130/2009.CTS004R2C.

Wentworth, C.M., Blake, M.C., Jr., McLaughlin, R.J., and Graymer, R.W., 1998, Preliminary geologic map of the San Jose 30×60-minute quadrangle, California—a digital database: U.S. Geological Survey Open-File Report 98–795, scale 1:100,000.

Wentworth, C.M., Hanson, R.T., Jachens, R.C., Langenheim, V.E., McLaughlin, R.J., Phelps, G., Simpson, R.W., Stanley, R.G., and Williams, R.A., 2003, Varied evidence for a blind thrust beneath the southwestern Santa Clara (Silicon) Valley, California—a product of 3-dimensional map analysis [abs.]: Geological Society of America, Abstracts with Programs, v. 35, no. 6, p. 74.

Wentworth, C.M., and Tinsley, J.C., 2005a, Tectonic subsidence and cyclic Quaternary deposition controlled by climate variation, Santa Clara Valley, California [abs.]: Geological Society of America, Abstracts with Programs, v. 37, no. 4, p. 59.

Wentworth, C.M., and Tinsley, J.C., 2005b, Geologic setting, stratigraphy, and detailed velocity structure of the Coyote Creek borehole, Santa Clara Valley, California, *in* Asten, M.W., and Boore, D.M., eds., Blind comparisons of shear-wave velocities at closely spaced sites in San Jose, California: U.S. Geological Survey Open-File Report 2005–1169, part 2_01, 26 p., available at http://pubs.usgs.gov/of/2005/1169/.

Wentworth, C.M., Tinsley, J.C., Andersen, D.W., Graham, S.E., Jachens, R.C., Mankinen, E.A., and Williams, R.A., 2005, Quaternary deposits of the Santa Clara Valley, California [abs.]: Geological Society of America, Abstracts with Programs, v. 37, no. 4, p. 58.

Wentworth, C.M., Williams, R.A., Jachens, R.C., Graymer, R.W., and Stephenson, W.J., 2010, The Quaternary Silver Creek Fault beneath the Santa Clara Valley, California: U.S. Geological Survey Open-File Report, 2010–1010, 50 p.

Williams, C.F., Galanis, S.P., Jr., Grubb, F.V., and Moses, T.H., Jr. 1994, The thermal regime of Santa Maria Province, California: U.S. Geological Survey Bulletin 1995–F, 25 p. [available only in Bulletin 1995_F-G], also available at http://pubs.usgs.gov/bul/1995f-g/report.pdf.

Williams, R.A., Stephenson, W.J., Jachens, R.C., Wentworth, C.M., Odum, J.K., and Stanley, R.G., 2004, Seismic-reflection profiling across the urban area of Santa Clara Valley, California; images of the northeastern margin of the Cupertino Basin [abs.]:, Eos (American Geophysical Union Transactions), Fall Meeting Supplement, Abstract S31A-1022.

Williams, R.A., Stephenson, W.J., Wentworth, C.M., Jachens, R.C., Hanson, R.T., Simpson, R.W., Odum, J.K., and Stanley, R.G., 2005, Constraints on faults and basins within the Santa Clara Valley, California, from seismic-reflection data [abs.]: Geological Society of America, Abstracts with Programs, v.37, no. 4. p. 59.

Williams, R.A., Stephenson, W.J., Wentworth, C.M., Odum, J.K., Hanson, R.T., and Jachens, R.C., 2002, Definition of the Silver Creek Fault and Evergreen Basin sediments from seismic reflection data, San Jose, California [abs.]: Eos (American Geophysical Union Transactions), Fall Meeting Supplement, Abstract T71E-1207.

Witter, R.C., Knudsen, K.L, Sowers, J.M., Wentworth, C.M., Koehler, R.D., Randolph, C.E., Brooks, S.K., and Gans, K.D., 2006, Maps of Quaternary deposits and liquefaction susceptibility in the central San Francisco Bay region, California: U.S. Geological Survey Open-File Report 2006-1037, scale 1:200,000, available at http://pubs.usgs.gov/of/2006/1037/.

Appendix A. Description of Cores

Cores were taken in six of the new wells as they were drilled. For five of these wells, available funding limited the coring to about 20 percent of the well depth, or 200 feet per nominally 1,000-foot hole. In one well, GUAD, funding was obtained to core most of the upper 1,000 feet of the well. The practical result was to recover 662 feet of core from the 883 feet attempted in GUAD, 205 of 339 feet in well CCOC, and similar smaller amounts in the four other partially cored wells (EVGR, MGCY, STPK, and WLLO). Core positions (depths) in the partially cored holes, ideally intended to sample contacts and coarser intervals, were selected on the basis of CPT soundings at the drill site and nearby well logs where available, but more generally by an attempt to spread the cores fairly evenly down the depth of the well. In most attempts the drill was advanced 5 feet to take a nominal 5-ft-long core, although in some cases only a 2.5 ft advance was used where difficulty in drilling or in retaining core in the barrel was anticipated. Once the coring advance was completed, the core barrel with its contents was retrieved from within the drill string by wire line.

After removal from the core barrel, the cores were prepared at the drill site and transported to Menlo Park, where they are maintained in refrigerated storage. Cores are identified by well, sequential number down the hole, and the depth interval that the drill advanced during coring. In the laboratory they were split longitudinally and described carefully at centimeter scale. Although the core depths are recorded in feet, the depth positions of described intervals within the cores are recorded in centimeters, measured down from the top of the core.

Coring

The core barrel (Christensen 94-mm wireline) was loaded with a hollow plastic cylinder (the liner) that would accept and hold the core itself (core diameter 6.2 cm), and a short cylindrical metal shoe with a tapered wall was attached at the front of the barrel to capture the core and feed it upward into the liner within the core barrel. This assembly was then lowered down into the well within the drill string on wire line and attached behind the donut-shaped coring bit.

Drilling then proceeded for the 5 (or 2.5) ft of coring advance, after which the core barrel was retrieved from the well by wire line and the shoe and liner removed. Typically both contained core, although rarely one as long as the 5 (or 2.5) ft that the drill bit was advanced. The length of shoe sample and of core in the liner were recorded, any empty liner at the top of the core was sawed off, the liner was capped at both ends, and the shoe sample was stored in a separate section of liner. Both were labeled by well and core number (such as CCOC-24C-1) and by depth interval of the core (such as 150–155 ft), and the top of the core was clearly marked.

Core Descriptions

The descriptive information obtained for the cores is presented in six data tables, which are summarized here and described in more detail below. Each table contains information for all the cored wells, with the cores uniquely identified by well and core depth ranges. The data tables and their general contents are:

- scv-core—Basic information about the cores, including well code, core number, depth range of the core, and details about the length of core that was actually recovered. This table is where the core numbers are recorded (for example, CCOC-24C-1); to determine the core number for a depth interval described in another table, match that depth range with the range in this table for the appropriate well.
- scv-lith—Textural and bedding information. The use of grain size terms follows Shepard (1954).
- scv-accessory—Description of other features of the material, such as sedimentary structures and bioturbation, sorting and rounding of grains, organic fragments, soil characteristics, carbonate, and degree of mechanical disturbance by coring.
- scv-remarks—Any additional remarks about the sediment, such as maximum clast size, clast rock type, sedimentary structures, soil characteristics, color, coring issues such as mechanical disturbance, intrusion of drilling fluid, empty core space, and sediment infall.
- scv-penetrometer—Approximate unconfined compressive strength of cohesive intervals measured by resistance to intrusion of a metered probe (pocket penetrometer).
- scv-color—Munsell color of described intervals and any subordinate phases.

Summary of Data Fields in the Tables

The Core field (only in the scv-core table) uniquely identifies each core. Several basic fields in each table identify the well and the relevant depth ranges.

- Core—the well code combined with the core number uniquely identifies each core. For example, CCOC-1C-1 identifies the first core taken in well CCOC. The 1C identifies this as the first core taken, using a Christiansen coring device (C). The -1 suffix is the core section number. For most cores, there is only one section, but for a few, some core material was found above the liner in the core barrel or for some other reason was separated from the main core. This material was placed in a separate core liner and labeled section 2. The core number itself is listed only in the scv-core table.
- Well—well code, such as CCOC. Table 1 lists well codes and equivalent well names.

Depths:

- From (ft)—Beginning (top) of the cored interval, in feet (scv-core table only)

- To (ft)—End (bottom) of the cored interval, in feet (scv-core table only)
- Top Depth (ft)—Depth of the top of the actual recovered core, in feet. Cores shorter than the cored interval were assumed to begin at the top of that interval.
- Bot Depth (ft)—Depth of the bottom of the actual recovered core, in feet
- From (cm)—Top of the described interval, in centimeters
- To (cm)—Bottom of the described interval, in centimeters
- Depth (ft)—Depth at point of measurement, in feet (scv-penetrometer table only)
- Depth (cm)—Depth at point of measurement, in centimeters (scv-penetrometer table only)
- Source—the source of the material described, either core (Cr) or cuttings (Ct) (listed in all tables except scv-core)
- Date of Entry—date on which the data were recorded in the database. All basic laboratory properties were recorded as each core was being examined and described, typically over a period of an hour or so.

List of Data Tables and Description of Data Fields

scv-core

The fields for Core, Well, basic depths, and Date of Entry are described above

- Core Number—The number of the core, counted sequentially down the hole
- Core Section—Generally 1, but in some cases a second piece of core was packaged separately as section 2
- Offset (cm)—Distance in cm the recovered core is moved upward, because empty core space or material at the top of the core (such as infall from farther up the borehole) was judged not to be part of the core.
- Recovery (cm)—The length, in centimeters, of the actual recovered core in the liner
- Shoe Recovery (cm)—The length, in centimeters, of material recovered from the shoe
- Total Length (cm)—The sum of the material recovered from liner and shoe
- Attempted Length (ft)—The distance that the core bit was advanced in taking this core
- Net Recovery (cm)—The actual length of cored material recovered, in centimeters. This is generally the same as the Total Length. It can differ, however, where adjustment is required because core material has been lost or the length has been distorted by mechanical disturbance
- Recovery (%)—The percent of attempted core length actually recovered
- Corrected Recovery (%)—Generally equal to Net Recovery, but recovered length for some cores was adjusted to accommodate shrinkage, lost materials, or expansion of the core upon removal of confining pressure.
- Remarks—Comments about such factors as recovered length, description of loose material, and corrections to lengths where the material expanded once unconfined. Comments about paint refer to portions of liner that were painted black on the outside before use to exclude light from the core. This anticipated the possibility of whole core sampling for optically stimulated or thermal luminescence dating (samples were taken, but no luminescence dating has been done).

scv-lith

- Lithology—The texture of each lithologic phase (primary, secondary, possibly tertiary) is described in terms of median grain size and subordinate sizes for the <2 mm fraction, as: sand, silty sand, sandy silt, silt, clayey silt, silty clay, sand-silt-clay mixtures, clayey sand, sandy clay, and clay. A standard grain-size card is used to calibrate size estimates. Where grains coarser than 2 mm exceed 15 percent, the modifier gravelly is added, and where they exceed 50 percent, the texture is gravel. Other lithologic descriptors include: clast-supported—sand and fines fill pore space, but gravel clasts are in contact with each other.
- Soils—Features of pedogenic soils (using the concepts and terminology of Birkeland, 1984) are described in several places in these tables: Basal Contact in scv-lith, Accessory in scv-accessory, and Remarks in scv-remarks
- The fields for Well, basic depths, Source, and Date of Entry are described above
- Lith1 (USC)—Field estimate of class in the Unified Soil Classification System for the primary lithology
- Lith1 Descr—Texture of the primary phase
- Lith2 (USC)—USC class of secondary phase
- Pct2—Volume percent of secondary phase
- Lith2 Descr—Texture of the secondary phase
- Lith3 (USC)—USC class of tertiary phase
- Pct3—Volume percent of tertiary phase
- Lith3 Descr—Texture of tertiary phase
- Bedding—Presence and thickness of bedding, as: bedding not observed, laminated, massive, thickly bedded (>dm), medium bedded (cm-dm), or thinly bedded (<cm)

- Grain Size—Range in grain size, in mm, of the size fraction less than 2 mm. See Remarks table for any comments about coarser grains
- Basal Contact—Nature of basal contact of described interval, as: sharp; slightly thicker clear; gradual; or even thicker diffuse (transition zone); contact topology as: smooth, wavy, or a more extreme irregular, broken (discontinuous), uncertain (indeterminable), or unknown (not observed)

scv-accessory

- The fields for Well, basic depths, Source, and Date of Entry are described above
- Accessory—Description of features of the material other than basic texture, such as sedimentary structures and bioturbation, sorting and rounding of grains, organic fragments, soil characteristics, carbonate, and degree of mechanical disturbance by coring. Each such feature is described for a given depth interval separately from others, such that described intervals for different accessories can overlap each other. The same depth interval can, for example, be separately described as "Slightly Disturbed," "No hydrocarbon indications," and "Bimodal sorting." More than 100 different descriptors are used.
- Abundance—The abundance of the accessory, where appropriate, such as accessory = "Ripup clasts," abundance = "Few-moderate (5-10%)"

scv-remarks

- The fields for Well, basic depths, Source, and Date of Entry are described above
- Remarks—Any additional comments about the sediment, such as maximum clast size, clast rock type, sedimentary structures, soil characteristics, color, coring issues such as mechanical disturbance, intrusion of drilling fluid, empty core space, and sediment infall. The entries are free form, with the longest approaching 450 characters. Quoted identifications (such as "gabbro") are visual interpretations that may not be completely accurate.

scv-color

- Colors—Primary and secondary colors of the core are described as soon as possible after the core is split, because oxidation can cause colors to change rapidly. Colors are recorded both as Munsell color notation and color names (Munsell Color, 2000).
- The fields for Well, basic depths, Source, and Date of Entry are described above
- Munsell1—Color notation for the primary color phase
- Color1 Descr—Color name for the primary color phase
- Munsell2—Color notation for the secondary color phase
- Color2 Descr—Color name for the secondary color phase

scv-penetrometer

- A quick measure of the unconfined compressive strength of cohesive sediment is determined using a pocket penetrometer (the CL-700 tool manufactured by Soiltest—now ELE International). The spring-mounted probe is pressed into the flat surface of the core until a penetration of 1 cm is achieved, and the maximum load required is recorded in tons per square feet. Loads in excess of 4.5 ton/ft^2 (the maximum measurement for this instrument) are recorded as >4.5 tons/sq. ft., and the degree of penetration at refusal is recorded as a percentage of the required 1-cm depth of penetration.
- The fields for Well, basic depths, Source, and Date of Entry are described above
- UCS (ton/ft^2)—Measures unconfined compressive strength in tons per square foot
- Remarks—Any comments about the measurement or the material, including the percent depth of penetration for tests where the probe reaches the 4.5 ton/ft^2 maximum at less than 1 cm penetration.
- Lith Descr—Texture of the measured sediment (from the scv-lith table)

Appendix B. Well Correlation Sections

The wells with driller's logs in our primary dataset (104 wells, excluding 917) are here interleaved with the geophysically logged wells of figures 11 and 14 (21 wells, excluding HTOR) along the section lines shown in figure B1 and, using the symbology of figure B2 (and see figs. 4 and 5*A*), are shown in figures B3–B21. The result is to greatly expand the framework defined by those wells with geophysical logs both by filling gaps and by expanding the areal coverage. Because these additional wells are all represented by driller's logs, they are generally less confident representatives of the stratigraphic section than are the geophysical logs. Well 917 is not included because it contains control only for cycle 1; well HTOR is excluded because it lies west of the Monte Vista frontal fault.

The diagram for each well in a section shows the well column in gray overlain by the logs, coarse intervals, and bedrock (if present). The wells are hung from a horizontal line, and thus compare depth, not elevation. The maximum difference in ground elevation within the well dataset is 236 ft (excluding HTOR), with surface elevations ranging from near sea level around the bay to as high as 200–239 ft near the heads of the alluvial fans. See data files bndys.xls and subdivs.xls (appendix E) for additional details.

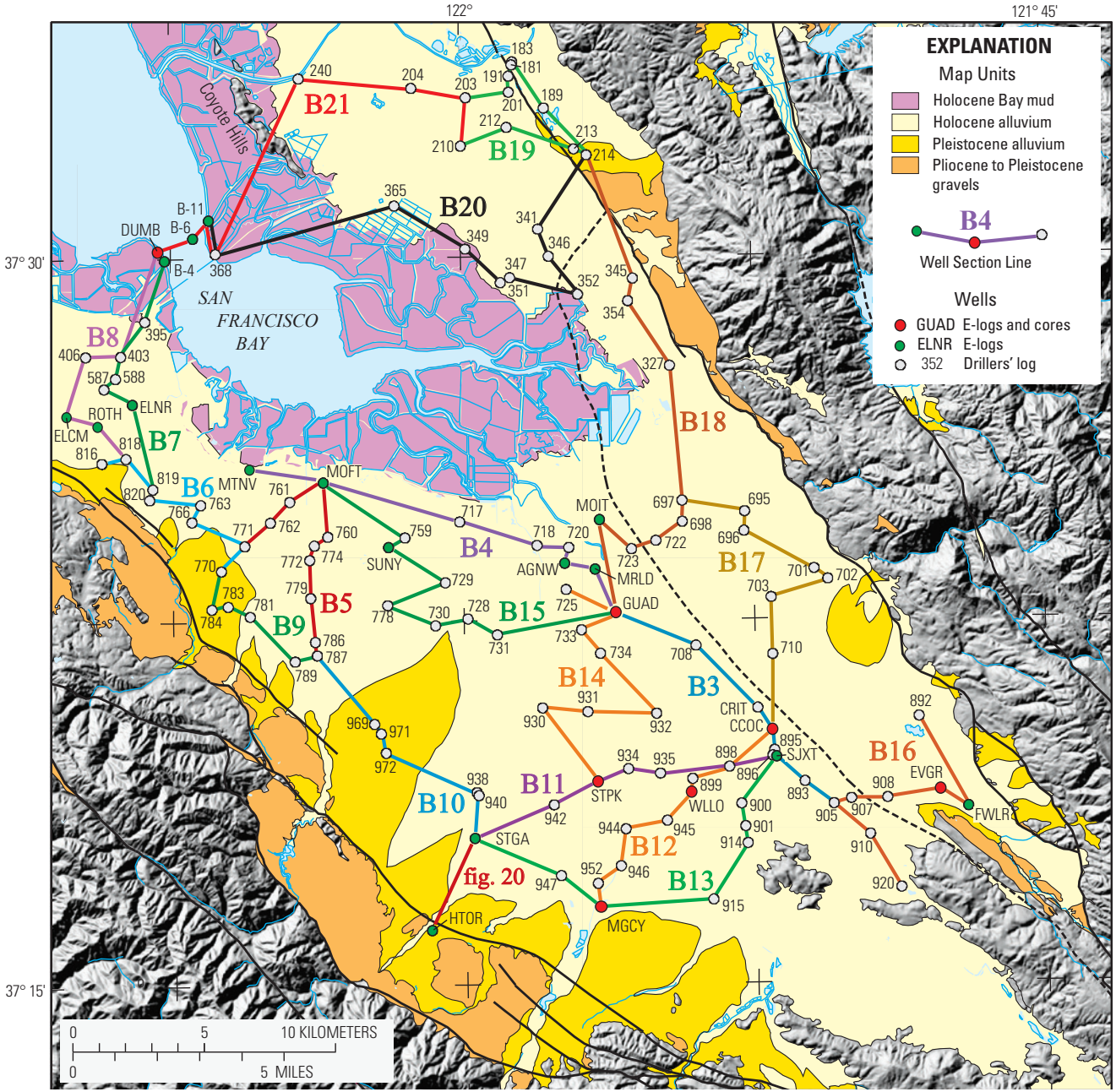

Figure B1. Map showing locations and numbers of the well sections in figures B3-B21 and in figure 20, together with the wells used in those sections. These wells, identified by well code, constitute the principal suite of wells used in this study. Surface geology and shaded relief as for figure 2.

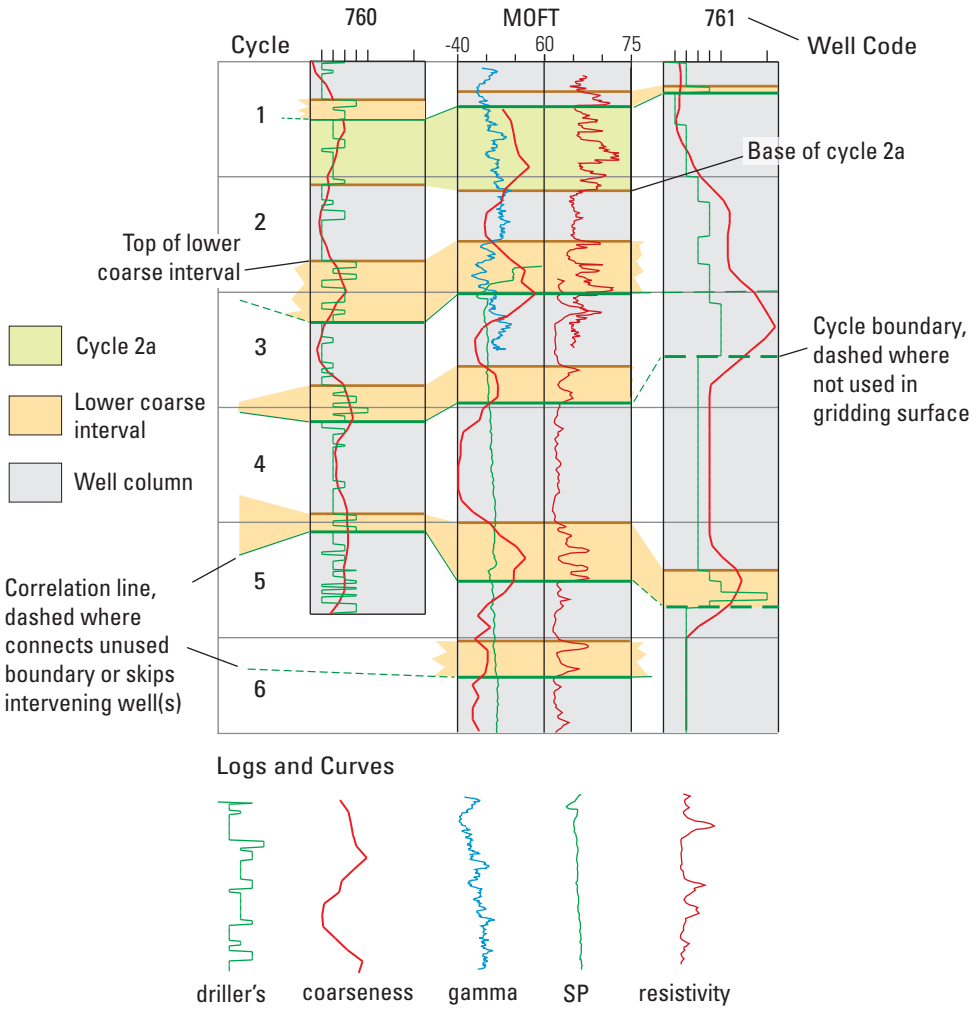

Figure B2. Explanation of symbols used in figures B3-B21. See also figures 4 and 5*A*, which provide explanation for the symbols used in the similar well diagrams of figures 5*B*, 14, and 15. Each well is identified by a well code and represented by a column within which the log information is plotted as a function of depth. For wells with geophysical logs, the column is divided into two parts vertically with different logs plotted in each. Values for the logs increase to the right, with resistivity typically ranging from 0 to 75 or 100 ohm-meters and natural gamma from 0 to 100 API units. Only one value is shown at the centerline, generally the high end of the left hand scale, as the resistivity scales all start at 0. Numeric driller's logs have values of 1 to 5, and 9. Values for the coarseness curve range from 0 to 100 percent within its column.

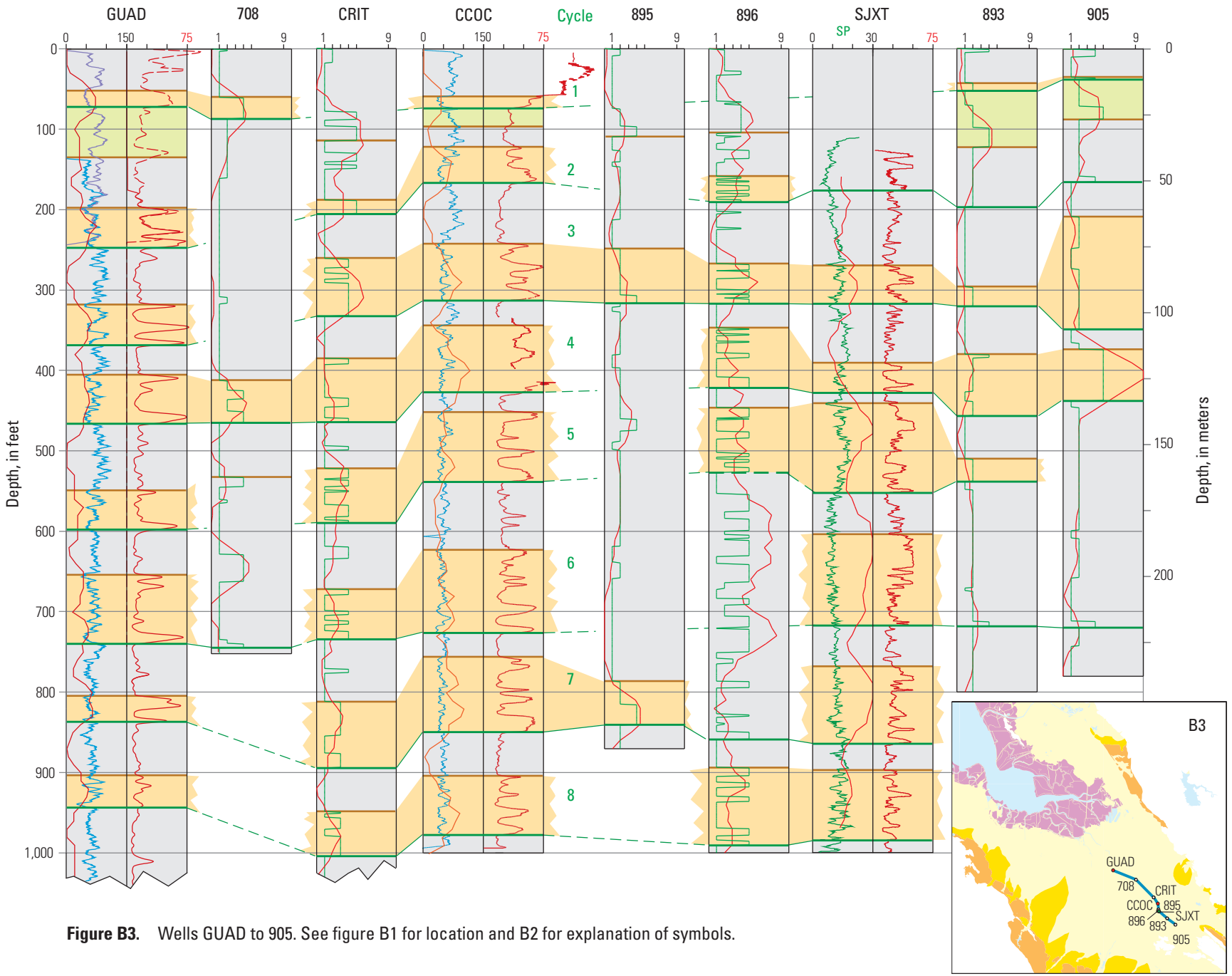

Figure B3. Wells GUAD to 905. See figure B1 for location and B2 for explanation of symbols.

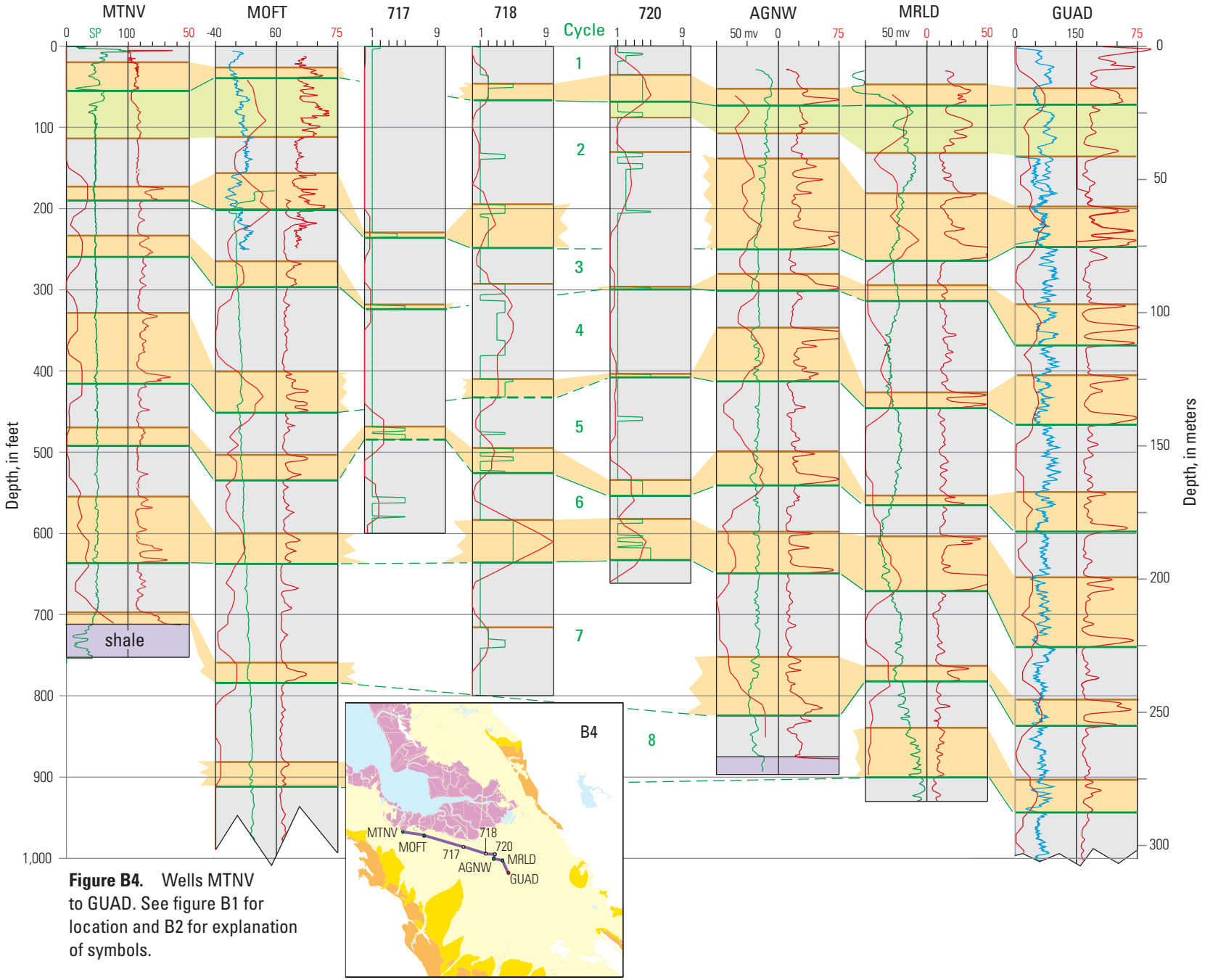

Figure B4. Wells MTNV to GUAD. See figure B1 for location and B2 for explanation of symbols.

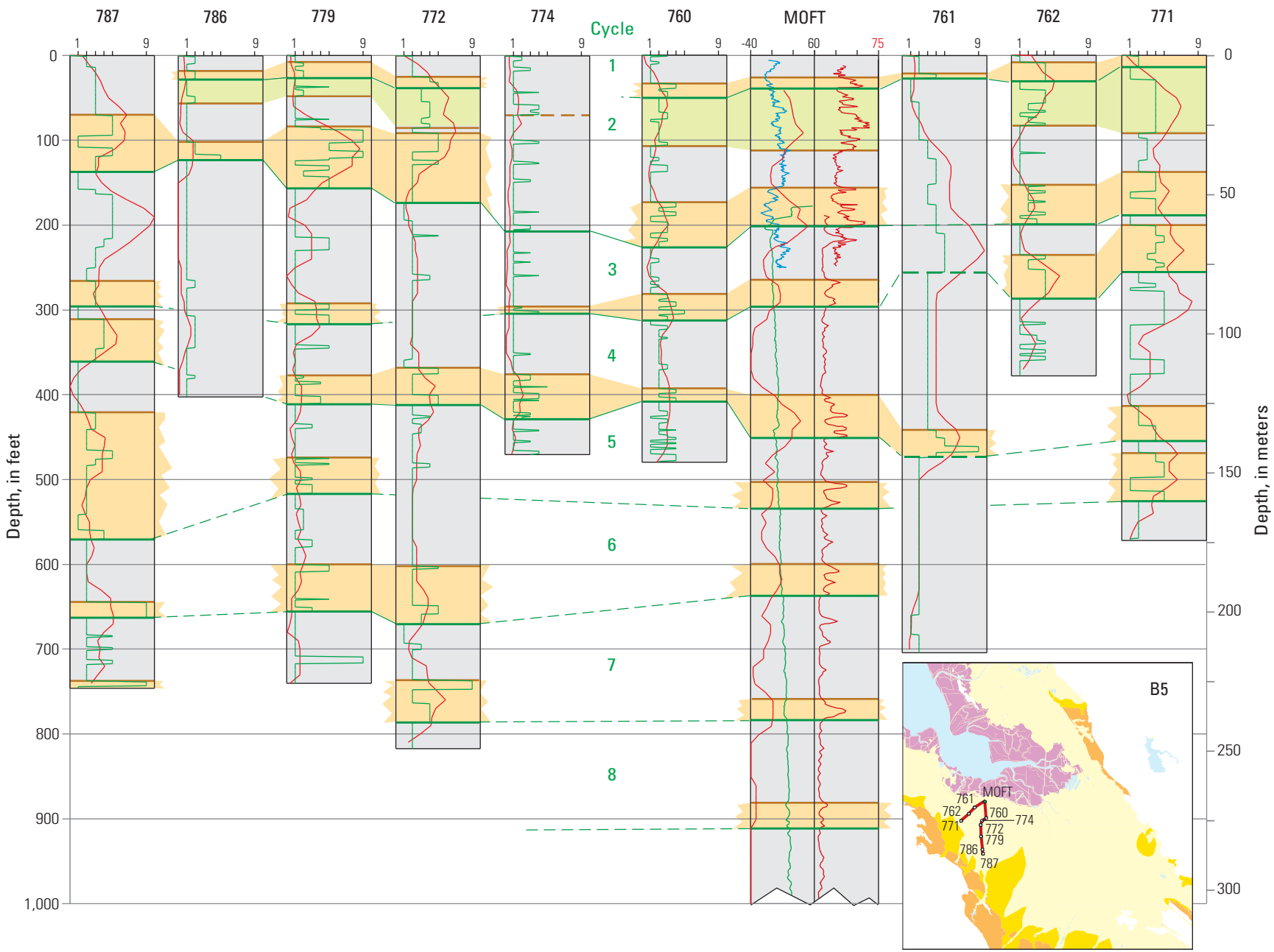

Figure B5. Wells 787 to 771. See figure B1 for location and B2 for explanation of symbols.

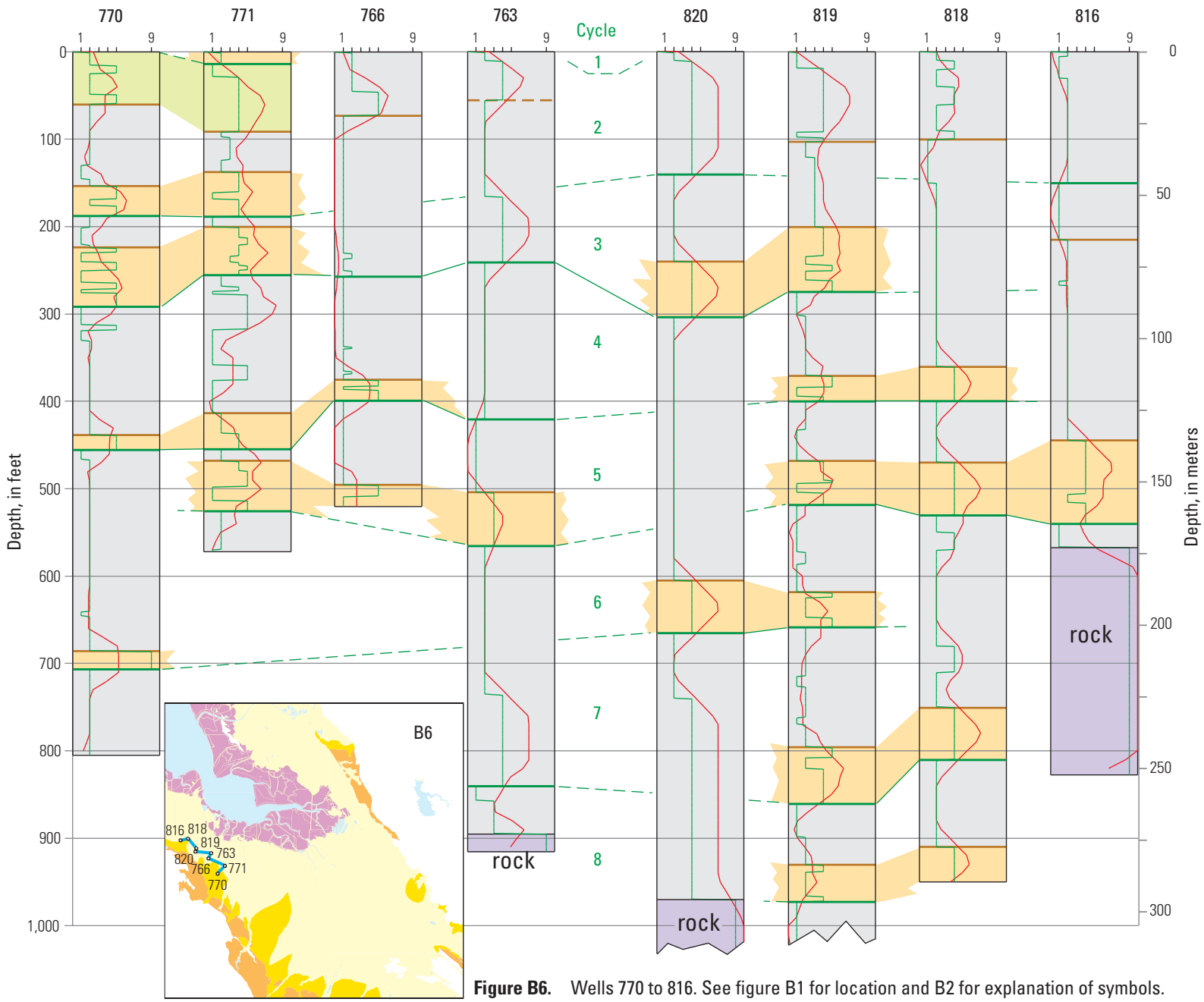

Figure B6. Wells 770 to 816. See figure B1 for location and B2 for explanation of symbols.

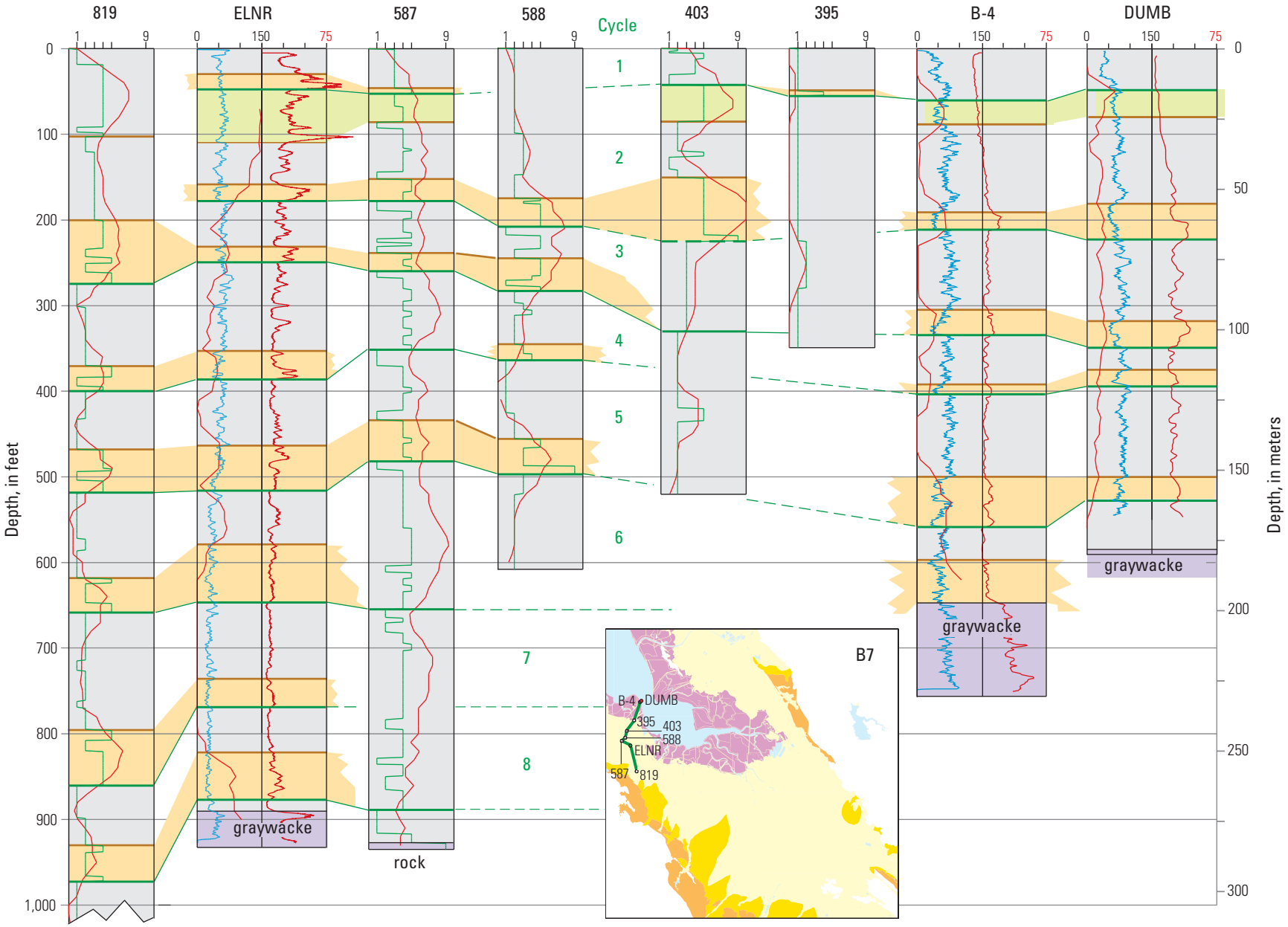

Figure B7. Wells 819 to DUMB. See figure B1 for location and B2 for explanation of symbols.

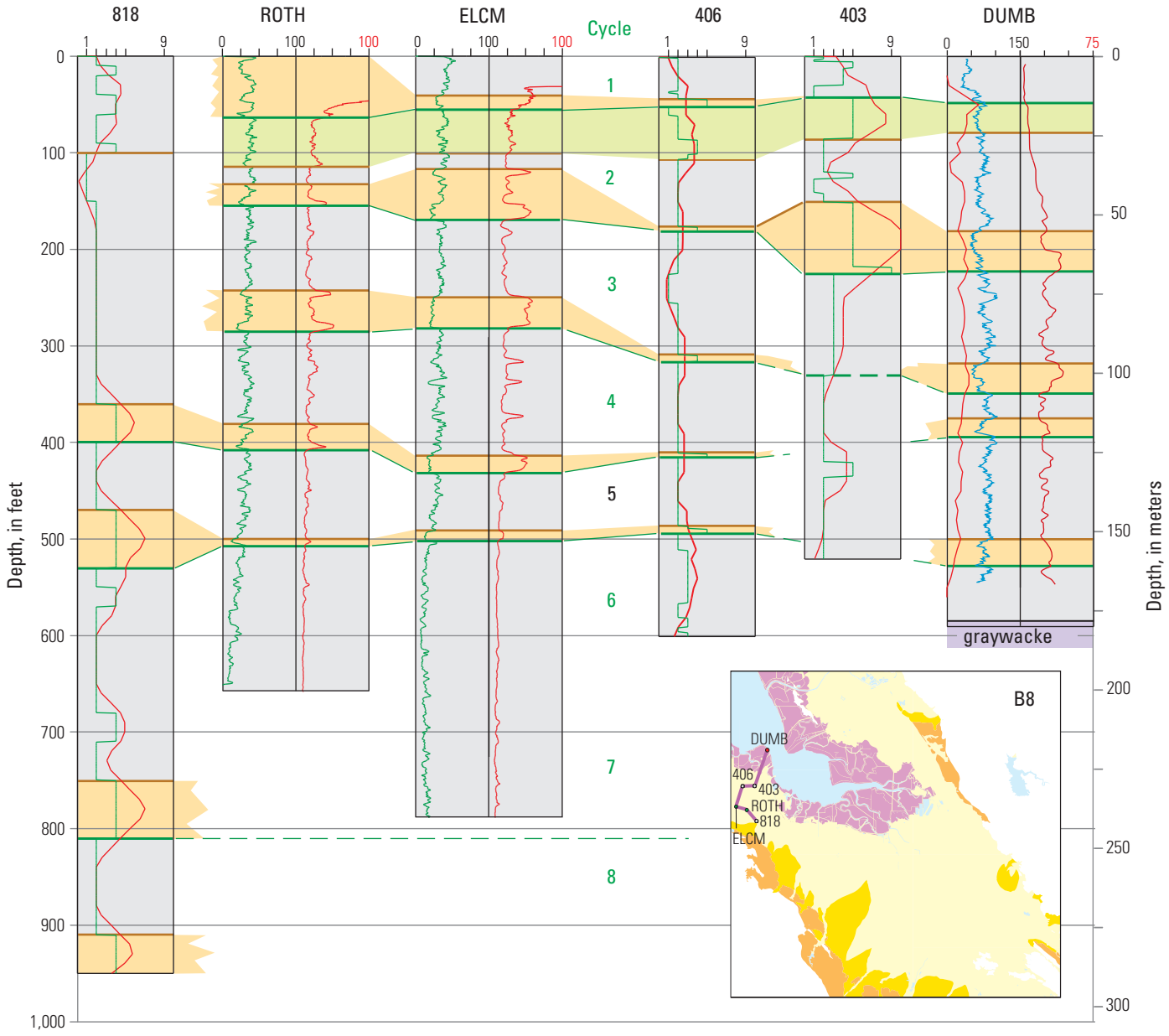

Figure B8. Wells 818 to DUMB. See figure B1 for location and B2 for explanation of symbols.

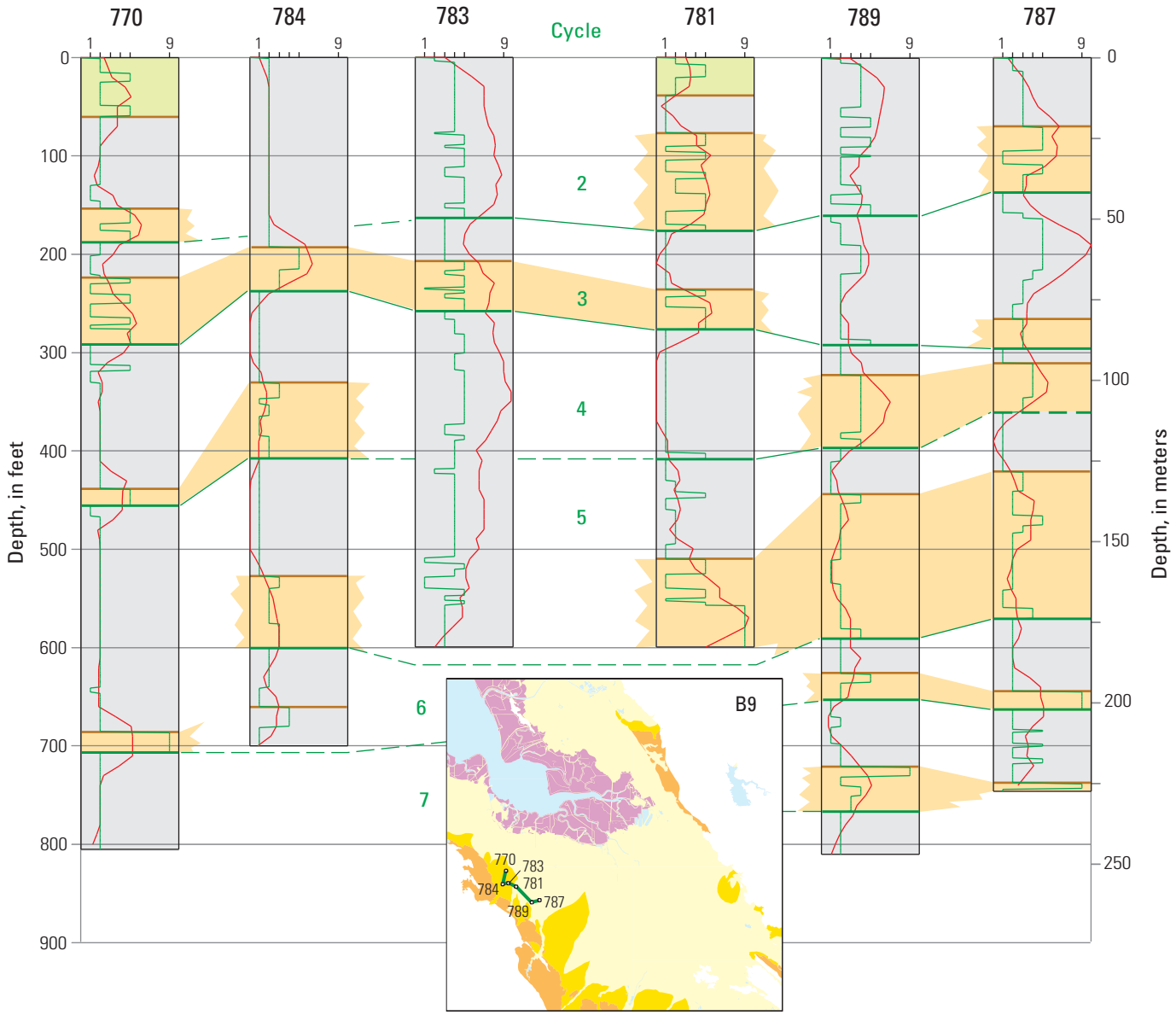

Figure B9. Wells 770 to 787. See figure B1 for location and B2 for explanation of symbols.

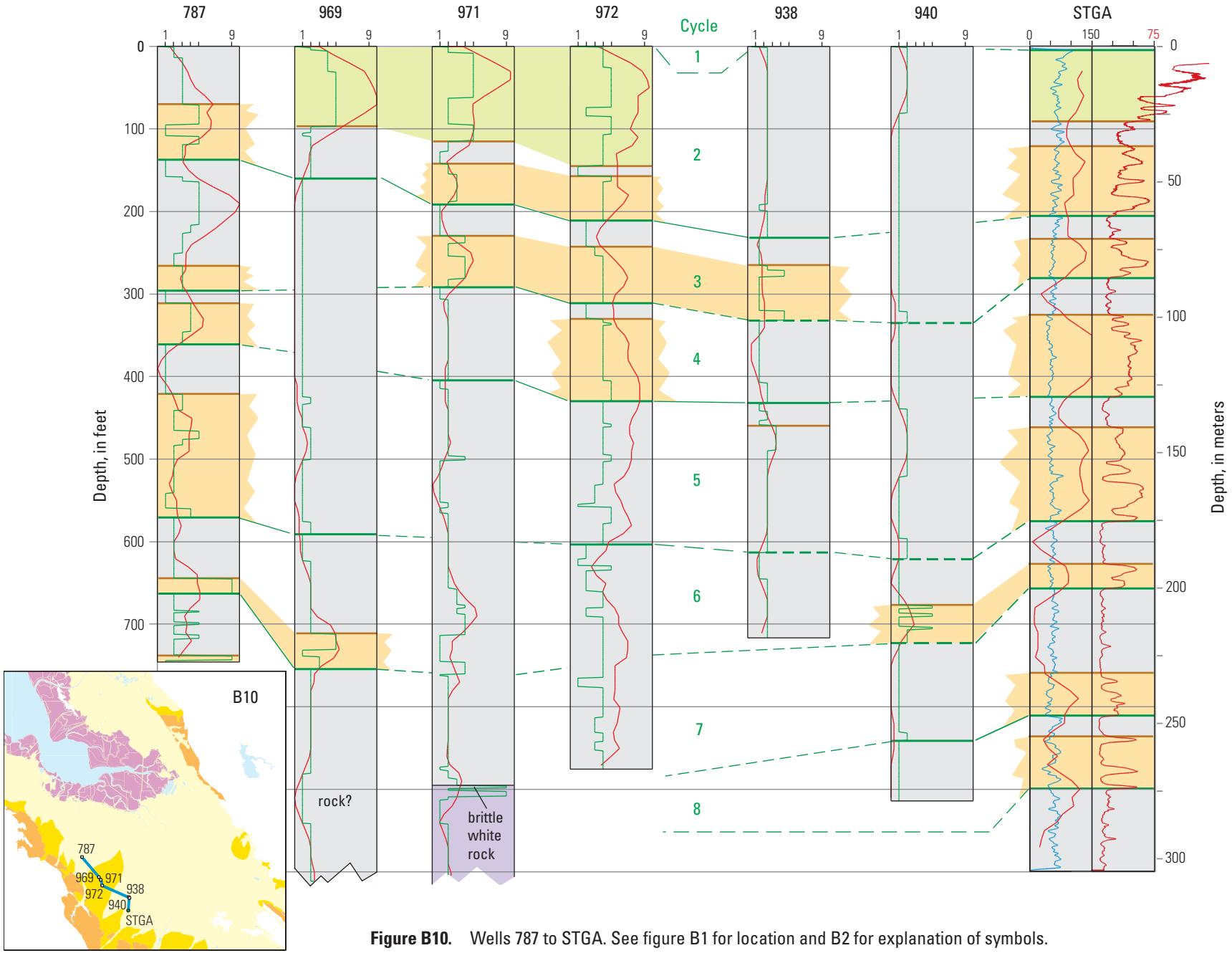

Figure B10. Wells 787 to STGA. See figure B1 for location and B2 for explanation of symbols.

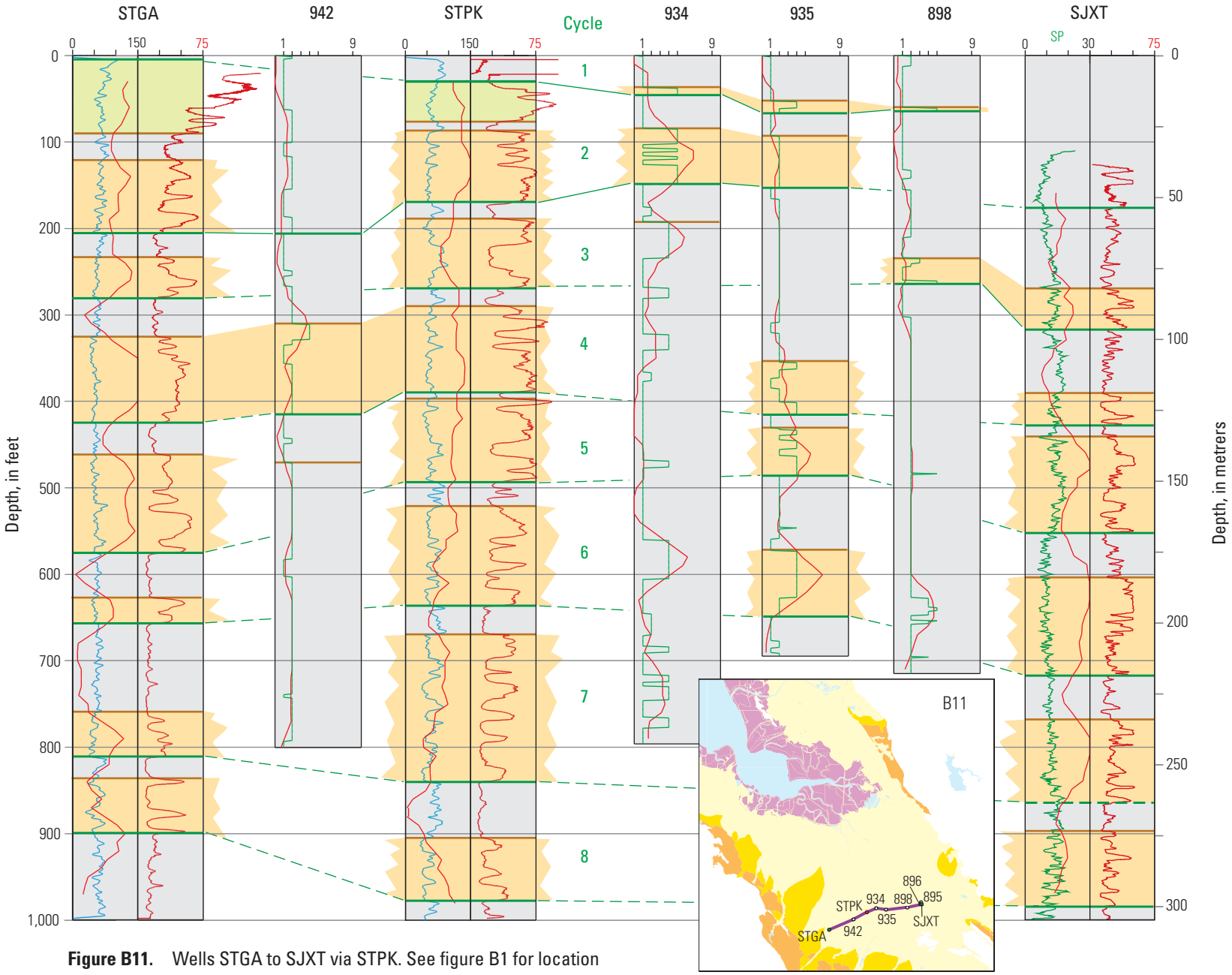

Figure B11. Wells STGA to SJXT via STPK. See figure B1 for location and B2 for explanation of symbols.

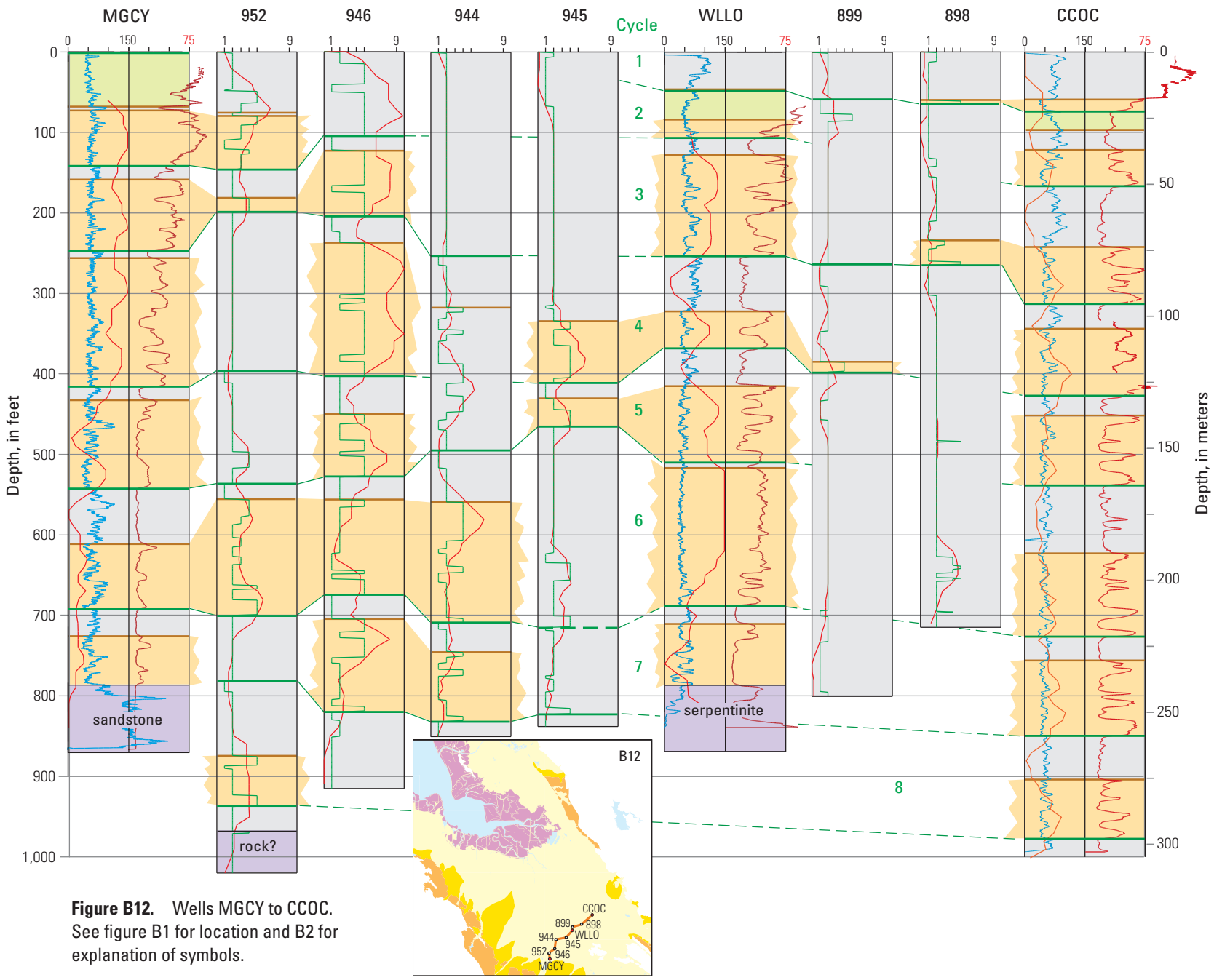

Figure B12. Wells MGCY to CCOC. See figure B1 for location and B2 for explanation of symbols.

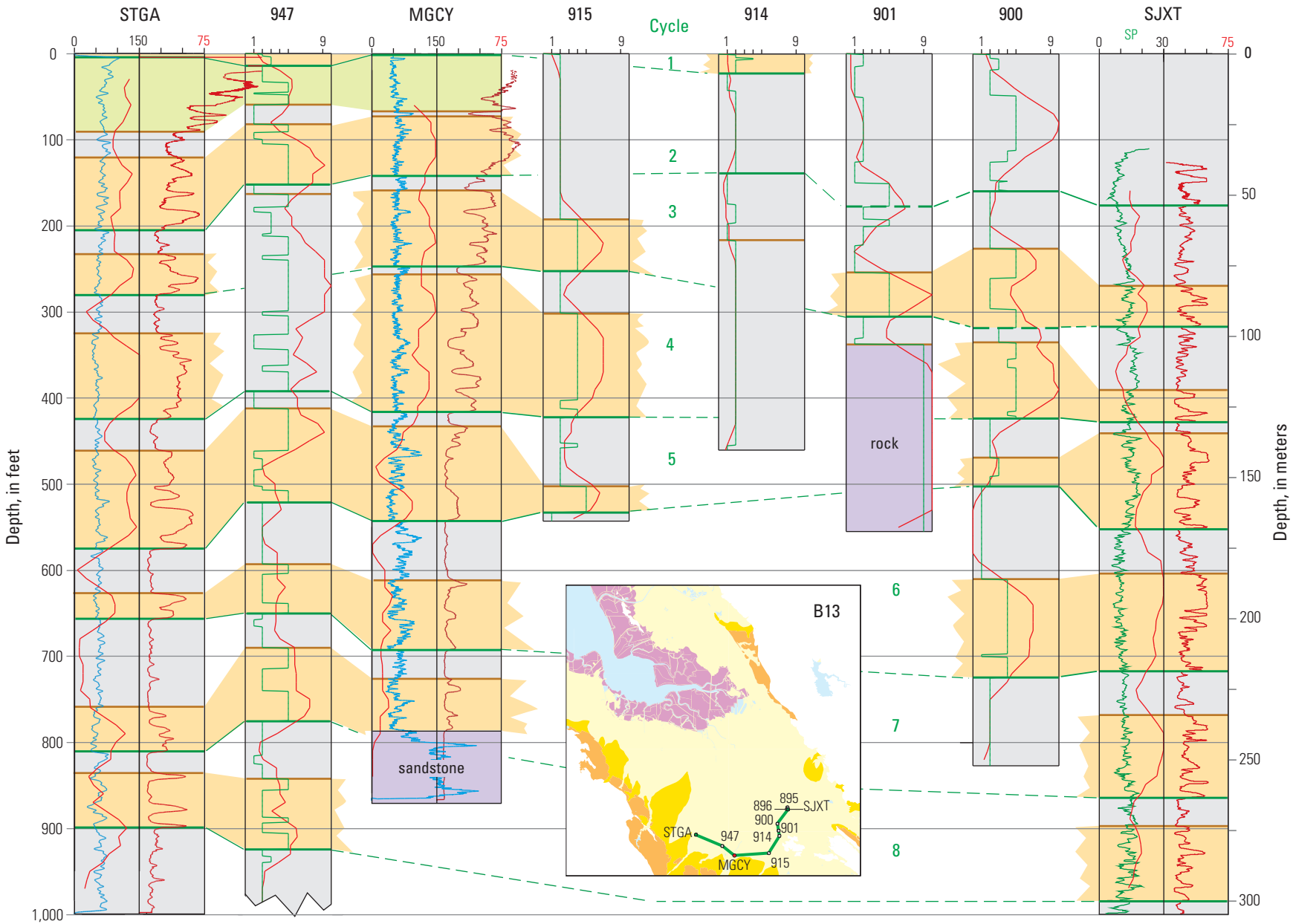

Figure B13. Wells STGA to SJXT via MGCY. See figure B1 for location and B2 for explanation of symbols.

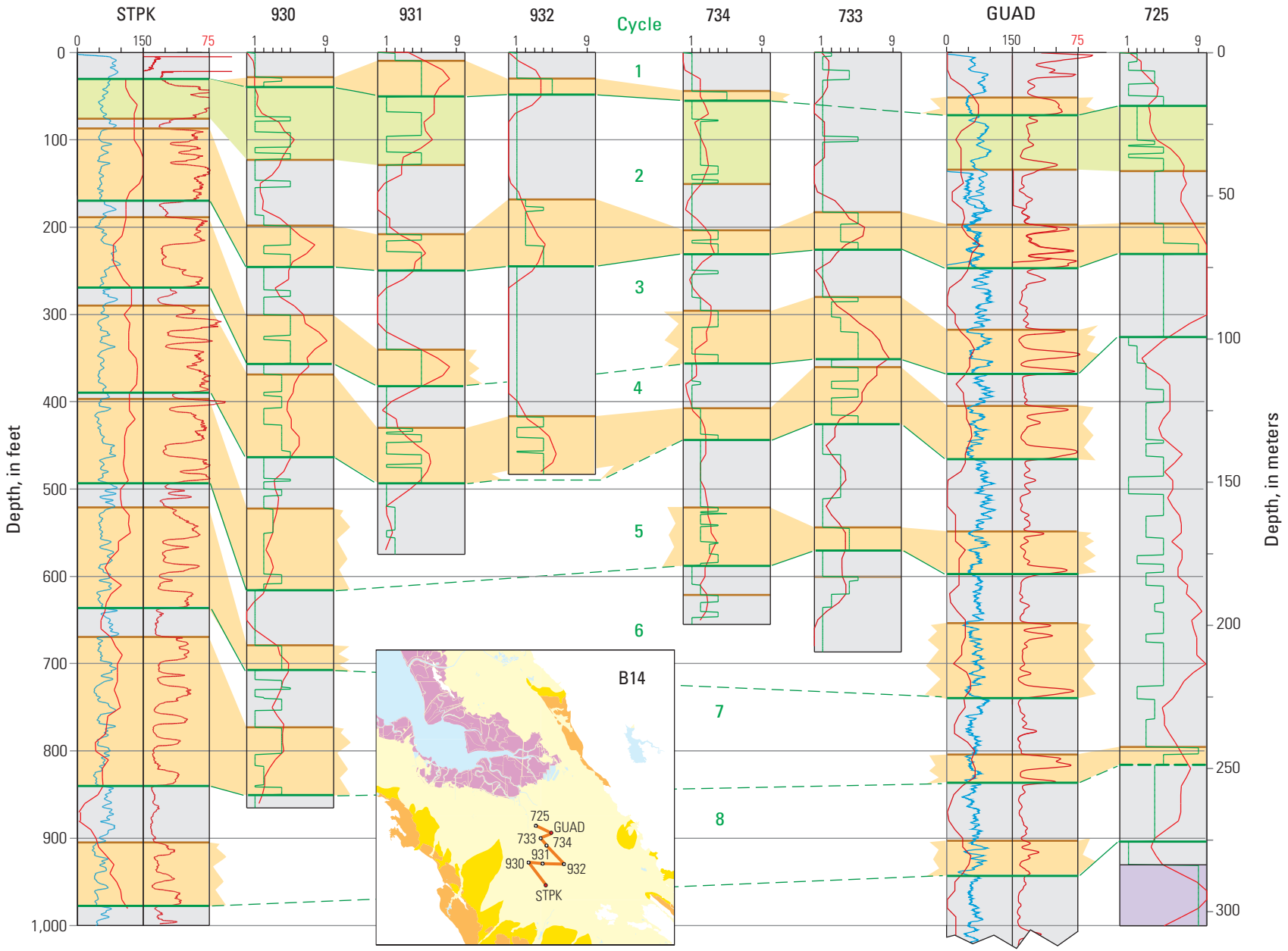

Figure B14. Wells STPK to 725. See figure B1 for location and B2 for explanation of symbols.

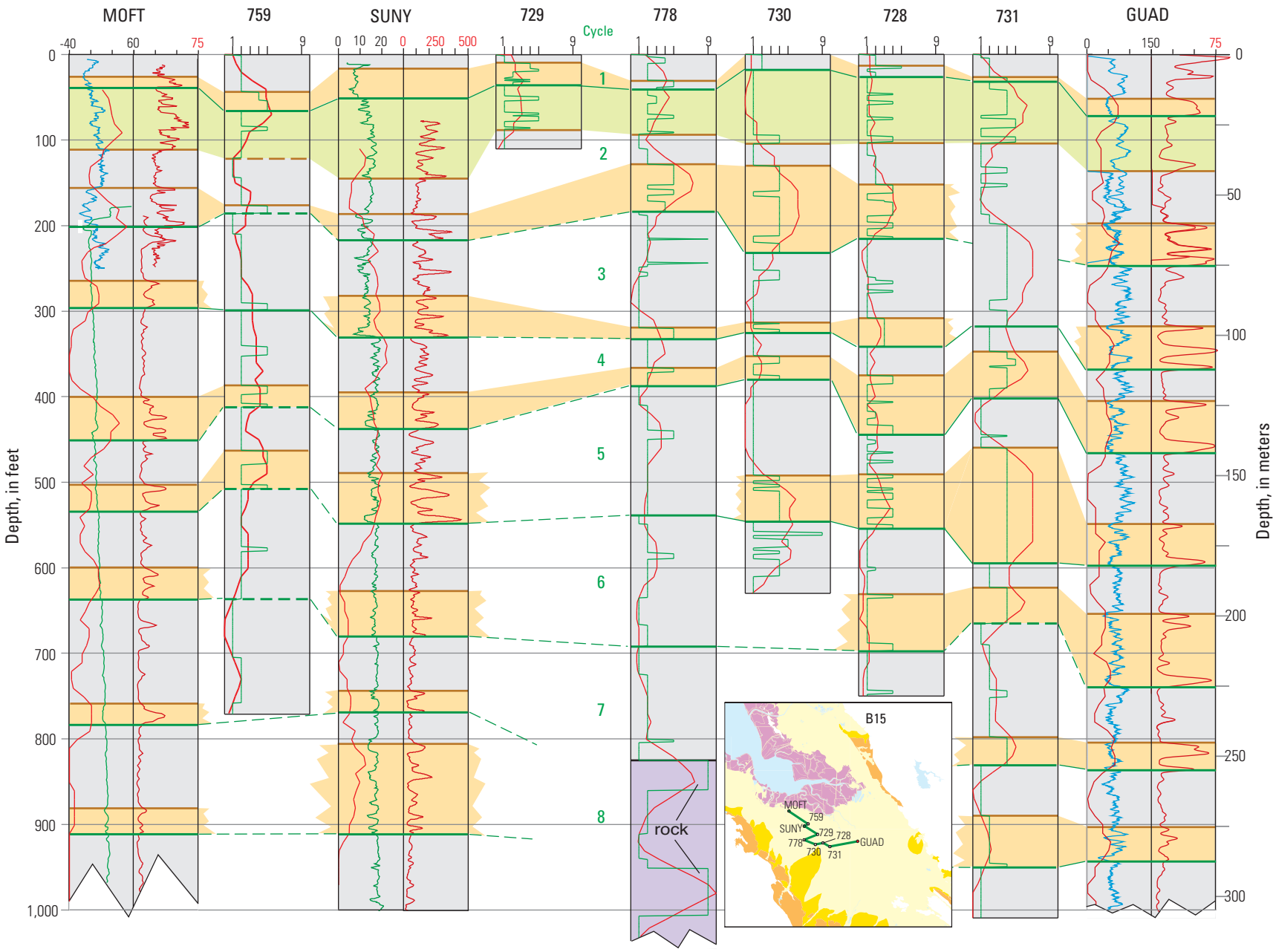

Figure B15. Wells MOFT to GUAD. See figure B1 for location and B2 for explanation of symbols.

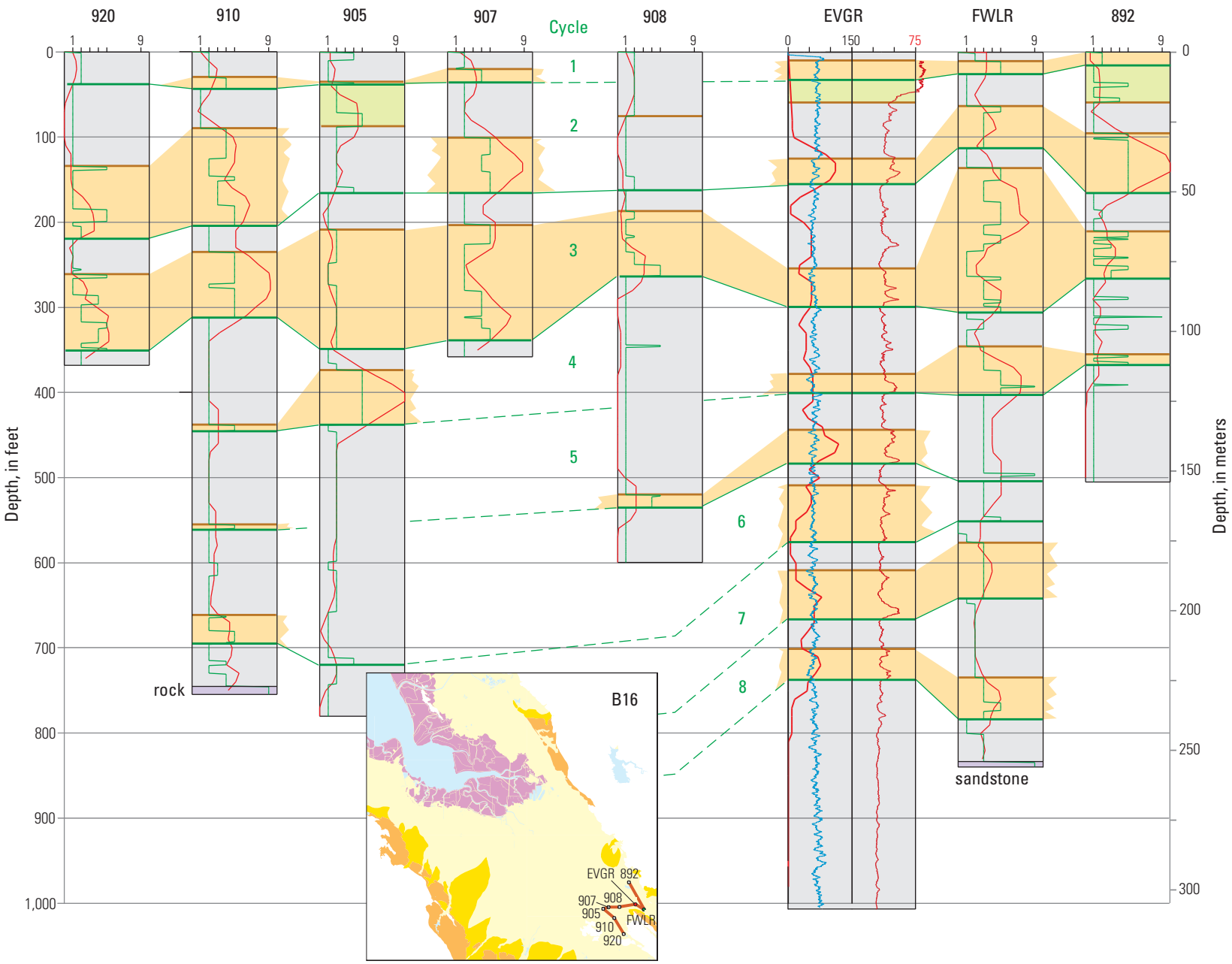

Figure B16. Wells 920 to 892. See figure B1 for location and B2 for explanation of symbols.

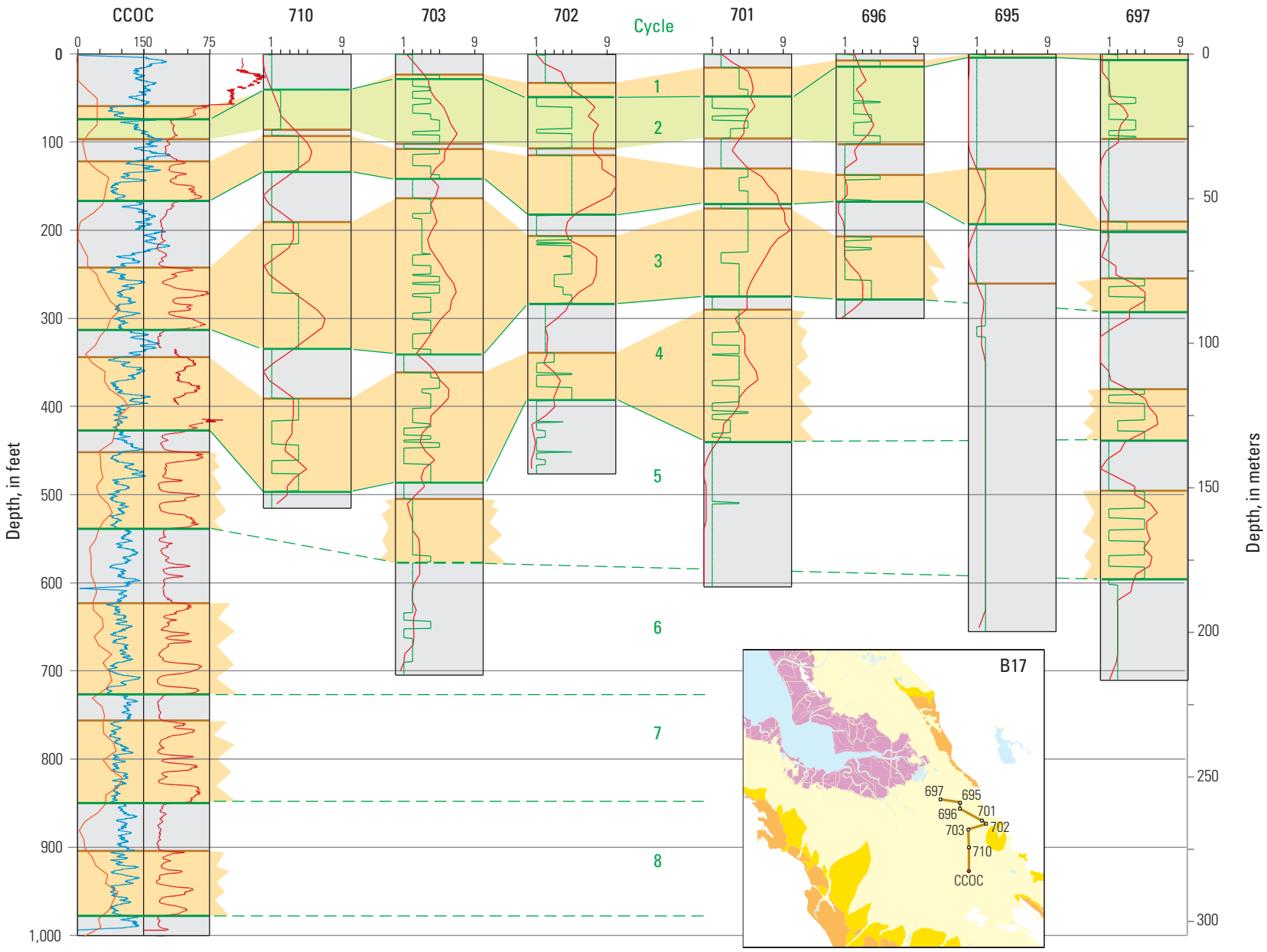

Figure B17. Wells CCOC to 697. See figure B1 for location and B2 for explanation of symbols.

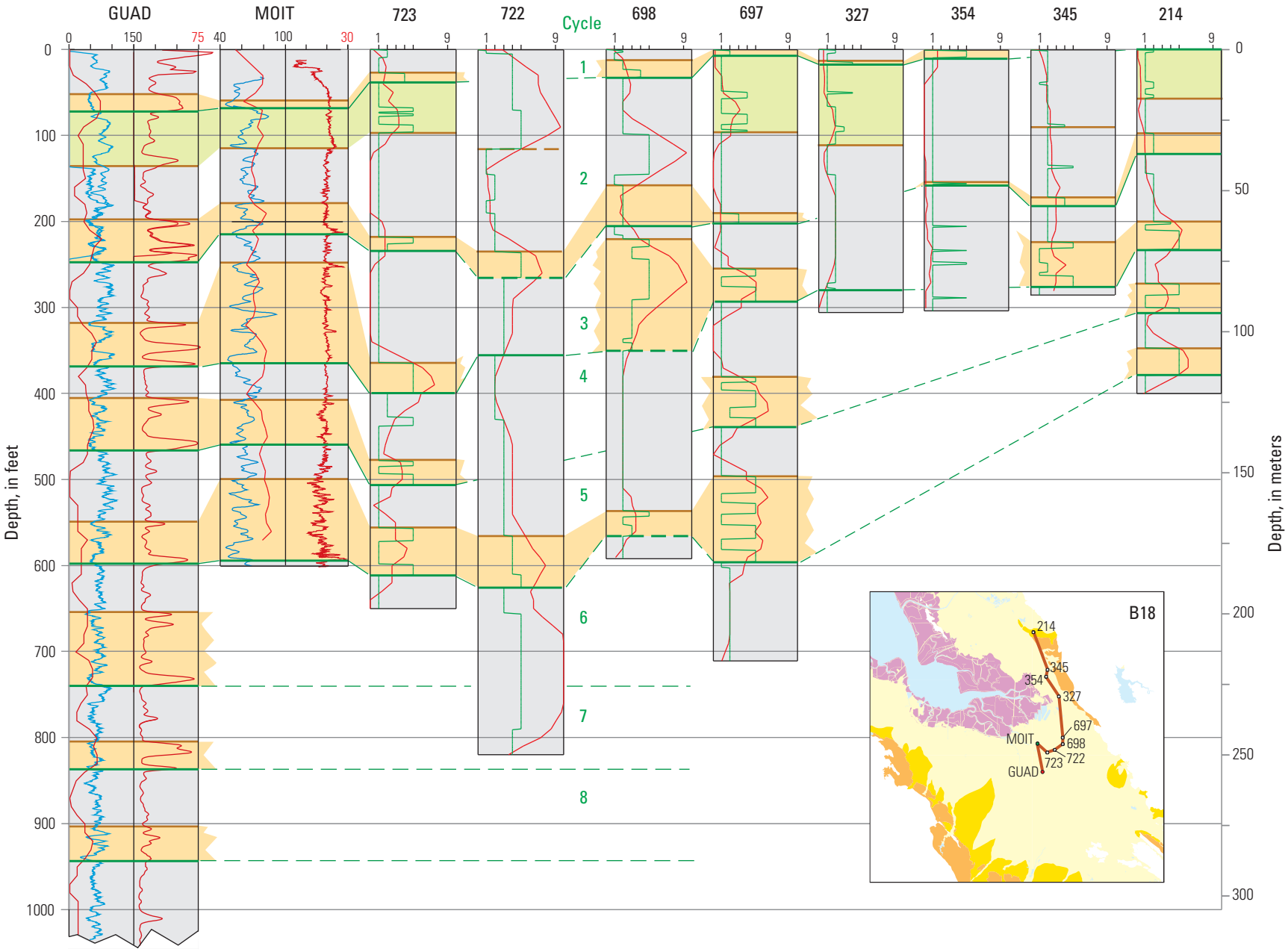

Figure B18. Wells GUAD to 214. See figure B1 for location and B2 for explanation of symbols.

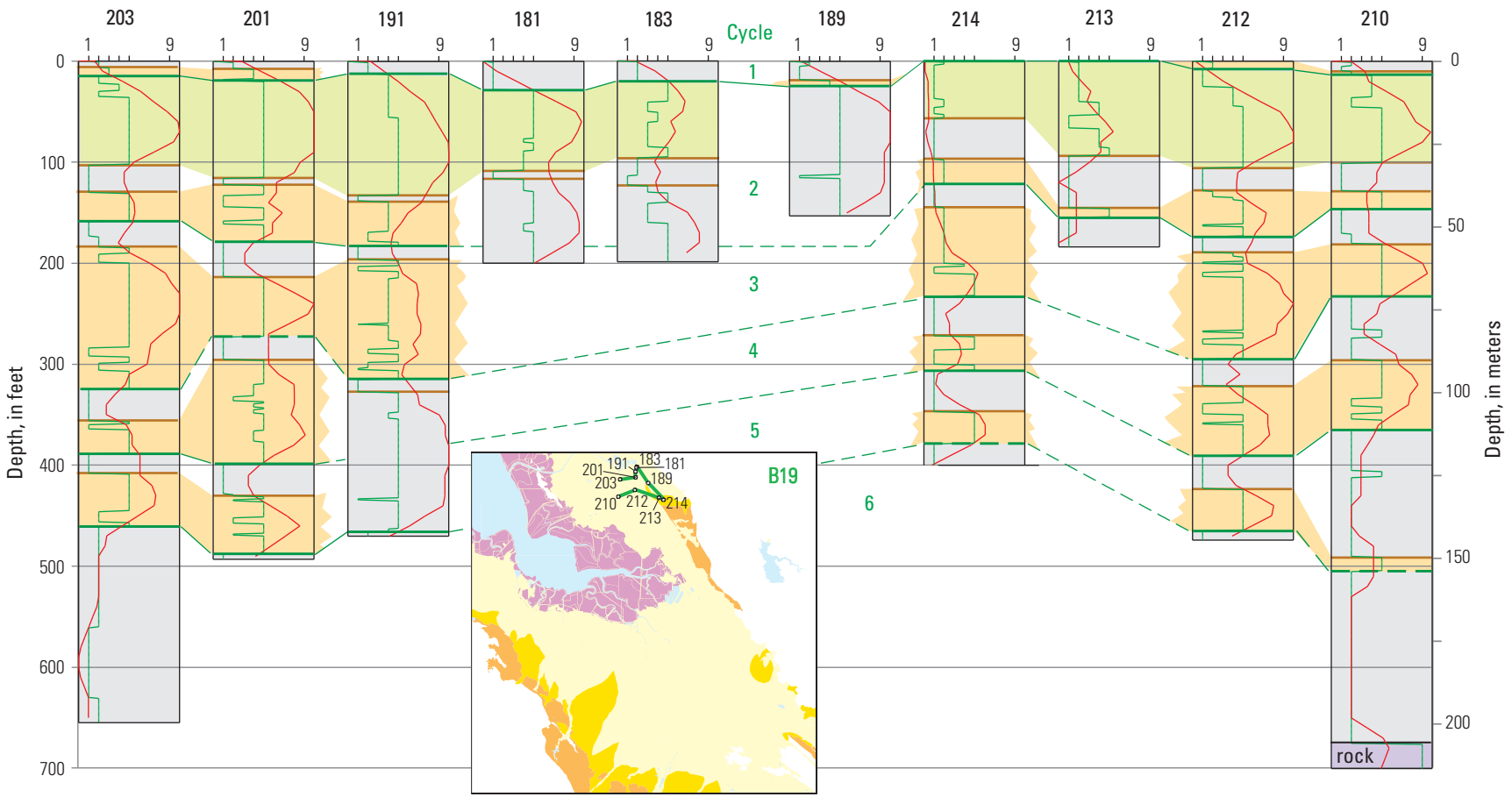

Figure B19. Wells 203 to 210. See figure B1 for location and B2 for explanation of symbols.

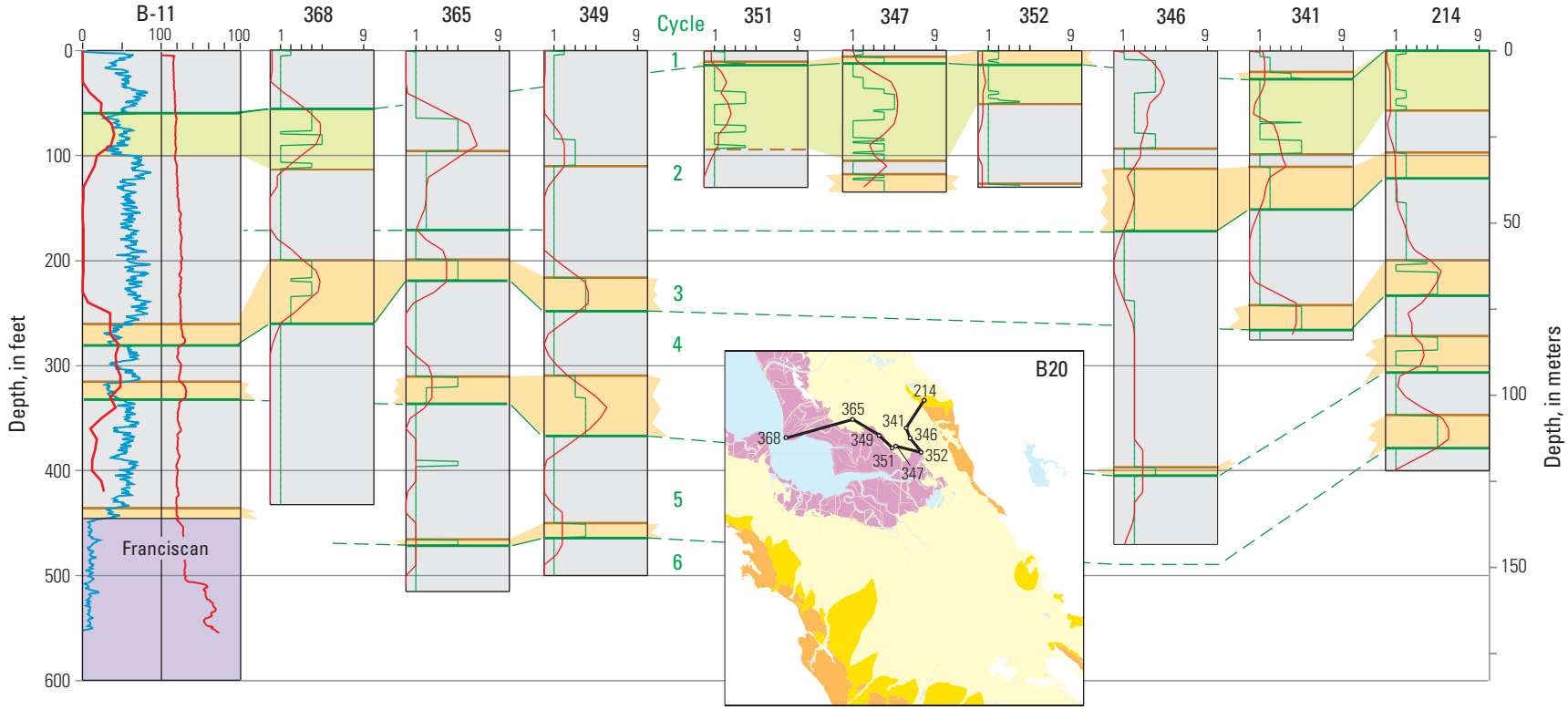

Figure B20. Wells B-11 to 214. See figure B1 for location and B2 for explanation of symbols.

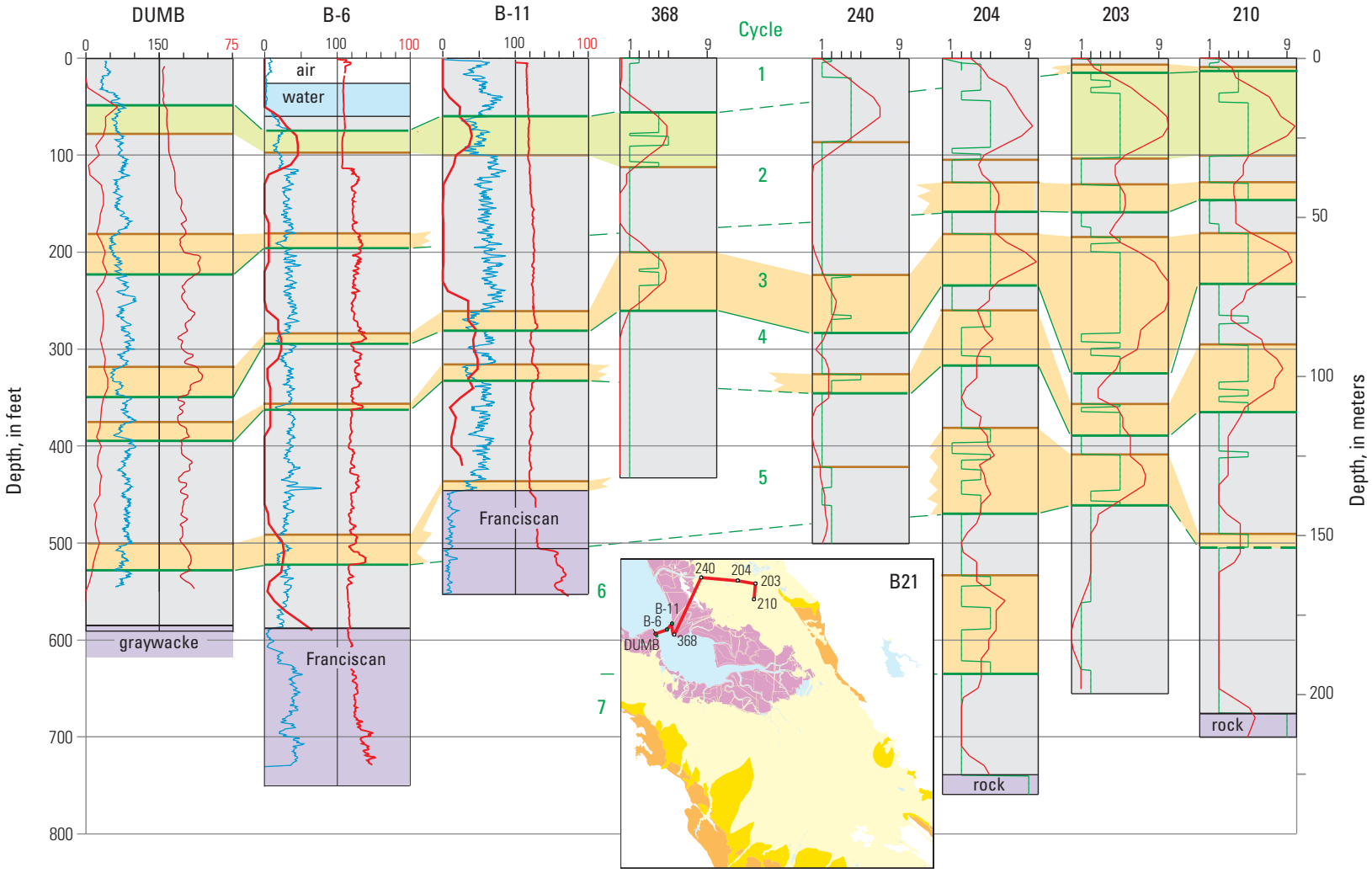

Figure B21. Wells DUMB to 210. See figure B1 for location and B2 for explanation of symbols.

The shallow logs used to supplement the deep logs in well MOFT (figs. 11*B*, 14*B*, 15, and B4, B5, and B15) were obtained from a log of a nearby shallow geotechnical well that was collected in 1988 as part of a study at Moffett Field, California, by Geo-Hydro-Data Inc. of Tehachapi, California, for The Water Development Corporation, apparently under contract to the U.S. Navy.

Appendix C. Gridding the Cycle Boundaries and Other Properties

Available control was used to prepare spatially continuous elevation surfaces (digital raster grids) for the cycle boundaries, the base of the upper coarse interval (C2a) in cycle 2, the internal boundaries between upper fine and lower coarse intervals in each cycle (top/bottom, or T/B, boundaries), and the buried bedrock surface. From these surfaces, grids representing the thickness of the cycles and of their upper fine and lower coarse intervals were prepared. Grids were also prepared for the varying abundance of coarse layers within the lower coarse intervals of the cycles. The grids are necessarily rectangular, and all of them cover most or all of the full study area, regardless of the extent of control for a particular surface. In the map presentations of plates 1 and 2, the outlying areas for which there is no control are masked as areas of no data and bedrock, and in some of the grids those areas have null values (NODATA).

Several gridding routines available in the commercial geographic information system (GIS) ArcInfo were tested before making these grids, including various splines and the function TOPOGRID, which was designed for topographic surfaces. Graham and Wentworth (2005) had previously selected TOPOGRID in a similar comparison. In the present test, the splines produced relatively high-amplitude bulges in uncontrolled areas, with the result that adjacent surfaces tended to intersect each other locally, a problem that was much less common with the TOPOGRID surfaces. For these reasons, and the fact that the cycle boundary and bedrock surfaces were once topographic surfaces, TOPOGRID was used for all the gridding. It did prove necessary to limit the number of TOPOGRID iterations severely, however, to avoid progressively increased departures from the control elevations; here 4 iterations were used rather than the default of 30. The resulting gridded surfaces are generally smooth, with only modest high and low bulges in uncontrolled areas, although for some grids it was necessary to construct additional control points to limit such anomalies. Note that at the rising outer edge of an area of control the gridded surface map may turn downward or continue upward, thus defining uncontrolled arches or ramps.

Cycle Boundaries

The cycle boundary surfaces (plate 1, maps 1–10) were prepared sequentially, first using all available well control (see appendix B), then further constrained by rejecting any anomalous control points, and finally adding any needed constructed points (the control points used, those rejected, and those constructed for these surfaces are shown on the maps of plate 2, row A). The results of the initial gridding were inspected for local distortions unreasonable in an erosional topographic surface, the wells responsible for any such anomalies were rejected, and the surfaces then remade (see main text for discussion). The number of wells with depths (and therefore elevations) for individual cycle boundary surfaces ranged from 92 to 82 for cycles 1 through 4, 66 for cycle 5, and thence decreasing from 41 to, finally, 19 for cycle 8. Wells rejected as having anomalous elevations did not exceed 8, and for most cycles were 5 or fewer (table C1).

The testing of each gridded cycle boundary involved examination of the gridded surface itself, both as an image and as contours generated from that surface, but also by examining the cycle thickness determined by subtracting each cycle boundary from the overlying one. For cycle 1, this required a topographic surface, a smoothed version of which was prepared by intersecting a 500-m grid of points with a 30-m digital elevation model and then gridding the resulting elevations. The sources for the topographic data are Graham and Pike (1998) for 30-m subaerial data and a National Oceanic and Atmospheric Administration (NOAA) Web site accessed in 2005 for 30-m estuarine bathymetry of San Francisco Bay (the 2014 Web address is http://estuarinebathymetry.noaa.gov/bathy_htmls/P090.html).

Control for the base of cycle 1 involved both elevations in wells, of which there were 84, and, beyond the outer limit of cycle 1 deposits, a scattering of points on the surfaces of exposed cycle 2 sediment at the heads of the alluvial fans (Pleistocene alluvium of fig. 2). Local uncontrolled bulges in the surface east and west of the south end of San Francisco Bay were constrained with three additional control points from the dataset of the California Geological Survey (Clahan and others, 2002). In some uncontrolled outer areas where the cycle is thin, the cycle 1 base rose above the smoothed topographic surface. There, the cycle 1 surface was arbitrarily set 1 foot below

Table C1. Wells rejected in the cycle-boundary gridding process.

Cycle	Rejected Wells
1	0 of 85
2a	5 of 87: 351, 722, 759, 763, 774
2	4 of 96: 722, 759, 901
3	7 of 99: 403, 698, 761, 900, 938, 940
4	3 of 86: 718, 759, 761
5	8 of 74: 210, 698, 703, 717, 759, 896, 938, 940
6	4 of 45: 731, 759, 940, 945
7	1 of 29: 725
8	0 of 22

that topographic surface (see plate 2, map 1, adjusted areas). No other cycle boundary encountered this intersection problem, but some further adjustments (see below) were required to prevent intersection of the internal top/bottom surfaces with the overlying cycle boundaries.

The well control for cycles 3, 5, and 8 was supplemented east of the Silver Creek Fault with points determined from the Evergreen seismic reflection profile (see fig. 13 and discussion in the section on "Mapping the Cycles"). There were 10 such points used for cycle 3, 12 for cycle 5, and three for cycle 8.

Top/Bottom Surfaces, Thicknesses, and Abundance of Coarse Sediment

Control for gridding the top/bottom internal boundary for each cycle (plate 2, maps 10–18) was more limited than for gridding the base of the cycle, because information for that internal boundary was not available for all the wells used to define the cycle base. This resulted in a decrease in the number of control wells for most cycles by 0 to 6, by 9 for cycle 3, and by 16 for C2a. Testing for intersection of these internal boundaries with the overlying cycle boundaries in areas of no control indicated a number of problems. To resolve these, one or two additional control points were created using elevations and thicknesses from nearby wells for most of the cycles (shown on the maps of plate 2). Cycle 1 posed a special problem, because it is relatively thin but also because available well detail tends to be poor and a coarse bottom is not everywhere present or discriminated. As a result, to prevent the scattered negative thicknesses that resulted, the C1 top/bottom surface was set equal to the basal C1 surface where those negatives occurred. Inasmuch as the internal top/bottom boundaries occur within continuous alluvial depositional sequences and are not necessarily the same age everywhere, the few anomalous depressions were not corrected.

The cycle thickness grids were determined by subtracting the cycle boundary elevation grid from the next overlying cycle boundary. Thickness grids for the upper fine and lower coarse intervals were similarly determined from the cycle boundary grids and grids for the top/bottom internal surfaces. Grids for the percentage of coarse sediment and the aggregate thickness of that sediment in the lower coarse intervals (plate 2, maps 19–36) were determined from the wells and values listed in data table subdivs.xls. The control points shown for these maps on plate 2 are those well locations. No additional constraints were imposed for these grids.

Bedrock Surface

Control on the position of the buried bedrock surface (plate 1, map 11) is provided both by wells that bottom in rock and by those that do not but are deep enough to constrain the surface. Other control is provided by seismic reflection profiles by Williams and others (2002, 2004, and 2005), refraction profiles by Hazelwood and bedrock wells reported by him (1974 and 1976), and the elevation of mapped depositional contacts of alluvium on bedrock. The digital GIS vector map bdrk (see appendix E) contains the data points used from these sources, and for the bedrock wells (other than those from Hazelwood) includes a brief description of the bedrock encountered (database field LITH).

The bedrock wells consist of 28 from our primary dataset and 17 others (including those shown by Hazelwood). Reports of rock types encountered in the bottom of these holes range from confident geologic identifications of greywacke and argillite of the Franciscan Complex, serpentinite, and Miocene marine sandstone to such driller's descriptions as serpentine, shale, rock, Hill Formation, and, in one case, "brittle white rock." No information on rock type is provided by Hazelwood for the bedrock wells that he shows.

Seismic reflections from the basement surface in the Guadalupe and Evergreen seismic profiles are relatively clear, whereas, in the Cupertino profile, selection of where to pick the bedrock is guided by the –650 to –750 foot elevations of rock in nearby wells. That depth range matches a change in the character of subhorizontal reflections in the Cupertino profile from regular and continuous below to discontinuous and somewhat irregular above, which is interpreted to mark the bedrock contact. This contrasts with an earlier interpretation of the profile in which a deeper angular unconformity was judged to mark that contact (Williams and others, 2004). One guide to identifying the bedrock surface in the wells near the reflection profile is well 971, west of the profile, which encountered "brittle white rock" at elevations of –676 and –682, with intervening "sandy clay and gravel." The white brittle rock is probably porcellanite, a common lithology in Miocene Monterey Formation and related rocks. Deeper in that well, and interbedded with clay, sand, and gravel, the driller reported "sandstone," "cemented gravel," "hard blue shale," and "hard sand." This section below the top of the first white brittle rock is judged to be Miocene bedrock, here including both porcellanite and less siliceous clastics. Well 778, almost 5 km to the north, also encounters reported rock (–739 to –774 and –865 to –919) with intervening and underlying clastic sediment. Well WW-3, about 1.3 km east of the reflection profile, bottoms in 67 ft of "blue clay and shale" below an elevation of –659 feet, which is far too shallow to mark the angular relation located nearby in the profile at almost –1,600 feet.

All the direct control was used to grid the bedrock surface in the same fashion used for the sedimentary cycles. Intersection of that surface with all the wells in our dataset identified several that are deeper than that surface but do not reach rock. Because the surface must

be deeper than those wells, elevations just below the bottoms of 19 wells were added to force the final gridded surface to pass beneath them (plate 1, map 11, points shown as "well, no rock"). Remaining artifacts in the surface around the north side of Oak hill were constrained by the addition of two constructed elevation points.

The final bedrock surface shown on plate 1 contains prominent closed depressions at wells 819 and MOFT and a small one in the topographic reentrant east of Oak hill. Probably, were there a denser array of control points, these would prove to be along drainage ways and are simply artifacts of the present distribution of control.

Subcrop Areas

The sedimentary cycles terminate laterally outward against the bedrock surface, and because that surface slopes inward toward the center of the Quaternary basin and to the edge of the Evergreen Basin, shallower cycles have larger areas than deeper ones. Thus, in the maps of plates 1 and 2, the area of bedrock increases downward through the cycles. This increased area of bedrock at the base of each cycle—the bedrock subcrop area—is shown on those maps in light green. The subcrop boundaries were determined by intersecting the digital grids for each cycle boundary with that for the bedrock surface. Although each sedimentary cycle gradually onlaps the bedrock surface such that the top of the cycle (the base of the next overlying cycle) has a larger area than its base, subcrop depiction in the maps makes the simplification that the full thickness of the cycle terminates at the subcrop boundary. For cycle 8, however, because the bedrock surface slopes particularly gently along the west side of the basin beneath that cycle, the subcrop boundary shown for its upper fine interval (plate 2, map 18) is that for its internal top/bottom surface, not its base.

Appendix D. Construction of the Cross Sections

The cross sections of figure 17 were prepared from the gridded surfaces described in appendix C, with minor modifications to better fit nearby well control (wells shown on the sections in that figure). The cross-section lines were defined in map space and points then created along them at 500-m spacing. These points were intersected with the cycle and top/bottom boundaries to obtain elevations of those surfaces at each point. Distances along the sections to each point, and elevations of the surfaces at that point, were then moved into cross-section space to define the surfaces there.

Simplified representations of control wells on or near the section lines (see fig. 17) were prepared from the well diagrams (fig. 22) and overlaid on the cross sections. The cross sections were then adjusted to better match those wells. Most of the mismatches were small. Reasonable mismatches for control wells that were more than 100 m or so from the section lines were retained. The dashed base of cycle 6 shown in section FG to the west of well 210 is based on depiction of that cycle in section AC.

Appendix E. Digital Data Files

Numerous tabular and geographic information system (GIS) files are included with this report. The tabular files include six files of descriptive data about the cores collected from the newly drilled wells (see appendix A) and two files listing depths in wells and other information about the sedimentary cycles. Two vector point GIS files contain the wells and well information, one contains control for the bedrock surface, and one vector polygon file is a framework geologic map. There are 18 raster elevation grids of cycle boundaries and subboundaries, and 9 each of aggregate thickness of coarse material and percent of coarse layers within the bottom coarse intervals of the cycles. Also included are the two shadesets (tables of colors) and two remap tables (correlation tables) used to assign colors to those raster grids. The tabular files are presented as Microsoft Excel tables. The vector GIS layers are presented as ArcInfo export files, the raster layers as ArcInfo grids, and the shadesets as both ArcInfo export and text files. The remap tables are text files.

Tables

- scv-core.xls—core data: basic information about the cores, including well code, core number, depth range, and length of the core.
- scv-lith.xls—core data: textural and bedding information.
- scv-accessory.xls—core data: description of other features of the sediment.
- scv-remarks.xls—core data: any additional remarks about the sediment.
- scv-penetrometer.xls—core data: approximate unconfined compressive strength of cohesive intervals.
- scv-color.xls—core data: Munsell color of described intervals and any subordinate phases.
- bndys.xls—depths to cycle boundaries in the 125 control wells.
- subdivs.xls—details of cycle subdivisions in the 125 wells: for each cycle top and each bottom (where discernable), thickness, aggregate thickness of coarse layers, thickness of the thickest individual fine layer, and number of layers.

GIS Files

Vector Maps

- qbdys.e00—map of the study area containing boundaries of south San Francisco Bay, the surrounding Bay mud, the outer Quaternary alluvium boundary, and the Holocene/Pleistocene alluvium boundary. The principal areas thus defined are identified as H2O, Qhbm, Qh, Qp, and br (bedrock).
- wels1.e00—points representing wells and other control points used to define the base of cycle 1, attributed with depths to and elevations of the cycle 1 boundary.
- wells.e00—points representing all 127 control wells used in the study, attributed for all eight cycles, with depths to and elevations of the cycle boundaries and internal top/bottom boundaries.
- bdrk.e00—points representing control on the elevation of the buried bedrock surface.
- subs.e00—points representing the 125 control wells used in the study, attributed for all eight cycles, with the subdivision data of data table subdivs.xls.

Raster Grids

Cycle and Top/Bottom Elevation Surfaces

- el-c0—smoothed topographic surface that forms the top of cycle 1.
- el-c1b—the internal top/bottom surface of cycle 1.
- el-c1—the bottom surface of cycle 1.
- el-c2a—the bottom of the anomalous upper coarse interval of cycle 2.
- el-c2b—the internal top/bottom surface of cycle 2.
- el-c2—the bottom surface of cycle 2.
- el-c3b—the internal top/bottom surface of cycle 3.
- el-c3—the bottom surface of cycle 3.
- el-c4b—the internal top/bottom surface of cycle 4.
- el-c4—the bottom surface of cycle 4.
- el-c5b—the internal top/bottom surface of cycle 5.
- el-c5—the bottom surface of cycle 5.
- el-c6b—the internal top/bottom surface of cycle 6.
- el-c6—the bottom surface of cycle 6.
- el-c7b—the internal top/bottom surface of cycle 7.
- el-c7—the bottom surface of cycle 7.
- el-c8b—the internal top/bottom surface of cycle 8.
- el-c8—the bottom surface of cycle 8.
- bdrk—the surface of underlying bedrock

Aggregate Thickness of Coarse Layers in Coarse Intervals Within Each Cycle

- ag-c1b—aggregate coarse thickness in bottom of cycle 1.
- ag-c2a—aggregate coarse thickness in cycle 2a.
- ag-c2b—aggregate coarse thickness in bottom of cycle 2.
- ag-c3b—aggregate coarse thickness in bottom of cycle 3.
- ag-c4b—aggregate coarse thickness in bottom of cycle 4.
- ag-c5b—aggregate coarse thickness in bottom of cycle 5.
- ag-c6b—aggregate coarse thickness in bottom of cycle 6.
- ag-c7b—aggregate coarse thickness in bottom of cycle 7.
- ag-c8b—aggregate coarse thickness in bottom of cycle 8.

Percent of Coarse Layers in Cycle Bottoms

- pc-c1b—percent of coarse layers in bottom of cycle 1.
- pc-c2a—percent of coarse layers in cycle 2a.
- pc-c2b—percent of coarse layers in bottom of cycle 2.
- pc-c3b—percent of coarse layers in bottom of cycle 3.
- pc-c4b—percent of coarse layers in bottom of cycle 4.
- pc-c5b—percent of coarse layers in bottom of cycle 5.
- pc-c6b—percent of coarse layers in bottom of cycle 6.
- pc-c7b—percent of coarse layers in bottom of cycle 7.
- pc-c8b—percent of coarse layers in bottom of cycle 8.

Color Files

Shadesets

- thick.shd.e00—shadeset containing a spectrum of 250 CMYK colors ranging from dark blue through green and yellow to magenta.
- pct.shd.e00—shadeset containing a spectrum of 100 CMYK colors ranging from dark blue through green and yellow to magenta.
- thick.txt—thick shadeset as a text file, containing the same colors in CMYK format.
- pct.txt—pct.shd shadeset as a text file, containing the same colors in CMYK format.

Remap Tables

- thick.rmt – text table assigning the colors of thick.shd to values ranging from 0 to 275.
- pct.rmt – text table assigning the colors of pct.shd to values ranging from 0 to 100.

Metadata Files

- Qbndys-metadata.txt
- Wells1-metadata.txt
- wells-metadata.txt
- bdrk-metadata.txt
- subdivs-metadata.txt
- uncon-metadata.txt
- el_grids-metadata.txt
- crs-pct_grids-metadata.txt

Produced in the Menlo Park Publishing Center
Manuscript approved for publication February 3, 2015
Edited by Peter H. Stauffer
Layout by Jeanne S. DiLeo

ISSN 2328-0328 (Online)
http://dx.doi.org/10.3133/sir20155017